JAERI-Research
2001-025

ACTIVATION CROSS SECTION MEASUREMENT AT NEUTRON ENERGY FROM 13.3 TO 14.9 MEV USING FNS FACILITY

March 2001

Yoshimi KASUGAI, Yujiro IKEDA, Yoshitomo UNO,
Hiroshi YAMAMOTO* and Kiyoshi KAWADE*

日本原子力研究所
Japan Atomic Energy Research Institute

本レポートは、日本原子力研究所が不定期に公刊している研究報告書です。
入手の問合わせは、日本原子力研究所研究情報部研究情報課（〒319-1195　茨城県那珂郡東海村）あて、お申し越し下さい。なお、このほかに財団法人原子力弘済会資料センター（〒319-1195　茨城県那珂郡東海村日本原子力研究所内）で複写による実費頒布を行っております。

This report is issued irregularly.
Inquiries about availability of the reports should be addressed to Research Information Division, Department of Intellectual Resources, Japan Atomic Energy Research Institute, Tokai-mura, Naka-gun, Ibaraki-ken 〒319-1195, Japan.

編集兼発行　日本原子力研究所

JAERI－Research 2001－025

Activation Cross Section Measurement at Neutron Energy From 13.3 to 14.9 MeV Using FNS Facility

Yoshimi KASUGAI, Yujiro IKEDA, Yoshitomo UNO, Hiroshi YAMAMOTO*
and Kiyoshi KAWADE*

Center for Neutron Science
Tokai Research Establishment
Japan Atomic Energy Research Institute
Tokai-mura, Naka-gun, Ibaraki-ken

(Received February 16, 2001)

Sixty activation cross sections have been measured in the neutron energy between 13.4 and 14.9 MeV using intense D-T neutrons source (Fusion Neutronics Source, FNS) at JAERI. The following reactions are included in this work: (1) 32 reactions mainly for lanthanide isotopes, (2) 19 reactions for short-lived products (the half-lives are from 1 s to 20 min) and (3) 9 (n, nα) reactions. The experimental results were compared with the data reported previously and the evaluated data of ENDF/B-VI Rev.4, JENDL-3.2 and FENDL/A-2.0. The present data for the (n, p) and (n, α) reactions were compared with the values estimated by using the empirical formulae proposed by our group in order to validate the systematics for the reactions for the lanthanide isotopes. Systematic trend of (n, nα) reactions were discussed based on the present data.

Keywords: Activation Cross Section, Fusion Reactor, Neutron Dosimetry, D-T neutron, FNS, (n, 2n), (n, n'), (n, p), (n, α), (n, nα) , JENDL-3, ENDF/B-VI, FENDL/A-2, Systematics, Empirical Formula

* Nagoya University

FNSを用いた13.3から14.9 MeVの中性子に対する放射化断面積測定

日本原子力研究所東海研究所中性子科学研究センター
春日井　好己・池田　裕二郎・宇野　喜智・山本　洋*・河出　清*

（2001年2月16日受理）

原研FNSの強力中性子源を用いて、エネルギーが13.4から14.9 MeVの中性子に対する60反応の放射化断面積を測定した。測定した放射化断面積には、次のような反応が含まれている。(1)主に希土類核を標的核とする32反応、(2) 19反応の短寿命核（半減期が1秒から20分）生成反応、(3) 9反応の(n, nα)反応。今回測定した実験値を、過去に報告された測定値およびENDF/B-VI Rev.4、JENDL-3.2及びFENDL/A-2.0の評価データと比較検討した。今回測定した(n, p)または(n, α)反応のデータについては、われわれのグループによって提案された経験式を使って計算した値と比較し、その経験式の希土類核領域に対する妥当性を検討した。また、今回得られたデータを使って、(n, nα)反応の系統性を議論した。

東海研究所：〒319-1195　茨城県那珂郡東海村白方白根2-4
*　名古屋大学

CONTENTS

目次

List of Tables

List of Figures

This is a blank page.

1. Introduction

Neutron activation cross section data around 14 MeV are a physical constant that is required for the design of a fusion reactor. For calculation of the induced activities in the structural materials of a fusion reactor, a complete set of evaluation of the cross section data is needed. Those data are also important for neutron dosimetry of fusion environments. Although plenty of experimental data for various elements have been reported, there are often inconsistencies among the experimental data. Some of these discrepancies can be explained in terms of the different experimental technique, different neutron sources, different decay data used in deducing the cross sections, and so on. Most of them still can not be explained. In the evaluations, therefore, judgement of quality of experimental data is critical. Practically, the evaluation of the cross sections is made using statistical process of the selected experimental data, an empirical formula and nuclear reaction theory. Some evaluation data set, ENDF/B-VI [1], JENDL-3.2 [2] and FENDL/A-2.0 [3] etc., are available. In order to keep the reliability of the data set, the evaluation should be regularly consider the latest experimental data.

The cross sections by 14 MeV neutrons have been systematically measured by using D-T neutron source by using FNS (Fusion Neutronics Source) facility at JAERI since 1984. More than 250 reactions for 50 elements have been already reported at 1988 and 1994 [4-7]. In the measurement, the cross sections in the neutron energy range from 13.4 to 14.9 MeV were obtained. The first report published in 1988 described the measuring technique and data reduction process in detail, and the activation cross sections of the 110 reactions for fusion structural materials were reported. The second report published in 1993 compiled 89 measured reaction cross sections not only for fusion structural materials but also for other elements in the viewpoint of the systematic study. The experimental data set has been used as one of the most reliable standard in the evaluations. In the meantime, we proposed the empirical formula for the (n, p) and (n, α) reaction cross sections and the slope of the excitation curve at 14.0 MeV on the basis of the experimental data. [8, 9]

Since 1995 we have been focused on the cross sections which are classified into three categories as follows: (1) the cross sections mainly for lanthanide isotopes, (2) the cross sections for the short-lived products and (3) the (n, nα) reaction cross sections. For category (1), the 32 reactions mainly for the lanthanide isotopes were systematically measured. These new data are very useful to check the validity of the empirical formula[8, 9] in the region of the lanthanide isotopes. As for category (2), the cross sections for 19 reactions, which produce the short-lived activities with the half-lives from 1 s to 20 min, were measured for the elements of boron, magnesium, silicon, sulfur, titanium, iron, copper, zinc, germanium, strontium, zirconium, ruthenium, tin, barium and hafnium. For category (3), the cross sections for 9 (n, nα) reactions were measured.

In this paper, we report the results of the cross sections measured for the above-mentioned 60 reactions. The measured reactions are summarized in Table 1 with the associated nuclear data taken form Table of Isotopes[10]. The present data were compared with the data in the literature and the evaluated data of JENDL-3.2, ENDF/B-VI Rev.4 and FENDL/A-2. For the (n, p) and (n, α) reactions, the cross section curves estimated by using the empirical formula are compared with the experimental data to check the validity of the formula for the lanthanide nuclei. Systematics of the (n, nα) reactions are discussed on the basis of the present experimental data.

2. Experiment

2.1 Neutron Source

D-T neutrons were produced via the $^{3}T(d, n)^{4}He$ reaction by bombarding d^{+} beams with a tritium-target using the FNS (Fusion Neutronics Source) facility. The d^{+} beam current and energy were 2 mA and 350 keV, respectively. Normal neutron yield was about 3×10^{11} /s.

2.2 Samples

Separated isotopes were used whenever they were available, in order to distinguish contribution of reactions that produce the same nucleus. Natural materials were used when separated isotopes were not obtained. The samples in powder form were wrapped with a thin cartridge paper. The effective area of these samples was 10×10 mm^2 and nominal thickness was 1 mm. The chemical compositions, weights, thickness and abundance of samples are summarized in Table 2.

2.3 Irradiation

The samples were placed at a distance of 100 mm from the D-T neutron source. They were set at various angles of 0°, 45°, 70°, 95° 120° and 155° with respect to the d^{+} beam in order to cover the neutron energies ranging from 13.4 to 14.9 MeV.

A pneumatic sample transport system was used for the irradiation of samples when we measured short-lived products. Pneumatic tubes were set at angles of 0°, 45°, 70°, 95° 120° and 155°. The schematic view of the typical setting of the pneumatic is shown in Fig.1. The distance between the neutron source and the irradiation positions are 10 cm. Typical neutron fluxes at each positions were 2×10^{8} /cm^{2}s.

2.4 Neutron flux monitor

The neutron flux at the sample position was measured with use of the $^{93}Nb(n,2n)^{92m}Nb$ reactions for long- lived products. The samples were sandwiched between two niobium foils of 10 mm × 10 mm and 0.1 mm in thickness. The schematic drawing of the sample and the cartridge are shown in Fig. 2. The value 464 mb (±4.2%) was adopted as the standard cross section of the $^{93}Nb(n,2n)^{92m}Nb$ reaction with the neutron energy between 13.3 to 14.9 MeV. This value was measured at FNS using the evaluated cross section of the $^{27}Al(n,\alpha)^{24}Na$ reaction in ENDF/B-VI as a standard. Recently we absolutely measured the cross sections of the $^{93}Nb(n,2n)^{92m}Nb$ reaction.[5] According to the absolute measurement, the adopted cross section values of the $^{93}Nb(n,2n)^{92m}Nb$ reaction are high by 1-2%. The difference between two data is no large. Therefore, in order to keep the consistency with the previous results, the present experiment adopted 464 mb as the standard cross section of the $^{93}Nb(n,2n)^{92m}Nb$ reaction.

When we measured the short-lived products with the half-lives less than 30 min, the $^{27}Al(n,p)^{27}Mg$ reaction cross sections were used as a neutron flux monitor. The samples were sandwiched between two aluminum foils of 10 mm×10 mm and 0.2 mm in thickness. The cross section values were determined using the standard cross section of the $^{93}Nb(n,2n)^{92m}Nb$ reaction.

2.5 Gamma-ray measurement

Gamma rays emitted from the irradiated samples were measured with HPGe detectors. The niobium and aluminum monitor foils were measured separately. A low-energy-photon-spectrometer (LEPS) with a thin Be-window was also used to measure low-energy gamma-rays below 100 keV. The cross sections of the ^{65}Cu(n,nα)^{61}Co reaction were measured using the LEPS because ^{61}Co emits 67.4 keV γ-ray. Each detector was covered with 5 mm thick acrylic absorbers in order to reduce β-rays. Absolute gamma-ray detection efficiency for each detector was calibrated at 5.0 cm from the detector surface using standard gamma-ray sources. The calibrated detection efficiencies at various gamma-ray energies were fitted with a numerical function for each detector. The efficiency curve of a detector is shown in Fig. 3. The accuracy of the fitting function is estimated to be ±2%. The irradiated samples were normally put at 5.0 cm from the detector surface (standard position). If the induced activities of the sample were weak, the samples were put just on the acrylic absorbers at 5 mm from the detector surface (close position). The efficiency at the close position was calibrated by measuring the same sample at both of the standard and the close positions. The sample for the calibration was prepared by irradiating at a position close to the DT neutron source in order to produce higher intensity activity.

2.6 Cross-section determination

The reaction rate, RR, was derived using the following equation,

$$RR = \frac{\lambda CAF}{W\varepsilon_f abN_A\left(1-e^{-\lambda t_i}\right)e^{-\lambda t_c}\left(1-e^{-\lambda t_m}\right)},$$

where

λ : decay constant of radioactivity,
C : gamma-ray count,
A : atomic weight of target sample,
F : correction factor,
W : sample weight,
ε_f : detector efficiency,
a : isotopic abundance of target nuclide,
b : gamma ray brunching ratio,
N_a : Avogadro's number,
t_i : irradiation time,
t_c : cooling time,
t_m : measuring time.

All decay data were taken from the Table of Isotopes [10]. The correction factor F includes fluctuations of the neutron flux during the irradiation, self-absorption of gamma ray in the samples, contribution of low energy neutrons, counting losses due to the coincidence sum effects and deviation in the measuring position coming from the difference thickness of each sample.

The average of reaction rates for the two monitor foils at front and back of the sample was adopted as that at the sample position. The difference between the reaction rate of the two monitor foils was 2-3% due to the difference of the distances from the neutron source to the monitor foils.

The cross section for the reactions of interest was obtained from the following equation,

$$\sigma = \frac{RR}{RR_m}\sigma_m$$

where,

RR : reaction rate of the reaction under investigation,
RR_m : averaged reaction rate of the monitor reactions,
σ_m : cross section of the monitor reaction.

In a case where two different reactions produce the same activity in one sample, two samples with different isotopic abundance were irradiated, and the contributions from these reactions were resolved.

Whenever a meta-stable state nucleus decayed to ground state nucleus by an isomeric transition during the gamma ray measurement, the contribution of that meta-stable state was subtracted in deducing the reaction cross section corresponding to production of the ground state nuclei.

The effective reaction energy of the incident neutrons was determined by using the measured cross section curve and neutron spectrum calculated with the Monte Carlo code, MORSE-DD [11]. The details of this procedure are described in Ref 4. In our previous work, the effective reaction energy was determined by considering a cross section curve for each measurement. In this work effective neutron energy was fixed for each irradiation angle because some of the cross section data were not measured at enough data points to estimate the cross section curve. The fixed values are 14.94, 14.68, 14.37, 14.02, 13.68 and 13.36 MeV which correspond to the irradiation angles of 0°, 45°, 70°, 95° 120° and 155°, respectively. The error of the fixed effective neutron energy was estimated to be less than ±50 keV by considering an extreme case of the cross section curve.

2.7 Error estimation

The sources and typical values of the experimental errors are summarized in Table 3. The dominant error sources were due to gamma ray detector efficiency, counting statistics and the standard cross sections for the neutron flux monitor. For some reactions, the errors of the gamma ray branching ratios were larger than 10%.

3. Results and Discussion

All of the measured cross sections are shown in Figs. 4.1 to 4.60 together with corresponding values from the literature and results from the comprehensive evaluation ENDF/B-VI Rev.4 [1], JENDL-3.2 [2] and FENDL/A-2.0 [3]. (Below we use ENDF/B-VI, JENDL-3 and FENDL/A-2 instead of ENDF/B-VI Rev.4 , JENDL-3.2 and FENDL/A-2.0, respectively) Numerical values for the measured cross sections are given in Table 4 along with the experimental errors. Discussion concerning each reaction is given below.

3.1 ^{11}B(n, p)^{11}Be (Fig.4.1)

The present data agree with the previous data within the uncertainties. The JENDL-3 evaluation is more consistent with the present data than the ENDF/B-VI evaluation. The FENDL/A-2 evaluation adopted the same values as the ENDF/B-VI evaluation.

3.2 ^{26}Mg(n, p)^{26}Na (Fig. 4.2)

The JENDL-3 evaluation is higher by 10-20% than the present data. The FENDL/A-2 evaluation adopted the same values as the JENDL-3 evaluation.

3.3 ^{30}Si(n, p)^{30}Al (Fig. 4.3)

The present data is consistent with the data measured by Satoh et al. [12] The ENDF/B-VI evaluation is consistent with the present data within the uncertainty. The JENDL-3 evaluation is lower by 50% than the present data. The FENDL/A-2 evaluation, which adopted the experimental data measured by Schantl[13], is much higher than the present data by a factor of more than 2.

3.4 ^{34}S(n, p)^{34}P (Fig. 4.4)

The JENDL-3 and FENDL/A-2 evaluation are consistent with the present data within the uncertainties thought the errors of the present data are so large.

3.5 ^{46}Ti(n, p)^{46m}Sc (Fig. 4.5)

The cross sections were measured using the samples enriched with the ^{46}Ti isotope. The contribution of the ^{47}Ti(n, np)^{46m}Sc reaction was taken into account by using the enriched samples with the ^{47}Ti isotope.

The present data agree with the recent experimental data obtained by Viennot[14], Ribansky[15] and Molla[16] within the experimental errors. All of the previous data were obtained at one neutron energy point. The present data show for the first time that the excitation function around 14 MeV has decreasing trend with increasing the neutron energy. The FENDL/A-2 evaluation has also decreasing trend around 14 MeV though the cross section is lager than the present data by 10-20%.

3.6 ^{47}Ti(n, np)^{46m}Sc (Fig. 4.6)

The contribution of the ^{46}Ti(n, p)^{46m}Sc reaction was taken into account using the ^{46}Ti-enriched samples. The present data are the first experimental data for this reaction.

Sum of the (n, np) and (n, d) cross sections in the FENDL/A-2 file are plotted in the figure. In the 14 MeV region, the FENDL/A-2 evaluation are larger than the present experimental data by more than a factor of 2. The present data shows that the excitation function rises up about 13 MeV though the evaluated excitation function are rising up at 12 MeV.

3.7 $^{51}V(n, n\alpha)^{47}Sc$ (Fig. 4.7)

A sample with natural abundance was used to measure this reaction cross section. The natural sample includes ^{50}V isotope with abundance of 0.25%. ^{47}Sc is produced via the $^{51}V(n, n\alpha)^{47}Sc$ and $^{50}V(n, \alpha)^{47}Sc$ reaction. Though the natural abundance of ^{50}V is very small, the cross section of the (n, nα) reaction is much smaller than that of the (n, α) reaction by a factor of more than 100. Therefore the contribution of the $^{50}V(n, \alpha)^{47}Sc$ reaction to the production of ^{47}Sc have to be considered to deduce the $^{51}V(n, n\alpha)^{47}Sc$ reaction. There are no available experimental data of the $^{50}V(n, \alpha)^{47}Sc$ reaction. In this work, the cross sections calculated using the empirical formula[9] are used. The error of the estimated (n, α) cross section is estimated to be ±30%. As a result, the upper limit of the (n, nα) cross section was obtained by subtracting the contribution of the (n, α) reaction.

Both of the cross sections reported by Qaim et al. [17] and Pepelnik et al. [18] are higher than the upper limit obtained in this work. It is possibly to say that their data were not properly taken the contribution of the (n, nα) reaction into account. We regard that the JENDL-3 and FENDL/A-2 evaluation is consistent with our data because the value of the evaluation is lower than the upper limit.

3.8 $^{57}Fe(n, p)^{57}Mn$ (Fig. 4.8)

The present data are good agreement with the data of Molla and Qaim[16]. However this agreement may be an accident, because the decay data used in this work are much different from the data used by Molla and Qaim. They used 87.9% as the 122 keV gamma-ray intensities with the decay of ^{57}Mn while we used 14%.

Viennot et al.[14, 19] measured the cross section data at 7 neutron energy points between 13.8 and 14.8 MeV. The data are much larger than our data.

The ENDF/B-VI evaluation data shows agreement in our data. The evaluation curve of the ENDF/B-VI has a peak at 14.5 MeV, though our data shows that the cross section values are slightly decrease as increase of the neutron energy in the energy range from 13.4 to 15.0 MeV. The JENDL-3 evaluation, which seems to be based on the data of Singh[20], is much smaller than our data. A re-evaluation is required for the evaluation. The FENDL/A-2 evaluation is much larger than the present data by 40%.

3.9 $^{63}Cu(n, 2n)^{62}Cu$ (Fig. 4.9)

In this measurement, we paid special attention to determination of the activities of ^{62}Cu.[21] We measured annihilation γ-rays converted from the β^+-rays, which is emitted with the decay of ^{62}Cu because the gamma-ray branching ratios are very small. The Cu-sample was covered with a lead capsule with the thickness of 0.8 mm to stop all positrons in a restricted region. By covering the samples, we could avoid the annihilation events far form the samples. The mean position of the sample for the Ge detectors was slightly different. The annihilation γ-rays were absorbed in the lead cover. The cross sections were deduced by taking such kinds of effects into consideration.

There are many experimental data available for the reaction. (In the figure, the data obtained

after 1965 are plotted.) However there are considerably large scattering. At 14.5 MeV, the largest data is about 600 mb and the smallest one is 400 mb. Our data are close to the smallest one. The evaluation seemed to be performed by statistical process; averaging all available data, for example. In conclusion, we recommended re-evaluating the cross section for this reaction.

3.10 ^{65}Cu(n, nα)^{61}Co (Fig. 4.10)

A low-energy-photon-spectrometer (LEPS) was used to detect 67.4 keV gamma-ray associated with the decay of ^{61}Co.

Santry et al.[22] obtained the cross sections at 14.74, 14.50, 14.25 and 13.58 MeV. Their data are consistent with our data except the data at 14.74 MeV, which is smaller by 20% than our data.

The evaluations of ENDF/B-VI and JENDL-3 are consistent with our data. Note that FENDL/A-2 is just same as ENDF/B-VI.

3.11 ^{68}Zn(n, p)^{68m}Cu (Fig.4.11)

There are several kinds of multi-point data in the energy range from 13.4 and 15.0 MeV. Our data shows good agreement with the data of Kasugai et al.[23], which were measured by using DT neutron source at Osaka University in Japan. It is very important that the almost same values of the cross sections were obtained by using a different neutron source, different germanium detectors and different samples.

The data of Viennot et al.[14] are smaller by 20% than our data. The data of Kielan et al.[24] are 30% smaller at 13.4 MeV and 50% smaller at 14.9 MeV than our data. This means that the increasing trend shown by Kielan's data is not as steep as our data. The data of Ghorai et al.[25], which was reported most recently, is in agreement within the errors with our data.

The FENDL/A-2 evaluation is systematically lager than our data by about 1 mb in the region from 13.4 and 15.0 MeV.

3.12 ^{71}Ga(n, nα)^{67}Cu (Fig. 4.12)

Qaim [17] and Bramlitt et al. [26] measured the cross section at one neutron energy of 14.7 MeV. Those are consistent with our data. JENDL-3 and FENDL/A-2 are almost consistent with our data.

3.13 ^{74}Ge(n, p)$^{74m+g}$Ga (Fig. 4.13)

All experimental data reported previously agree with our data within the uncertainties except the data which is obtained by Hoang et al.[27] at 15.0 MeV. The JENDL-3 evaluation shows good agreement with our data. The excitation function of the FENDL/A-2 evaluation has a peak at the neutron energy at 14.5 MeV. The present data do not support the evaluated excitation function. The present data support the JENDL-3 evaluation whose excitation function shows the increasing trend in the energy range between 13.3 and 15.0 MeV.

3.14 ^{76}Ge(n, p)^{76}Ga (Fig. 4.14)

Previously only one data exist at 14.7 MeV. The data measured by Rieppo et al.[28] is in good agreement with our data though the error of their data is large.

The cross section curve of the JENDL-3 evaluation has an increasing trend, and the curve is

passing just through Rieppos' data. In the neutron energy region between 13.4 and 14.1 MeV, JENDL-3 is in good agreement with our data. In the energy region higher than 14.5 MeV, however, the curve shows smaller than our data. The present experimental data shows a rather steep slope of the cross section curve around 14.5 MeV.

The present experimental data do not support the the FENDL/A-2 evaluation whose excitation function has a peak at 15.5 MeV.

3.15 ^{76}Ge(n, 2n)^{75m}Ge (Fig. 4.15)

Our data agree with the data of Okumura et al.[29] within the uncertainties. The data of Borman et al.[30] are 10-20% larger than our data. The errors of our data are the smallest among the existing data. The slope of the FENDL/A-2 cross section curve is rather flat in the energy region between 13.5 and 15 MeV in comparison with the experimental data.

3.16 ^{76}Ge(n, nα)^{72}Zn (Fig. 4.16)

The data measured by Qaim et al.[31] is much higher than our data by a factor of about 100. FENDL/A-2 evaluation adopted the data of Qaim et al. The present cross section value, however, is close to the curve of the JENDL-3 evaluation.

3.17 ^{87}Rb(n, nα)^{83}Br (Fig. 4.17)

The cross section is measured for the first time in this work. The present values are higher than the values of ENDF/B-VI, JENDL-3 and FENDL/A-2 by a factor more than 10.

3.18 ^{84}Sr(n, p)^{84m}Rb (Fig. 4.18)

There is only one data measured by Molla and Qaim[16] previously. The data is 20% larger than our data. In this work we obtained the first multi-point data, which shows the decreasing trend of the excitation function with the neutron energy. The cross section curve of FENDL/A-2 is systematically higher than the present data by 10 mb.

3.19 ^{91}Zr(n, nα)^{87m}Sr (Fig. 4.19)

The cross section for this reaction was measured for the first time. The FENDL/A-2 is smaller by a factor 2~3 than the present results.

3.20 ^{96}Zr(n, np)^{95}Y (Fig. 4.20)

No data exists previously for the reaction. In this work the cross section data were obtained at only 14.9 MeV, but for the first time. The statistics of γ-ray peak counts were very poor (10±5 counts), so the statistical error was 50%. The JENDL-3 evaluation is much smaller than our data. Based on the present data, the excitation curve of the JENDL-3 evaluation is needed to be shifted by about -1 MeV. The FENDL/A-2 evaluation is much larger than the present data by a factor more than 2.

3.21 ^{96}Zr(n, nα)^{92}Sr (Fig. 4.21)

The cross section for this reaction was measured for the first time. The evaluated curve of JENDL-3 is higher than our data by a factor of 3. FENDL/A-2 shows lower values than the present data by a factor more than 10.

3.22 ^{93}Nb(n, nα)^{89m}Y(Fig. 4.22)

Previously three data obtained at one point of neutron energy were reported by Kim et al[32] , Pepelnik et al.[18] and Brammlitt et al.[26] In this work the cross section at multiple energy points were obtained. The previous data are consistent with our data. FENDL/A-2 agrees with the present data.

3.23 ^{100}Ru(n, p)^{100}Tc (Fig. 4.23)

It has been difficult to measure activities of the product of ^{100}Tc due to the short half-life of 15.8 s. Previously only one data was given by Prasad[33]. The data is smaller by 50% in comparison with our data. The JENDL-3 evaluation was also smaller than our data. The evaluated cross section curve of FENDL/A-2 shows relatively better agreement with the present data.

3.24 ^{109}Ag(n, nα)$^{105m+g}$Rh (Fig. 4.24)

The cross section for this reaction was measured for the first time. The value of JENDL-3 is higher by a factor of 3 in comparison with our data. ENDF/B-VI curve is relatively in better agreement with the present results.

3.25 ^{111}Cd(n, p)$^{111m+g}$Ag (Fig. 4.25)

The activity of ^{111g}Ag ($T_{1/2}$=7.45 d) was measured after cooling the samples for more than one day. The short-lived isotope of ^{111m}Ag almost decayed out to the ground state by isomeric transition; the isomeric transition ratio is 99.7%. By measuring the ^{111g}Ag activity after enough cooling-time, we obtained the total cross section for the products of ^{111m}Ag and ^{111g}Ag.

Bayhurst et al.[34] obtained the cross section data in the neutron energy range between 7 and 20 MeV. The data of Grallert et al.[35], which was reported recently, support Bayhursts' data. The evaluation curve of ENDF/B-VI was drawn using those experimental data as bases. Those data are larger by 20~30% compared with our data.

The data obtained by Pepelnik et al.[36], which was adopted in the evaluations of JENDL-3 and FENDL/A-2, were higher by a factor of 2 than our data.

3.26 ^{113}Cd(n, p)$^{113m+g}$Ag (Fig. 4.26)

The activity of ^{113g}Ag ($T_{1/2}$=5.37 d) was measured after cooling the samples for more than one hour. The short-lived isomer ^{113m}Ag decayed out during the measurement. The decay mode of the isomer is isomeric transition and β-decay; the isomeric transition ratio is 64%. The cross sections for $0.64\sigma_m+\sigma_g$ were obtained in this work, where σ_m and σ_g are the cross sections for the ^{113m}Ag and ^{113g}Ag production, respectively.

The cross section data of Yu et al.[37] and Levkovskiy et al.[38] were deduced without considering existence of isomeric state.

Grallert et al.[35] measured a cross section for the production of the isomer and the ground state, separately. Their data for σ_m is almost equal to our data for $0.64\sigma_m+\sigma_g$. This shows $\sigma_m \approx 0.64\sigma_m+\sigma_g$, if Grallerts' data is correct. Then we could estimate that the isomer ratio σ_m/σ_g is 2.8.

The ENDF/B-VI and JENDL-3 evaluation curves for $\sigma_m+\sigma_g$ are drawn in the figure. To compare our data for $0.64\sigma_m+\sigma_g$ with the evaluations, the value of $\sigma_m+\sigma_g$ was estimated by using the isomer ratio $\sigma_m/\sigma_g \approx 2.8$. As a result, the estimated cross section for $\sigma_m+\sigma_g$ at 14.95 MeV is about 22 mb. (The estimated value of $\sigma_m+\sigma_g$ is 30% as large as our cross section data for $0.64\sigma_m+\sigma_g$.) This estimation for $\sigma_m+\sigma_g$ is very rough and has larger uncertainties including the error of the experimentally determined values for $0.64\sigma_m+\sigma_g$ and σ_m/σ_g. Even if the large uncertainties are taken into account, both of the evaluations are underestimated as a result.

In the evaluated data-file of FENDL/A-2, the values of both σ_m and σ_g were compiled. In the figure, the values of $0.64\sigma_m+\sigma_g$ were plotted. The evaluated cross section curve is almost consistent with the measured value in the energy range between 13.7 and 15 MeV. However, the evaluated cross section values are not compiled in the energy range between 15 and 20 MeV. Therefore, in the figure, the data-point at 15.0 MeV and 20.0 MeV was connected with a line.

3.27 ^{120}Sn(n, np)^{119g}In (Fig. 4.27)

There exist an isomer of ^{119g}In with the half-life of 18.0 min. The isomer has a branch of isomeric transition; the isomeric transition rate is 5.6%. In this work, we measured the activity of the ground state (^{119g}In) by detecting 763.1 keV γ-rays. To check the contribution of the isomeric transition to the activity of ^{119g}In, we follow the decay process by detecting the γ-rays at several of cooling times. As a result of the measurement, the half-life of 763.1 keV γ-ray is almost equal to that of ^{119g}In. We concluded that the contribution of the isomer was negligibly small.

This cross section is measured for the first experimental data for this reaction. The evaluated values of FENDL/A-2 are much higher than the present data by a factor of more than ten.

3.28 ^{132}Ba(n, 2n)^{131m}Ba (Fig. 4.28)

The natural abundance of ^{132}Ba is very low as 0.101%. The data of Rurartz et al.[39] agree with our data within the uncertainty though the errors of there data are large. The excitation function of the FENDL/A-2 evaluation shows the increasing trend around the 14 MeV region. Our data, which is obtained at the neutron energies of 14.94, 14.68 and 13.68 MeV, show the decreasing trend for the neutron energy in the energy region between 13.4 and 15.0 MeV.

3.29 ^{137}Ba(n, n')^{137m}Ba (Fig. 4.29)

The samples enriched with ^{137}Ba by 64% were used. The samples also contain ^{138}Ba by 34%. The contribution of the ^{138}Ba(n,2n)^{137m}Ba reaction to the production of ^{137m}Ba was estimated using the experimental cross section data of Ikeda et al.[3] As a result of the estimation, the ^{138}Ba(n,2n)^{137m}Ba reactions contributed by 50% to the ^{137m}Ba production.

In the 14 MeV region, two kinds of data were previously reported by Pepelnik et al.[40] and Rurartz et al.[41] Pepelniks' data shows good agreement with our data. Rurartzs' data is larger by 50% than our data. The ENDF/B-VI excitation function, which is supposed to be evaluated on the basis of the data reported by Hannapel et al.[42], shows extremely large values in comparison with the present data. The evaluated cross sections of JENDL-3 are also larger than the present data by about 300 mb.

3.30 ^{139}La(n, p)^{139}Ba (Fig. 4.30)

Previously, Achour et al.[43] reported multi-point data for the reaction cross section, and others are one-point data as shown in Fig 4.30. The data of Achor et al. is 20~30% smaller than our data. JENDL-3 evaluation shows relatively a good agreement with our data though the slope of the excitation curve of the evaluation is slightly steeper than that of our data. The cross section curve of FENDL/A-2 is also in good agreement.

3.31 ^{139}La(n, t)^{137m}Ba (Fig. 4.31)

A well-type Ge detector with a high efficiency was used to detect the activity of the products ^{137m}Ba because the ^{137m}Ba activity was expected to be small. The efficiency of the detector for 661 keV γ-ray emitted from ^{137m}Ba was calibrated using a ^{137}Ba-enriched sample. Strong activities of ^{137m}Ba were obtained via the ^{137}Ba(n, n')^{137m}Ba reaction. After the irradiation, the 661 keV γ-rays were counted with the standard detector and the well-type detector. The measurement time was 1 min for each detector, and the efficiency ratio for the γ-ray was obtained. The detection efficiency for the well-type detector could be obtained by multiplying the ratio by the standard detector efficiency.

Previously one-point data were reported by Woo et al.[44] and Qaim et al.[45] Those data show an agreement with our data at 14.68 MeV. FENDL/A-2 is extremely low in comparison with all the experimental data.

3.32 ^{140}Ce(n, 2n)^{139m}Ce (Fig. 4.32)

Bormann et al.[46] reported cross section data for the reaction in the wide energy range. Their data shows a different trend of the excitation curve from our data; our data shows an increasing trend, and on the other hand their data shows a decreasing trend with the neutron energy. Qaims' data[47] shows a good agreement with our data. The agreement between the present data and FENDL/A-2 is also good.

3.33 ^{140}Ce(n, 2n)$^{139m+g}$Ce (Fig. 4.33)

Considerable number of data were reported. Our data is in agreement with the previous data except the data of Eapen et al.[48] and Cuzzocrea et al.[49] JENDL-3 is 10% larger than our data, and FENDL/A-2 shows a good agreement with the present data.

3.34 ^{140}Ce(n, p)^{140}La (Fig. 4.34)

The data reported by Teng Dan[50] et al. show an excellent agreement with the present data. The JENDL-3 and FENDL/A-2 are also in agreement with our data, though the slope of both evaluation curves is slightly gradual compared with the curve expressed by the present multi-points data, and the present data of 13.36 MeV is slightly higher than the evaluation curves.

3.35 ^{140}Ce(n, α)^{137m}Ba (Fig. 4.35)

The data reported by Bormann et al.[51] are quite different from our data. The data of Havlik et al.[52] shows an agreement with our data. FENDL/A-2 curve shows a good agreement with the present data.

3.36 ^{142}Ce(n, 2n)^{141}Ce (Fig. 4.36)

The data obtained by Teng Dan[50] et al. at multiple energy points almost agree with our data. The evaluation curves of JENDL-3 and FENDL/A-2 is almost same in the neutron energy region less than 13.4 MeV, and those evaluations agree with our data at 13.4 MeV. The decreasing tendency of the FENDL/A-2 curve at energies more than 13.5 MeV is more rapid than that of JENDL-3. Compared with our data, the decreasing trend of FENDL/A-2 is too steep.

3.37 ^{141}Pr(n, 2n)^{140}Pr (Fig. 4.37)

The present data are lower than the evaluated curves of ENDF-B/VI, JENDL-3 and FENDL/A-2 by 20-30%. Those data are based mainly on the experimental data repored by Rayburn et al. [53] and Koehler et al. [54]. The data of Sigg et al. [55], Valkonen et al. [56] and Arammininowicz et al. [57] agree with the present data.

3.38 ^{141}Pr(n, p)^{141}Ce (Fig. 4.38)

All the one-energy-point data reported previously are consistent within the uncertainties except one. The JENDL-3 and FENDL/A-2 evaluations are slightly smaller than our data by 10%. The evaluation curve of ENDF-B/VI is smaller by 40% than our data.

3.39 ^{142}Nd(n, 2n)$^{141m+g}$Nd (Fig. 4.39)

The data obtained by Jong Do et al.[58] at multiple energy points are lower by 20% in comparison with our data. The present data are consistent with other experimental data of Frehaut et al. [59], Kumabe et al. [60], Qaim et al. [61], etc. JENDL-3 almost agrees with the present data. FENDL/A-2, which is supposed to be evaluated based on the experimental data reported by Jong Do et al.[58], shows lower values by 15-20% than the present data.

3.40 ^{144}Nd(n, α)^{141}Ce (Fig. 4.40)

There exist three data reported by Grallert et al.[62], Gmuca et al.[63] and Prasad et al.[64] The data of Prasad et al. are extremely large in comparison with others. The others are larger by a factor of 1.2-1.5 than our data. The data of Grallert et al. and Gumuca et al. were adopted for the FENDL/A-2. The excitation curve of FENDL/A-2 data starts at 8 MeV and gradually increases. However the present data at three neutron energy points indicate that the excitation function effectively starts at 13-14 MeV and rapidly increases.

3.41 ^{145}Nd(n, p)^{145}Pr (Fig. 4.41)

Only one experimental data of Gmuca et al. [63] was reported previously. Their data agree with our data. JENDL-3 and FENDL/A-2 show good agreements with our data. ENDF/B-VI is smaller by 50% than our data at 14.94 MeV.

3.42 ^{146}Nd(n, p)^{146}Pr (Fig. 4.42)

Our data agree with the data of Gmuca et al. [63] and Qaim et al. [65] The data of Bari et al. [66] is smaller by 50% than our data. JENDL-3 and FENDL/A-2 are in agreement within the errors with our data. ENDF/B-VI is much smaller in comparison with all the experimental data.

3.43 ^{148}Nd(n, p)^{148m}Pr (Fig. 4.43)

The isomer ^{148m}Pr has no branch of isomeric transition; that decays only with β^--decay. The isomer ^{148m}Pr decays with the gamma-rays of 301 and 450 keV with the intensities of 95% and 50%, respectively. ^{148g}Pr also emit the gamma-rays of 301 and 450 keV. For the decay of ^{148g}Pr, the intensities of the 450 keV gamma-ray is very weak; the intensities of 301 and 450 keV are 61% and 3%, respectively. This means that almost all counts of the 450 keV gamma-rays came from the decay of ^{148m}Pr.

Previously only one data are obtained by Gmuca et al. [63] The excitation curve of FENDL/A-2 is in good agreement with the present data.

3.44 ^{148}Nd(n, α)^{145}Ce (Fig. 4.44)

Our data agree well with the data of Gmuca et al. [63] and that of Majeddin et al.[67]

JENDL-3 is in good agreement with our data. ENDF/B-VI is smaller in comparison with the experimental data at around 14.8 MeV. The slope of the excitation curve given by our data is steeper than the ENDF/B-VI evaluation curve. FENDL/A-2, which was evaluated using the data of Wille et al. [68], is much higher than our data.

3.45 ^{150}Nd(n, 2n)^{149}Nd (Fig. 4.45)

Many experimental data were reported previously, and almost all the data show good agreements with our data. Our data shows a decreasing trend with increase of the neutron energy. ENDF/B-VI is just same as FENDL/A-2. The evaluation curves show also a decreasing trend, but the slope of the curve is much steeper in comparison with our data.

3.46 ^{144}Sm(n, 2n)^{143m}Sm (Fig. 4.46)

Our data shows an excellent agreement with the data of Murahira et al. [69], Jong Do et al. [58] obtained the cross section data at several neutron energy points, though the data are systematically lower in comparison with our data. FENDL/A-2 shows an excellent agreement with the present data.

3.47 ^{144}Sm(n, α)$^{141m+g}$Nd (Fig. 4.47)

Previously only one data were reported by Alford et al.[70] Their data shows a good agreement with our data. JENDL-3 and FENDL/A-2 are slightly lower than our data.

3.48 ^{154}Gd(n, 2n)^{153}Gd (Fig. 4.48)

The data of Weigel et al. [71] are quite lower than the present data. The data reported by Qaim et al. [61] and Dilg et al. [72] are consistent with our data though Dilgs' data is slightly small.

JENDL-3 and ENDF-B/VI are just same. The excitation curve shows an agreement with our data. FENDL/A-2 is slightly smaller than the present data in the 14 MeV region because the cross section data of Dilg et al. [72] was adopted for the evaluation..

3.49 ^{154}Gd(n, p)^{154m}Eu (Fig. 4.49)

The cross section is measured for the first time in this work. FENDL/A-2 is much larger than the present values by a factor more than ten.

3.50 ^{160}Gd(n, 2n)^{159}Gd (Fig. 4.50)

Errors of the present data are large. The errors of the present data encompass almost all the other experimental data and the evaluations of ENDF/B-VI and FENDL/A-2. The data of Bari [73] and Paul et al. [74] locate out of the region covered by the error bars of the present data.

3.51 ^{162}Dy(n, p)^{162}Tb (Fig. 4.51)

The previous data of Antov [75] and Qaim [76] show an excellent agreement with the present data. FENDL/A-2 shows an excellent agreement with the present data.

3.52 ^{162}Dy(n, α)^{159}Gd (Fig. 4.52)

The present data agree with the value of Bari et al. [66] and Qaim et al. [76] The data reported by Coleman et al.[77] is lager by a factor of 1.5-2 than our data.

FENDL/A-2 is in good agreement with the present results.

3.53 ^{164}Dy(n, p)^{164}Tb (Fig. 4.53)

Previously only one data was reported by Qaim et al [65]. Their data is consistent with out data. FENDL/A-2 shows an agreement with the present data.

3.54 ^{164}Dy(n, np)^{163}Tb (Fig. 4.54)

The present data are for the first time. Contribution of the ^{163}Dy(n, p)^{163}Tb reactions to the production of ^{163}Tb was considered. For estimating the contribution, the ^{163}Dy(n, p)^{163}Tb reaction cross sections were estimated using the empirical formula[8]. The estimated values were 2.6 mb, 2.1 mb, 2.0 mb, 1.3 mb, 1.1 mb and 0.8 mb at 14.94, 14.68, 14.37, 14.02, 13.68 and 13.36 MeV, respectively. The uncertainties of the estimated values are estimated to be ±30%. As a result, the rates of the contribution to the total production of ^{163}Tb were 10-20%. The statistics of the gamma-ray counts were poor, so the errors of the present data are large.

The curve of the FENDL/A-2 is lower than the present data. The result suggests that the curve should be sifted by -2 ~ -3 MeV along the horizontal axis of the neutron energy.

3.55 ^{164}Dy(n, α)^{161}Gd (Fig. 4.55)

There are four data reported previously. The data reported by Havlik et al. [78], Khurana et al. [79],

and Wille et al. [80] are consistent each other. The values of these data are ranging from 4 to 6 mb at the neutron energy at about 14.8 MeV. Though present data are considerable smaller than the three data, the data of Oms et al.[81], which is adopted in the FENDL/A-2 evaluation as a basis, is relatively close to our data.

3.56 ^{167}Er(n, p)^{167}Ho (Fig. 4.56)

The present data shows that the cross sections increase with the neutron energy. The cross section values reported by Liljavirta et al. [82], Prasad et al. [33] and Wille et al. [80] are consistent with the present data. The data of Lakshmana Das et al.[83] is lower than the present data by 30%. FENDL/A-2 shows an agreement with the present results.

3.57 ^{168}Er(n, p)$^{168m+g}$Ho (Fig. 4.57)

The existence of the isomer ^{168m}Ho is reported in 1990.[84] The half-life of the isomer is 132 s, and the decay mode is only isomeric transition. It is very difficult to detect the 59 keV gamma-ray associated with the isomeric transition because the gamma-ray intensity is weak. We follow the decay of 741 keV gamma-ray associated with the decay of the ground state to check the contribution of the isomer production.

All the previous data, which were obtained without considering the contribution of the isomer, were systematically low in comparison with the present data. FENDL/A-2 shows an agreement with the present result.

3.58 ^{176}Yb(n, np)^{175}Tm (Fig. 4.58)

The cross section is measured for the first time in this work. We obtained the cross section data at three points for the neutron energies. FENDL/A-2 is lower than the present results.

3.59 ^{176}Yb(n, α)^{173}Er (Fig. 4.59)

Previously only one data is reported by Antov et al. [75] The data is consistent with our data. FENDL/A-2 agrees well with our data.

3.60 ^{180}Hf(n, p)^{180}Lu (Fig. 4.60)

No previous experimental data existed. Significant deviations among ENDF/B-VI, JENDL-3 and FENDL/A-2 evaluation are seen. All of the evaluations are not consistent with our data.

4. Systematics of the reaction cross sections

In this chapter, we discuss the systematics of the (n, p), (n, α) and (n, nα) reactons based on the present experimental data.

As for the (n, p) and (n, α) reactions, considerable many different systematcs, including the empirical formulae, have been proposed. Nevertheless, the systematics proposed previously by our group[8, 9] has been unique because partial excitation functions in the neutron energy region between 13.4 and 15.0 MeV can be estimated by using the empirical formula we proposed. (A brief summary of our systematics was given in an Appendix.) The empirical formulae were deduced based on our experimental data. Some of the experimental data reported here were already referred for deducing the systematics; the referred data were the ^{57}Fe(n, p)^{57}Mn, ^{76}Ge(n, p)^{75m}Ge, ^{100}Ru(n, p)^{100}Tc and ^{180}Hf(n, p)^{180}Lu reactions. The empirical formulae, however, have not been validated yet thoroughly for the target nuclei around lanthanide isotopes. In the present data, (n, p) and (n, α) reactions for the target nuclei around lanthanide isotopes were included. By comparing with the experimental data, the empirical formulae can be validated for the target nuclei around lanthanide isotopes.

For the (n, p) reactions, the experimental data for the ^{111}Cd(n, p)$^{111m+g}$Ag, ^{139}La(n, p)^{139}Ba, ^{140}Ce(n, p)^{140}La, ^{141}Pr(n, p)^{141}Ce, ^{145}Nd(n, p)^{145}Pr, ^{146}Nd(n, p)^{146}Pr, ^{162}Dy(n, p)^{162}Tb, ^{164}Dy(n, p)^{164}Tb and ^{167}Er(n, p)^{167}Ho reactions were compared with the calculated partial excitation functions. In Fig. 5.1, the present experimental results and the estimated partial excitation functions are plotted. Though, for the ^{167}Er(n,p)^{167}Ho reaction, the estimated excitation function deviated from the experimental data by about 1 mb in the region from 13.4 and 14.7 MeV, the agreement for other reactions are satisfactory. Therefore it is demomstrated that the empirical formulae for the (n,p) reaction are effective for the target nuclei around lanthanide isotopes.

As for the (n,α) reactions, we employed the following data to validate the empirical formulae; ^{144}Nd(n,α)^{141}Ce, ^{148}Nd(n, α)^{145}Ce, ^{144}Sm(n, α)$^{141m+g}$Ce, ^{162}Dy(n, α)^{159}Gd, ^{164}Dy(n, α)^{161}Gd and ^{176}Yb(n, α)^{173}Er. The present experimental results and the estimated partial excitation functions are plotted in Fig.5.2. The calculated curves for the ^{144}Nd(n, α)^{141}Ce, ^{148}Nd(n, α)^{145}Ce, ^{144}Sm(n, α)$^{141m+g}$Nd and ^{164}Dy(n, α)^{161}Gd reactions dose not agree with the experimental data. The disagreement implies that the proposed empirical formulas should be improved to obtain a better agreement.

For the (n, nα) reactions, there has been no effective systematics proposed. The reaction with charged particle emission as (n, p), (n, α), etc., in general, have a trend that the cross section value decrease as a function of (N-Z)/A, where N, Z and A are neutron, proton and mass number of target nuclei for the reaction. In Fig. 5.3, the present data of the (n, nα) reactions are plotted as a function of (N-Z)/A. (The data for the ^{92}Mo(n, nα)^{88}Zr reaction were taken from Ref. 85.) In addition, as a trial, the (n, nα) cross section data are plotted as a function of the threshold energy in Fig. 5.4. In the figures, however, no distinct correlation like other (n, charged particle reaction) can be seen. At present, we conclude that more experimental data and further discussion will be required to establish the systematics of the (n, nα) reaction.

5. Conclusion

Neutron activation cross sections have been measured in the energy range between 13.3 and14.9 MeV for 60 reactions, which include 32 reactions mainly for the lanthanide isotopes, 19 reactions for the short-lived products and 9 reactions of (n, nα) reactions. The cross section measurement has been done using the intense neutron source (FNS) facility.

The cross section of the following reactions were obtained for the first time in this work: ^{47}Ti(n, np)^{46m}Sc, ^{96}Zr(n, np)^{95}Y, ^{120}Sn(n, np)^{119g}In, ^{154}Gd(n, p)^{154m}Eu, ^{164}Dy(n, np)^{163}Tb, ^{176}Yb(n, np)^{175m}Tm, ^{180}Hf(n, p)^{180}Lu, ^{87}Rb(n, nα)^{83}Br, ^{91}Zr(n, nα)^{87m}Sr, ^{96}Zr(n, nα)^{92}Sr and ^{109}Ag(n, nα)^{105}Rh. For the following reactions, where only one point data had been reported previously, the present experimental data covers the relatively wide energy range with multiple data points: ^{46}Ti(n, p)^{46m}Sc, ^{76}Ge(n, p)^{76}Ga, ^{84}Sr(n, p)^{84m}Rb, ^{100}Ru(n, p)^{100}Tc, ^{132}Ba(n, 2n)^{131m}Ba, ^{137}Ba(n, n')^{137m}Ba, ^{141}Pr(n, p)^{141}Ce, ^{144}Nd(n, α)^{141}Ce, ^{148}Nd(n, p)^{148}Pr, ^{148}Nd(n, α)^{145}Ce, ^{144}Sm(n, α)$^{141m+g}$Nd, ^{154}Gd(n, 2n)^{153}Gd, ^{162}Dy(n, α)^{159}Gd, ^{164}Dy(n, p)^{164}Tb, ^{167}Er(n, p)^{167}Ho, ^{168}Ho(n, p)^{168}Ho, ^{71}Ga(n, nα)^{67}Cu and ^{93}Nb(n, nα)^{89m}Y. These results provide new input data for consideration in the next versions of evaluated nuclear data files and for updating the activation cross section data library.

The present data were compared with the evaluated nuclear data of ENDF-B/VI and JENDL-3 along with FENDL/A-2 library data. As a result of the comparison, we recommended the reevaluation for some reactions.

The present experimental cross section data of the (n, p) and (n, α) reactions for lanthanide isotopes were compared with the excitation curve calculated using the empirical formula that we proposed in order to validate them in the lanthanide region. For the (n, p) reactions, the deduced curves were in good agreement with the experimental data. However, for (n, α) reactions, the deduced curves of the ^{144}Nd(n,α)^{141}Ce, ^{148}Nd(n,α)^{145}Ce, ^{144}Sm(n,α)$^{141m+g}$Nd and ^{164}Dy(n,α)^{161}Gd reactions did not agree with the experimental data. This implies that the proposed empirical formulas should be improved to obtain a better agreement. For the (n, nα) reaction, no distinct trends could be found using the present data. More experimental data accumulation and further discussion are required to establish the more realistic systematics of the (n, nα) reactions.

Acknowledgements

The authors gratefully acknowledge the contributions by students of Nagoya University in a part of measurements. They are indebted to Messrs. C. Kutsukake, S. Tanaka, Y. Abe and M. Seki for operation of the FNS accelerator.

This work was done in a part under the Cooperative Research Program between Japan Atomic Energy Research Institute and Nagoya University.

References

1) "Evaluated Nuclear Data File, Section B, Version VI, Revision 4 (ENDF/B-VI, Rev. 4)" , National Nuclear Data Center, Brookhaven National Laboratory (1998).
2) Nakagawa T., et al.: J. Nucl. Sci. Technol., 32, 1259 (1995).
3) Paschenko A. B.: "Summary Report for IAEA Consultants' Meeting on Selection of Evaluations for the FENDL/A-2 Activation Cross Section Library", INDC(NDS)-341, International Atomic Energy Agency (1996).
4) Ikeda Y., et al.: "Activation Cross Section Measurements for Fusion Reactor Structural Materials at Neutron Energy from 13.3 to 15.0 MeV Using FNS Facility", JAERI 1312 (1988)
5) Konno C., et al.: "Activation Cross Section Measurement at Neutron Energy from 13.3 to 14.9 MeV Using the FNS Facility", JAERI 1329 (1993).
6) Ikeda Y., et al.: J. Nucl. Sci. Technol., 30, 870 (1993).
7) Ikeda Y., et al.: J. Nucl. Sci. Technol., 30, 967 (1993).
8) Kasugai Y., et al.: Ann. Nucl. Energy, 23, 1429 (1996).
9) Kasugai Y., et al.: Ann. Nucl. Energy, 25, 421 (1998).
10) Firestone R. B.: "Table of Isotopes", 8th Edition, 1998 Updated, John Wiley & Sons, Inc. New York (1998).
11) Nakagawa M., Mori T.: "MORSE-DD; A Monte Carlo Code Using Multi-Grope Double Differential Form Cross Section", JAERI-M 84-126 (1984).
12) Satoh Y., et al.: "Proc. of the 1994 Symposium on Nuclear Data", JAERI-Conf 95-008, p. 189 (1995).
13) Schantl: EXFORE 21846.017 (1970).
14) Viennot M., et al.: Nucl. Sci. Eng., 108, 289 (1991).
15) Ribansky I., et al.: J. Phys., G9, 1537 (1983).
16) Molla N. I. and Qaim S. M.: Nucl. Phys., A283, 269 (1977).
17) Qaim S. M, Nucl. Phys., A458, 237 (1986).
18) Pepelnik R., et al.: Conf. on Nuclear Data for Basic and Applied Sci., Santa Fe (1985).
19) Viennot M., et al.: International Conference on Nuclear Data for Science and Technology, Antwerp, p. 406 (1982).
20) Singh J.: Trans. of American Nuclear Soc., 15, 147 (1972)
21) Ikeda Y., et al.: International Conference on Nuclear Data for Science and Technology, Gatlinburg, Tennessee, p. 944 (1994).
22) Santry D.C., et al.: Can. J. Phys., 44, 1183(1965).
23) Kasugai Y., et al.: Ann. Nucl. Energy, 25, 23 (1998).
24) Kielan D. and Marcinkowski A.: Z. Phys., 352, 137 (1995).
25) Ghorai S. K., et al.: Ann. Nucl. Energy, 22, 11 (1995).
26) Bramlitt E.T., et al.: Phys. Rev., 131, 2649 (1963).
27) Hoang H. M., et al.: Z. Phys., 342, 283 (1992).
28) Rieppo R., et al.: J. Inorg. Nucl. Chem., 38, 1927 (1976).
29) Okumura S., et al.: Nucl Phys., A93, 74 (1967).
30) Bormann M., et al.: EXFORE 21503.003 (1967).
31) Qaim S.M., et al.: EUR-5182E, 939 (1974).
32) Kim, Y.S., et al.: KNS, 18, (2), 92 (1986).
33) Prasad R. and Sarker D. C.: Nuovo Cimento, A3, 467 (1971).
34) Bayhurst B.P. and Prestwood R. J.: Inorg. Nucl. Chem., 23, 173 (1961).
35) Grallert A., et al.: EXFORE 31496.046 (1993).

36) Pepelnik R., et al.: EXFORE 21976.035 (1985).
37) Yu Y. W. and Gardner D.G.: Nucl. Phys., A98, 451 (1967).
38) Levkovskiy V. N.: JET, 18, 213 (1966).
39) Rurarz E., et al.: Acta. Phys. Polonica, B3, 637 (1972).
40) Pepelnik R., et al.: EXFORE 21976.047 (1985).
41) Rurarz E., et al.: Acta. Phys. Polonica, B1, 415 (1970).
42) Hannapel L, et al.: Nucl. Instrum. Methods, 167,289 (1979).
43) Achour M., et al.: EXFORE 31410.002 (1986).
44) Woo T. W., et al.: EXFORE 10806.012 (1979).
45) Qaim S. M., et al.: Inorg. Nucl. Chem., 35, 19 (1973).
46) Bormann M., et al.: Nucl. Phys., A115, 309 (1968).
47) Qaim S. M., et al.: Nucl. Phys., A224, 319 (1974).
48) Eapen P. K., et al.: Inorg. Nucl. Chem., 37, 1121 (1975).
49) Cuzzocrea P., et al.: Nuovo Cimento, B52, 476 (1967).
50) Teng Dan, et al.: Chinese J. of Nucl. Phys., 7, 307 (1985).
51) Bormann M., et al.: EXFORE 20900.005 (1966).
52) Havlik E., et al.: Acta. Phys. Austrica, A34, 209 (1971).
53) Rayburn L. A., et al.: Bull. of the American Physical Soc., 8, 60 (1963).
54) Koehler D. R., et al.: EXFORE 11785.006 (1962).
55) Sigg R. A., et al.: Inorg. Nucl. Chem., 37, 631 (1975).
56) Valkonen M., et al.: EXFORE 20673.028 (1976).
57) Araminowicz J.,et al.: EXFORE 30264.040 (1973).
58) Jong Do, et al.: J. Phys., G10, 91 (1984).
59) Frehaut J., et al.: EXFORE 20416.029 (1980).
60) Kumabe I., et al.: J. Nucl. Sci. Technol., 14, 319 (1977).
61) Qaim S. M. et al.: Nucl. Phys., 224, 319 (1974).
62) Grallert A., et al.: INDC(NDS)-286,131 (1993).
63) Gmuca S., et al.: Acta. Phys. Slovaca, 33, 9 (1983).
64) Prasad P. R., et al.: Nucl. Phys., A125, 57 (1969).
65) Qaim S. M., et al.: Radiochem. Radioanal. Lett., 25, 335 (1976).
66) Bari A.: J. Radioanal. Chem., 75, 189 (1982).
67) Majeddin A. D., et al.: EXFORE 31481.011 (1997).
68) Wille R.G., et al.: Phys. Rev., 118, 242 (1960).
69) Murahira S. et al.: INDC(JPN)-175/U, 171(1995).
70) Alford W. L., et al.: Bull. of the American Physical Soc., 10, 260 (1965).
71) Weigel H. et al.: Radiochim. Acta., 22,11 (1975).
72) Dilg W. et al.: Nucl. Phys, A118, 9 (1968).
73) Bari A.: EXFORE 10431.055 (1971).
74) Paul E. B., et al.: Can. J. Phys., 31, 267 (1953).
75) Antov A., et al.: Bulgarian J. Phys., 10, 601 (1983).
76) Qaim S. M. et al.: EXFORE 20933.011 (1974).
77) Coleman R. F. et al.: Proc. Physical Soc., London, 73, 215 (1959).
78) Havlik, E.: Acta Phys. Austrica, 34, 209 (1971).
79) Khurana C. S., et al.: Nucl. Phys., 69, 153 (1965).
80) Wille R. G., et al.: Phys. Rev., 118, 242 (1960).
81) Oms, L.A., et al.: Bull. American Physical Soc., 13, 1699 (1968).
82) Liljavirta H., et al.: Physica Scripta, 18, 75 (1978).

83) Lakshmana das N., et al.: Nuovo Cimento, A48, 500 (1978).
84) Chasteler R. M., et al.: Phys. Rev., C42, 1796 (1990).
85) Katoh T, et al.: JAERI-M, 89-083 (1989). [in Japanese]

Table 1 List of measured reactions and associated decay data

Target Nucleus	Natural Abundance	Reaction**	Product	Half-life	Gamma-ray Energy [keV]	Branching Ratio (%)	Q-value*** [MeV]
$^{11}B^{*}$	80.1	(n, p)	^{11}Be	13.8 s	2124.5	35.5±1.8	-10.72
^{26}Mg	11.01	(n, p)	^{26}Na	1.07 s	1808.6	99.0±0.4	-8.53
^{30}Si	3.10	(n, p)	^{30}Al	3.60 s	2235.2	65±1	-7.76
$^{34}S^{*}$	4.21	(n, p)	^{34}P	12.4 s	2127.5	15±2	-4.59
$^{46}Ti^{*}$	8.0	(n, p)	^{46m}Sc	18.75 s	142.6	62±2	-1.58
$^{47}Ti^{*}$	7.3	(n, np)	^{46m}Sc	18.75 s	142.6	62±2	-10.46
^{51}V	99.750	(n, nα)	^{47}Sc	3.345 d	159.4	67.9±1.5	-10.29
$^{57}Fe^{*}$	2.2	(n, p)	^{57}Mn	87.2 s	122.1	14±5	-1.91
^{63}Cu	69.17	(n, 2n)	^{62}Cu	9.74 m	511.0	195.6	-10.85
^{65}Cu	30.83	(n, nα)	^{61}Co	1.650 h	67.4	84.7±0.4	-6.79
$^{68}Zn^{*}$	18.8	(n, p)	^{68m}Cu	3.75 m	525.9	70.6±0.8	-3.66
$^{71}Ga^{*}$	39.9	(n, nα)	^{67}Cu	61.83 h	184.6	48.7±0.3	-5.26
$^{74}Ge^{*}$	36.5	(n, p)	$^{74m+g}Ga$	8.12 m	595.9	91.4±0.4	-4.58
$^{76}Ge^{*}$	7.8	(n, p)	^{76}Ga	32.6 s	562.9	66±3	-5.99
$^{76}Ge^{*}$	7.8	(n, 2n)	^{75m}Ge	47.7 s	139.7	38.8±0.8	-9.43
$^{76}Ge^{*}$	7.8	(n, nα)	^{72}Zn	46.5 h	144.7	82.9±0.2	-7.50
^{87}Rb	27.835	(n, nα)	^{83}Br	2.40 h	529.6	1.2±0.5	-8.01
$^{84}Sr^{*}$	0.56	(n, p)	^{84m}Rb	20.26 m	248.0	60.2±0.8	-0.11
$^{91}Zr^{*}$	11.22	(n, nα)	^{87m}Sr	2.803 h	388.5	82.1±0.5	-5.44
$^{96}Zr^{*}$	2.80	(n, np)	^{95}Y	10.3 m	954.0	15.8±0.7	-11.52
$^{96}Zr^{*}$	2.80	(n, nα)	^{92}Sr	2.71 h	1383.9	90.0±5.7	-4.91
^{93}Nb	100	(n, nα)	^{89m}Y	16.06 s	909.1	99.14±0.03	-1.93
$^{100}Ru^{*}$	12.6	(n, p)	^{100}Tc	15.8 s	539.5	7.0±1.2	-2.42
^{109}Ag	48.461	(n, nα)	$^{105m+g}Rh$	35.36 h	318.9	19.2±0.4	-3.29
$^{111}Cd^{*}$	12.80	(n, p)	$^{111m+g}Ag$	7.45 d	342.1	6.7±0.3	-0.25
$^{113}Cd^{*}$	12.22	(n, p)	$^{113m+g}Ag$	5.37 h	298.6	10	-1.23
^{120}Sn	32.59	(n, np)	^{119g}In	2.4 m	763.1	99.2±0.2	-1.55
$^{132}Ba^{*}$	0.101	(n, 2n)	^{131m}Ba	14.6 m	108.1	55.4	-9.08
$^{137}Ba^{*}$	11.23	(n, n)	^{137m}Ba	2.552 m	661.7	90.11±0.06	-6.38
^{139}La	99.91	(n, p)	^{139}Ba	83.06 m	165.9	24±4	-1.53
^{139}La	99.91	(n, t)	^{137m}Ba	2.552 m	661.7	90.11±0.06	-6.38
^{140}Ce	88.48	(n, 2n)	^{139m}Ce	54.8 s	754.3	92.45	-9.19
^{140}Ce	88.48	(n, 2n)	$^{139m+g}Ce$	137.640 d	165.9	79.899±0.001	-9.19
^{140}Ce	88.48	(n, p)	^{140}La	1.6781 d	1596.2	95.40±0.08	-2.98
^{140}Ce	88.48	(n, α)	^{137m}Ba	2.552 m	661.7	90.11±0.06	5.30
^{142}Ce	11.08	(n, 2n)	^{141}Ce	32.501 d	145.4	48.2±0.3	-7.17
^{141}Pr	100	(n, 2n)	^{140}Pr	3.39 m	306.9	0.151±0.019	-9.40
^{141}Pr	100	(n, p)	^{141}Ce	32.501 d	145.4	48.2±0.3	0.20
^{142}Nd	27.13	(n, 2n)	$^{141m+g}Nd$	2.49 h	1126.9	0.80±0.03	-9.82
$^{144}Nd^{*}$	23.80	(n, α)	^{141}Ce	32.501 d	145.4	48.2±0.3	7.34
$^{145}Nd^{*}$	8.30	(n, p)	^{145}Pr	5.984 h	748.3	0.525±0.009	-1.02
^{146}Nd	17.19	(n, p)	^{146}Pr	24.15 m	453.9	48±3	-3.38
$^{148}Nd^{*}$	5.76	(n, p)	^{148m}Pr	2.0 m	450.6	50.0±0.05	-4.18
$^{148}Nd^{*}$	5.76	(n, α)	^{145}Ce	3.01 m	724.3	99±7	5.33
$^{150}Nd^{*}$	5.64	(n, 2n)	^{149}Nd	1.73 h	211.3	25.9±1.4	-7.38

* Separated isotopes was used.

** (n,np) means (n,np)+(n,pn)+(n,d)

*** Q-value for the (n,np) reactions were calculated for (n,np) reactions. Q-value for the (n,d) reactions are calculated as follows: Q(n,d)=Q(n,np)+2.225 MeV, where Q-values of (n,np) and (n,d) are Q(n,d) and Q(n,np), respectively.

Table 1 List of measured reactions and associated decay data (continued)

Target Nucleus	Natural Abundance	Reaction**	Product	Half-life	Gamma-ray Energy [keV]	Branching Ratio (%)	Q-value*** [MeV]
$^{144}Sm^{*}$	3.1	(n, 2n)	^{143m}Sm	66 s	754.0	90±3	-10.52
$^{144}Sm^{*}$	3.1	(n, α)	$^{141m+g}Nd$	2.49 h	1126.9	0.80±0.03	0.23
$^{154}Gd^{*}$	2.18	(n, 2n)	^{153}Gd	241.6 d	103.2	21±4	-8.90
$^{154}Gd^{*}$	2.18	(n, p)	^{154m}Eu	46.3 m	100.9	27±4	-1.19
^{160}Gd	21.86	(n, 2n)	^{159}Gd	18.479 h	363.5	11±3	-7.45
$^{162}Dy^{*}$	25.5	(n, p)	^{162}Tb	7.60 m	260.1	80±5	-1.75
$^{162}Dy^{*}$	25.5	(n, α)	^{159}Gd	18.479 h	363.6	11±3	6.03
$^{164}Dy^{*}$	28.2	(n, p)	^{164}Tb	3.0 m	168.8	26±9	-3.08
$^{164}Dy^{*}$	28.2	(n, np)	^{163}Tb	19.5 m	351.1	26±3	-8.58
$^{164}Dy^{*}$	28.2	(n, α)	^{161}Gd	3.66 m	360.9	60.1±1.5	5.18
$^{167}Er^{*}$	22.95	(n, p)	^{167}Ho	3.1 h	346.5	56±12	-0.23
$^{168}Er^{*}$	26.8	(n, p)	$^{168m+g}Ho$	2.99 m	741.3	36.6±1.0	-1.94
$^{176}Yb^{*}$	12.7	(n, np)	^{175}Tm	15.2 m	514.9	65±7	-8.45
$^{176}Yb^{*}$	12.7	(n, α)	^{173}Er	1.4 m	199.2	48±2	5.92
$^{180}Hf^{*}$	35.1	(n, p)	^{180}Lu	5.7m	408.0	43±1	-2.32

* Separated isotopes was used.

** (n,np) means (n,np)+(n,pn)+(n,d)

*** Q-value for the (n,np) reactions were calculated for (n,np) reactions. Q-value for the (n,d) reactions are calculated as follows: Q(n,d)=Q(n,np)+2.225 MeV, where Q-values of (n,np) and (n,d) are Q(n,d) and Q(n,np), respectively.

Table 2 List of chemical properties, weights and abundance of samples

Target Nucleus	Chemical Form	Weight [mg]	Abundance [%]
^{11}B	B	200	^{10}Be: 0.05, ^{11}Be: 99.5,
^{26}Mg	Mg	80	Natural [^{24}Mg: 78.99 , ^{25}Mg: 10.00, ^{26}Mg: 11.01]
^{30}Si	Si	200	Natural [^{28}Si: 92.23 , ^{29}Si: 4.67, ^{30}Si: 3.10]
^{34}S	S	23	^{32}S: 5.53 , ^{33}S: 0.11, ^{34}S: 94.33, ^{36}S: 0.03
^{46}Ti	TiO_2	50	^{46}Ti: 81.20, ^{47}Ti: 2.10, ^{48}Ti: 14.50, ^{49}Ti: 1.10, ^{50}Ti: 1.10
^{47}Ti	TiO_2	50	^{46}Ti: 3.00, ^{47}Ti: 68.50, ^{48}Ti: 25.00, ^{49}Ti: 1.80, ^{50}Ti: 1.60
^{51}V	V	100	Natural [^{50}V: 0.250, ^{51}V: 99.750]
^{57}Fe	Fe	40	^{54}Fe: 0.12, ^{56}Fe: 6.52, ^{57}Fe: 93.31, ^{58}Fe: 0.05
^{63}Cu	Cu	350	Natural [^{63}Cu: 69.17, ^{65}Cu: 30.83]
^{65}Cu	Cu	350	Natural [^{63}Cu: 69.17, ^{65}Cu: 30.83]
^{68}Zn	ZnO	40	^{64}Zn: 0.32, ^{66}Zn: 0.21, ^{67}Zn: 0.10, ^{68}Zn: 99.36, ^{70}Zn: 0.01
^{71}Ga	Ga_2O_3	100	^{69}Ga: 0.41, ^{71}Ga: 99.59
^{74}Ge	GeO_2	40	^{70}Ge: 1.47, ^{72}Ge: 2.13, ^{73}Ge: 0.54, ^{74}Ge: 95.20, ^{76}Ge: 0.66
^{76}Ge	GeO_2	65	^{70}Ge: 1.30, ^{72}Ge: 2.00, ^{73}Ge: 0.63, ^{74}Ge: 3.25, ^{76}Ge: 92.82
^{87}Rb	RbCl	200	Natural [^{85}Rb: 72.165, ^{87}Rb: 27.835]
^{84}Sr	$SrCO_3$	10	^{84}Sr: 75.35, ^{86}Sr: 4.13, ^{87}Sr: 2.06, ^{88}Sr: 18.47
^{91}Zr	ZrO2	30	^{90}Zr: 3.24, ^{91}Zr: 94.59, ^{92}Zr: 1.63, ^{94}Zr: 0.46, ^{96}Zr: 0.08
^{96}Zr	ZrO_2	85	^{90}Zr: 1.54, ^{91}Zr: 0.40, ^{92}Zr: 0.73, ^{94}Zr: 1.70, ^{96}Zr: 95.63
^{93}Nb	Nb	200	Natural [^{93}Nb: 100]
^{100}Ru	Ru	40	^{96}Ru: 0.04, ^{98}Ru: 0.05, ^{99}Ru: 0.47, ^{100}Ru: 97.42, ^{101}Ru: 1.09, ^{102}Ru: 0.75 ^{104}Ru: 0.18
^{109}Ag	Ag	200	Natural [^{107}Ag: 51.839, ^{109}Ag: 48.161]
^{111}Cd	CdO	60	^{110}Cd: 0.63, ^{111}Cd: 96.44, ^{112}Cd: 1.82, ^{113}Cd: 0.43, ^{114}Cd: 0.59, ^{116}Cd: 0.10
^{113}Cd	CdO	60	^{110}Cd: 0.19, ^{111}Cd: 0.33, ^{112}Cd: 1.43, ^{113}Cd: 95.10, ^{114}Cd: 2.75, ^{116}Cd: 0.20
^{120}Sn	SnO_2	50	^{116}Sn: 0.13, ^{117}Sn: 0.11, ^{118}Sn: 0.61, ^{119}Sn: 0.66, ^{120}Sn: 98.05, ^{122}Sn: 0.34, ^{124}Sn: 0.10
^{132}Ba	$BaCO_3$	25	^{130}Ba: 0.10, ^{132}Ba: 8.20, ^{134}Ba: 10.80, ^{135}Ba: 11.00, ^{136}Ba: 8.60, ^{137}Ba: 9.60 ^{138}Ba: 51.70
^{137}Ba	$BaCO_3$	95	^{130}Ba: 0.02, ^{132}Ba: 0.02, ^{134}Ba: 0.06, ^{135}Ba: 0.23, ^{136}Ba: 1.55, ^{137}Ba: 64.04 ^{138}Ba: 34.12
^{139}La	La_2O_3	100	Natural (^{138}La: 0.09, ^{139}La: 99.91)
^{140}Ce	CeO_2	100	Natural (^{136}Ce: 0.19, ^{138}Ce: 0.25, ^{140}Ce: 88.48, ^{142}Ce: 11.08)
^{142}Ce	CeO_2	100	Natural (^{136}Ce: 0.19, ^{138}Ce: 0.25, ^{140}Ce: 88.48, ^{142}Ce: 11.08)
^{141}Pr	Pr_6O_{11}	100	Natural (^{141}Pr: 100)
^{142}Nd	Nd_2O_3	100	Natural (^{142}Nd: 27.13, ^{143}Nd: 12.18, ^{144}Nd: 23.80, ^{145}Nd: 8.30, ^{146}Nd: 17.19 ^{148}Nd: 5.76, ^{150}Nd: 5.64)
^{144}Nd	Nd_2O_3	45	^{142}Nd: 0.58, ^{143}Nd: 0.55, ^{144}Nd: 97.35, ^{145}Nd: 0.70, ^{146}Nd: 0.66, ^{148}Nd: 0.09 ^{150}Nd: 0.06
^{145}Nd	Nd_2O_3	50	^{142}Nd: 0.93, ^{143}Nd: 0.64, ^{144}Nd: 2.74, ^{145}Nd: 91.58, ^{146}Nd: 3.7, ^{148}Nd: 0.28 ^{150}Nd: 0.14
^{146}Nd	Nd_2O_3	100	Natural (^{142}Nd: 27.13, ^{143}Nd: 12.18, ^{144}Nd: 23.80, ^{145}Nd: 8.30, ^{146}Nd: 17.19, ^{148}Nd: 5.76, ^{150}Nd: 5.64)
^{148}Nd	Nd_2O_3	65	^{142}Nd: 1.25, ^{143}Nd: 0.6, ^{144}Nd: 1.27, ^{145}Nd: 0.59, ^{146}Nd: 2.17, ^{148}Nd: 93.11, ^{150}Nd: 1.03
^{150}Nd	Nd_2O_3	65	^{142}Nd: 1.45, ^{143}Nd: 1.02, ^{144}Nd: 1.50, ^{145}Nd: 0.92, ^{146}Nd: 1.52, ^{148}Nd: 1.07, ^{150}Nd: 92.53
^{144}Sm	Sm_2O_3	60	^{144}Sm: 85.91, ^{147}Sm: 3.88, ^{148}Sm: 2.18, ^{149}Sm: 2.19, ^{150}Sm: 1.02, ^{152}Sm: 2.80 ^{154}Sm: 2.02
^{154}Gd	Gd_2O_3	55	^{154}Gd: 98.27, ^{155}Gd: 1.18, ^{156}Gd: 0.29, ^{157}Gd: 0.11, ^{158}Gd: 0.1, ^{160}Gd: 0.05
^{160}Gd	Gd_2O_3	100	Natural (^{152}Gd: 0.20, ^{154}Gd: 2.18, ^{155}Gd: 14.80, ^{156}Gd: 20.47, ^{157}Gd: 15.65, ^{158}Gd: 24.84, ^{160}Gd: 21.86)

Table 2 List of chemical properties, weights and abundance of samples (continued)

Target Nucleus	Chemical Form	Weight [mg]	Abundance [%]
^{162}Dy	Dy_2O_3	50	^{158}Dy: 0.02, ^{160}Dy: 0.12, ^{161}Dy: 3.06, ^{162}Dy: 92.43, ^{163}Dy: 3.31, ^{164}Dy: 1.06
^{164}Dy	Dy_2O_3	55	^{161}Dy: 0.40, ^{162}Dy: 1.34, ^{163}Dy: 5.55, ^{164}Dy: 92.71
^{167}Er	Er_2O_3	60	^{164}Er: 0.05, ^{166}Er: 2.81, ^{167}Er: 91.77, ^{168}Er: 5.05, ^{170}Er: 0.32
^{168}Er	Er_2O_3	50	^{162}Er: 0.01, ^{164}Er: 0.05, ^{166}Er: 1.43, ^{167}Er: 2.47, ^{168}Er: 95.44, ^{170}Er: 0.61
^{176}Yb	Yb_2O_3	50	^{170}Yb: 0.05, ^{171}Yb: 0.28, ^{172}Yb: 0.51, ^{173}Yb: 0.53, ^{174}Yb: 1.59, ^{176}Yb: 97.04
^{180}Hf	HfO_2	50	^{174}Hf: 0.05, ^{176}Hf: 0.20, ^{177}Hf: 0.50, ^{178}Hf: 2.00, ^{179}Hf: 1.10, ^{180}Hf: 96.20

Table 3 Parameters needed to deduce the cross sections and their estimated errors

	Items	Estimated error(%)
1.	Statistics of gamma-ray counts	±0.3-50
2.	Detector efficiency	±2.0
3.	Sample weight	< ±0.1
4.	Irradiation, cooling and measuring time	< ±0.1
5.	Self-absorption of gamma-ray in a sample	< ±0.5
6.	Half-life (Decay constant)	< ±0.1-3
7.	Gamma-ray branching ratio	±0.1-20
8.	Correction factor for mean source position	< ±0.1
9.	Correction factor due to fluctuation of neutron flux during irradiation	< ±0.1
10.	Correction factor due to sum-peak of gamma-ray	< ±0.1
11.	Standard reaction cross section	±4.8

Table 4 Numerical values for the measured cross sections

$^{11}B(n, p)^{11}Be$

Neutron Energy [MeV]	Cross Section [mb]	Error [mb]
14.94	5.2	0.4

$^{26}Mg(n, p)^{26}Na$

Neutron Energy [MeV]	Cross Section [mb]	Error [mb]
14.94	31	4

$^{30}Si(n, p)^{30}Al$

Neutron Energy [MeV]	Cross Section [mb]	Error [mb]
14.94	34	5

$^{34}S(n, p)^{34}P$

Neutron Energy [MeV]	Cross Section [mb]	Error [mb]
14.94	100	22
14.68	88	19
14.37	88	20
14.02	90	20
13.68	82	20
13.36	88	22

$^{46}Ti(n, p)^{46m}Sc$

Neutron Energy [MeV]	Cross Section [mb]	Error [mb]
14.94	51	3
14.68	51	3
14.37	51	3
14.02	54	4
13.68	58	4
13.36	59	4

$^{47}Ti(n, np)^{46m}Sc$

Neutron Energy [MeV]	Cross Section [mb]	Error [mb]
14.94	10.6	0.9
14.68	7.6	0.7
14.37	5.0	0.6
13.68	2.8	0.6
13.36	1.8	0.4

$^{51}V(n, n\alpha)^{47}Sc$

Neutron Energy [MeV]	Cross Section [mb]	Error [mb]
14.94	0.048*	

* Upper limit

$^{57}Fe(n, p)^{57}Mn$

Neutron Energy [MeV]	Cross Section [mb]	Error [mb]
14.94	53	4
14.68	55	4
14.37	59	4
14.02	59	4
13.68	60	4
13.36	63	7

$^{63}Cu\ (n, 2n)\ ^{62}Cu$

Neutron Energy [MeV]	Cross Section [mb]	Error [mb]
14.94	518	22
14.68	464	20
14.37	430	18
14.02	370	16
13.68	350	15
13.36	299	13

$^{65}Cu(n, n\alpha)^{61}Co$

Neutron Energy [MeV]	Cross Section [mb]	Error [mb]
14.68	2.37	0.11
14.37	1.62	0.13
14.02	0.71	0.10

$^{68}Zn(n, p)^{68m}Cu$

Neutron Energy [MeV]	Cross Section [mb]	Error [mb]
14.94	6.3	0.3
14.68	4.9	0.4
14.37	5.0	0.4
14.02	3.9	0.4
13.68	4.3	0.4
13.36	3.5	0.4

$^{71}Ga(n, n\alpha)^{67}Cu$

Neutron Energy [MeV]	Cross Section [mb]	Error [mb]
14.94	3.29	0.30
14.68	2.66	0.24
14.37	1.49	0.19
14.02	1.37	0.18
13.68	0.91	0.08
13.36	0.86	0.19

$^{74}Ge(n, p)^{74m+g}Ga$

Neutron Energy [MeV]	Cross Section [mb]	Error [mb]
14.94	12.1	0.6
14.68	11.8	0.6
14.37	12.1	0.6
14.02	10.7	0.5
13.68	9.1	0.5
13.36	8.1	0.4

$^{76}Ge(n, p)^{76}Ga$

Neutron Energy [MeV]	Cross Section [mb]	Error [mb]
14.94	5.4	0.8
14.68	3.7	0.6
14.02	2.5	0.6
13.68	2.1	0.7
13.36	1.7	0.5

$^{76}Ge(n, 2n)^{75m}Ge$

Neutron Energy [MeV]	Cross Section [mb]	Error [mb]
14.94	960	50
14.68	910	50
14.37	830	40
14.02	790	40
13.68	800	40

$^{76}Ge(n, n\alpha)^{72}Zn$

Neutron Energy [MeV]	Cross Section [mb]	Error [mb]
14.94	0.011	0.003

$^{87}Rb(n, n\alpha)^{83}Br$

Neutron Energy [MeV]	Cross Section [mb]	Error [mb]
14.94	1.6	0.7

$^{84}Sr(n, p)^{84m}Rb$

Neutron Energy [MeV]	Cross Section [mb]	Error [mb]
14.68	31.5	1.9
14.37	33.0	1.2
14.02	35.9	1.5
13.68	34.7	1.6
13.36	39.3	1.9

$^{91}Zr(n, n\alpha)^{87m}Sr$

Neutron Energy [MeV]	Cross Section [mb]	Error [mb]
14.94	0.102	0.014
14.68	0.086	0.008
14.37	0.066	0.009

$^{96}Zr(n, np)^{95}Y$

Neutron Energy [MeV]	Cross Section [mb]	Error [mb]
14.94	0.52	0.21

$^{96}Zr(n, n\alpha)^{92}Sr$

Neutron Energy [MeV]	Cross Section [mb]	Error [mb]
14.94	0.047	0.007

$^{93}Nb(n, n\alpha)^{89m}Y$

Neutron Energy [MeV]	Cross Section [mb]	Error [mb]
14.94	2.4	0.5
14.69	2.1	0.4
14.37	1.4	0.3
14.02	1.2	0.3
13.68	0.8	0.3
13.36	0.9	0.3

$^{100}Ru(n, p)^{100}Tc$

Neutron Energy [MeV]	Cross Section [mb]	Error [mb]
14.94	35	8
14.68	33	8
14.37	26	7
14.02	18	6
13.68	22	8

$^{109}Ag(n, n\alpha)^{105m+g}Rh$

Neutron Energy [MeV]	Cross Section [mb]	Error [mb]
14.94	0.44	0.12

$^{111}Cd\ (n,p)^{111m+g}Ag$

Neutron Energy [MeV]	Cross Section [mb]	Error [mb]
14.94	21	7
14.37	18	3

$^{113}Cd(n, p)^{113m+g}Ag$

Neutron Energy [MeV]	Cross Section [mb]	Error [mb]
14.94	17	4
14.68	13	3
14.37	15	3
13.68	9	3

^{120}Sn (n, np)^{119g}In

Neutron Energy [MeV]	Cross Section [mb]	Error [mb]
14.94	0.121	0.019

$^{132}Ba(n, 2n)^{131m}Ba$

Neutron Energy [MeV]	Cross Section [mb]	Error [mb]
14.94	640	20
14.68	650	21
14.37	629	20
13.68	666	22

$^{137}Ba(n, n)^{137m}Ba$

Neutron Energy [MeV]	Cross Section [mb]	Error [mb]
14.94	225	27
14.68	192	27
14.37	342	29
14.02	180	27
13.68	229	28
13.36	211	27

$^{139}La(n ,p)^{139}Ba$

Neutron Energy [MeV]	Cross Section [mb]	Error [mb]
14.94	4.5	0.4
14.68	4.2	0.3
14.37	4.1	0.3
14.02	3.8	0.3
13.68	3.5	0.3
13.36	3.0	0.3

$^{139}La(n, t)^{137m}Ba$

Neutron Energy [MeV]	Cross Section [μb]	Error [μb]
14.94	62	23
14.68	16	11

$^{140}Ce(n, 2n)^{139m}Ce$

Neutron Energy [MeV]	Cross Section [mb]	Error [mb]
14.95	1020	40
14.37	840	40
14.02	870	40
13.68	770	30
13.36	640	30

$^{140}Ce(n, 2n)^{139m+g}Ce$

Neutron Energy [MeV]	Cross Section [mb]	Error [mb]
14.94	1690	120
14.68	1630	90
14.37	1690	90
14.02	1650	80
13.68	1580	100
13.36	1560	90

$^{140}Ce(n, p)^{140}La$

Neutron Energy [MeV]	Cross Section [mb]	Error [mb]
14.68	7.5	0.4
14.37	6.5	0.4
14.02	6.5	0.3
13.68	5.5	0.3
13.36	5.3	0.3

$^{140}Ce(n, \alpha)^{137m}Ba$

Neutron Energy [MeV]	Cross Section [mb]	Error [mb]
14.94	2.2	0.5
14.68	2.2	0.5
14.37	1.2	0.4
14.02	2.0	0.5
13.68	1.3	0.4
13.36	1.5	0.4

$^{142}Ce(n, 2n)^{141}Ce$

Neutron Energy [MeV]	Cross Section [mb]	Error [mb]
14.94	1750	90
14.68	1760	80
14.37	1880	90
14.02	1870	80
13.68	1840	80
13.36	1890	80

$^{141}Pr(n, 2n)^{140}Pr$

Neutron Energy [MeV]	Cross Section [mb]	Error [mb]
14.94	1420	60
14.68	1450	70
14.37	1360	60
14.02	1320	50
13.68	1300	60

$^{141}Pr(n, p)^{141}Ce$

Neutron Energy [MeV]	Cross Section [mb]	Error [mb]
14.94	12.0	0.8
14.68	11.5	0.9
14.37	9.9	1.0
13.68	9.7	0.8
13.36	9.0	0.7

$^{142}Nd(n, 2n)^{141m+g}Nd$

Neutron Energy [MeV]	Cross Section [mb]	Error [mb]
14.94	1740	120
14.68	1680	110
14.37	1690	100
14.02	1690	100
13.68	1580	100
13.36	1500	110

$^{144}Nd(n, \alpha)^{141}Ce$

Neutron Energy [MeV]	Cross Section [mb]	Error [mb]
14.94	3.6	0.5
14.68	2.2	0.4
14.37	1.3	0.6

$^{145}Nd(n, p)^{145}Pr$

Neutron Energy [MeV]	Cross Section [mb]	Error [mb]
14.94	7.3	1.2
13.36	3.5	2.0

$^{146}Nd(n, p)^{146}Pr$

Neutron Energy [MeV]	Cross Section [mb]	Error [mb]
14.94	7.6	1.4
14.68	5.2	1.0

$^{148}Nd(n, p)^{148m}Pr$

Neutron Energy [MeV]	Cross Section [mb]	Error [mb]
14.94	2.2	0.3
14.68	2.0	0.3
14.37	2.0	0.3
14.02	1.4	0.2
13.68	0.8	0.2
13.36	0.7	0.2

$^{148}Nd(n, \alpha)^{145}Ce$

Neutron Energy [MeV]	Cross Section [mb]	Error [mb]
14.94	2.7	0.5
14.68	2.3	0.5
14.37	2.9	0.6
14.02	1.9	0.4
13.68	1.4	0.4
13.36	1.5	0.3

$^{150}Nd(n, 2n)^{149}Nd$

Neutron Energy [MeV]	Cross Section [mb]	Error [mb]
14.94	1430	100
14.68	1520	100
14.37	1690	110
14.02	1720	110
13.68	1790	120
13.36	1790	120

$^{144}Sm(n,2n)^{143m}Sm$

Neutron Energy [MeV]	Cross Section [mb]	Error [mb]
14.94	608	20
14.68	592	20
14.37	526	17
14.02	457	16
13.68	378	13
13.36	352	12

$^{144}Sm(n, \alpha)^{141m+g}Nd$

Neutron Energy [MeV]	Cross Section [mb]	Error [mb]
14.94	12.6	1.0
14.68	14.3	1.1
14.02	11.5	0.9

$^{154}Gd(n, 2n)^{153}Gd$

Neutron Energy [MeV]	Cross Section [mb]	Error [mb]
14.94	2140	210
14.37	2110	180
13.68	2170	200

$^{154}Gd(n, p)^{154m}Eu$

Neutron Energy [MeV]	Cross Section [mb]	Error [mb]
14.94	0.13	0.05

$^{160}Gd(n, 2n)^{159}Gd$

Neutron Energy [MeV]	Cross Section [mb]	Error [mb]
14.94	2000	500
14.68	2100	500
14.37	2100	500
14.02	2000	500
13.68	2200	500
13.36	1900	500

$^{162}Dy(n, p)^{162}Tb$

Neutron Energy [MeV]	Cross Section [mb]	Error [mb]
14.94	4.2	0.4
14.68	4.4	0.4
14.37	3.4	0.3
14.02	2.9	0.3
13.68	2.2	0.2
13.36	1.8	0.2

$^{162}Dy(n, \alpha)^{159}Gd$

Neutron Energy [MeV]	Cross Section [mb]	Error [mb]
14.94	1.2	0.5
14.68	1.8	0.8
13.68	1.3	0.6

$^{164}Dy(n, p)^{164}Tb$

Neutron Energy [MeV]	Cross Section [mb]	Error [mb]
14.94	2.8	0.6
14.68	2.1	1.0
14.02	2.1	0.5

$^{164}Dy(n, np)^{163}Tb$

Neutron Energy [MeV]	Cross Section [mb]	Error [mb]
14.94	0.7	0.3
14.68	0.7	0.3
14.37	0.3	0.2
14.02	0.5	0.2

$^{164}Dy(n, \alpha)^{161}Gd$

Neutron Energy [MeV]	Cross Section [mb]	Error [mb]
14.94	0.60	0.14

$^{167}Er(n, p)^{167}Ho$

Neutron Energy [MeV]	Cross Section [mb]	Error [mb]
14.94	5.0	1.1
14.68	2.8	0.6
14.37	2.6	0.6
14.02	1.7	0.4
13.36	1.5	0.4

$^{168}Er(n, p)^{168m+g}Ho$

Neutron Energy [MeV]	Cross Section [mb]	Error [mb]
14.94	3.5	0.7
14.68	4.2	0.8
14.37	3.3	0.7
14.02	2.3	0.5
13.68	2.8	0.5
13.36	2.2	0.4

$^{176}Yb(n, np)^{175}Tm$

Neutron Energy [MeV]	Cross Section [mb]	Error [mb]
14.94	0.34	0.11
14.68	0.27	0.09
14.37	0.16	0.06

$^{176}Yb(n, \alpha)^{173}Er$

Neutron Energy [MeV]	Cross Section [mb]	Error [mb]
14.94	1.1	0.3
14.02	0.8	0.3

$^{180}Hf(n, p)^{180}Lu$

Neutron Energy [MeV]	Cross Section [mb]	Error [mb]
14.94	3.2	0.6
14.68	2.5	0.5
14.37	2.1	0.4
14.02	2.0	0.4
13.68	1.4	0.3
13.36	0.9	0.2

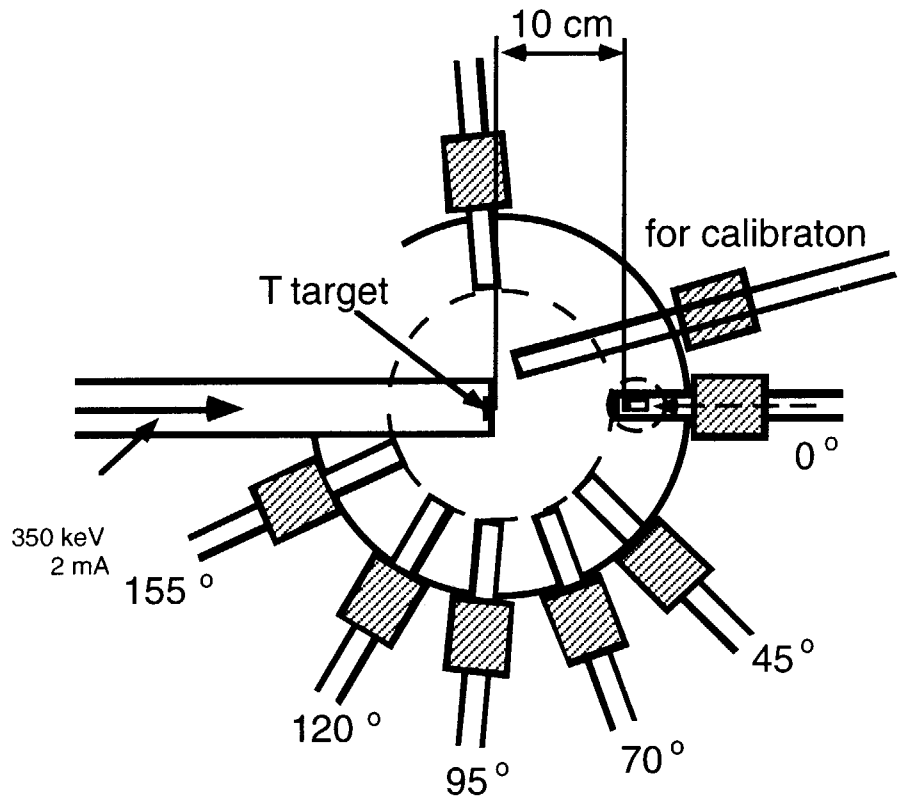

Fig. 1 A schematic drawing of typical irradiation setting (up-view).

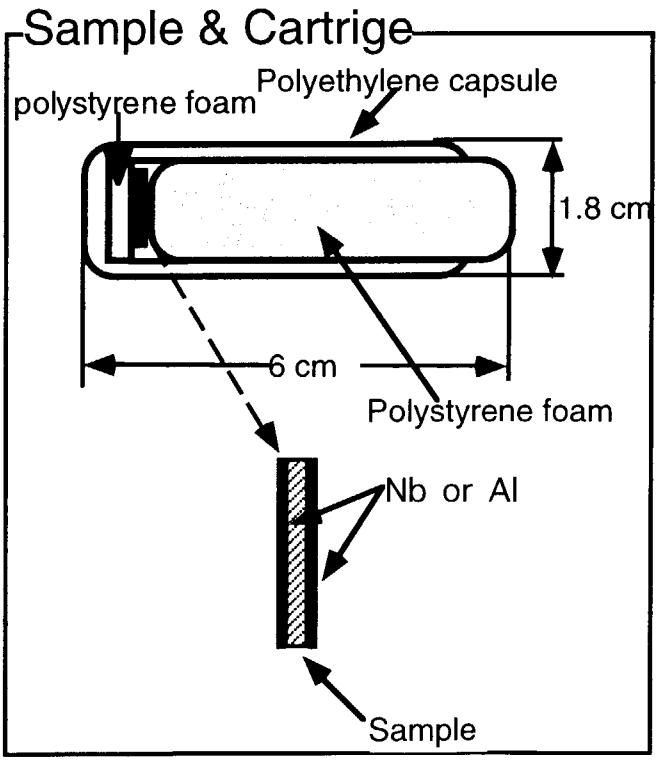

Fig. 2 A schematic drawing of the sample and the cartridge.

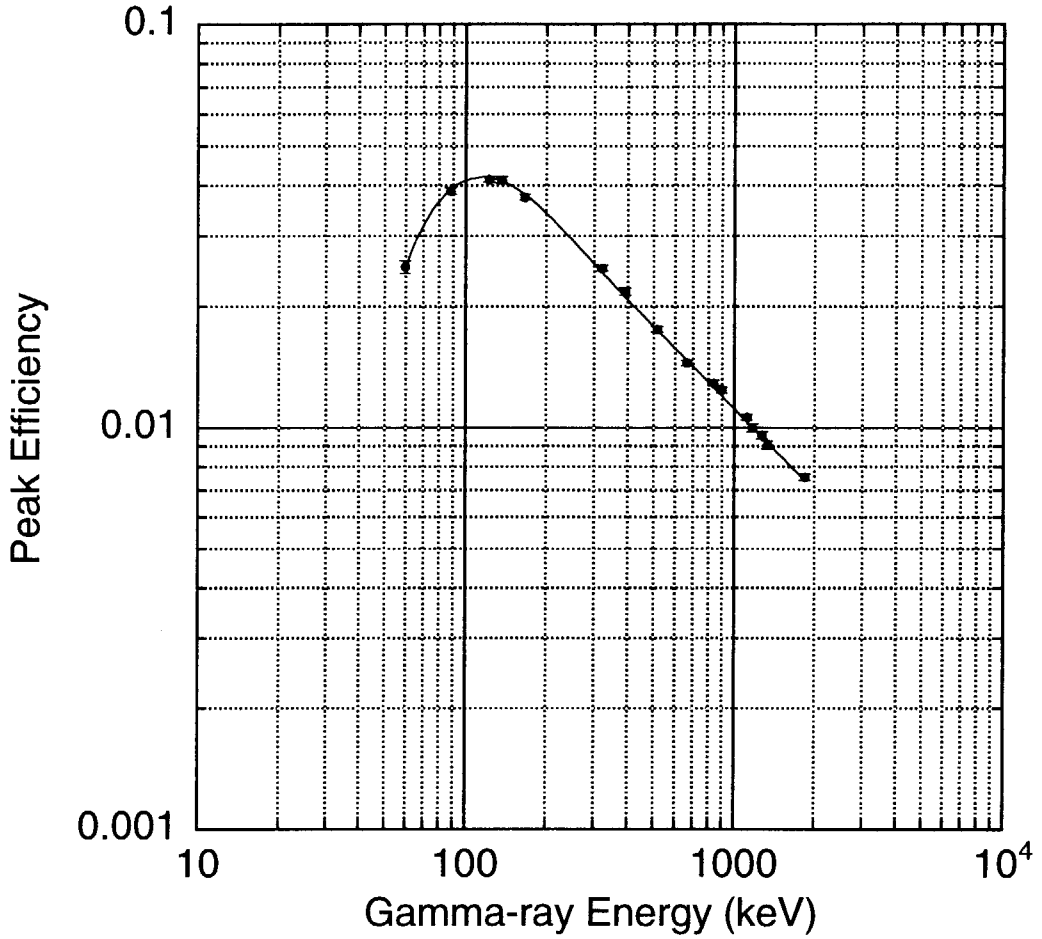

Fig. 3 Efficiency curve of the 75% HPGe detector. The dots show the data measured by using standard gamma-ray sources and the line show the fitting function.

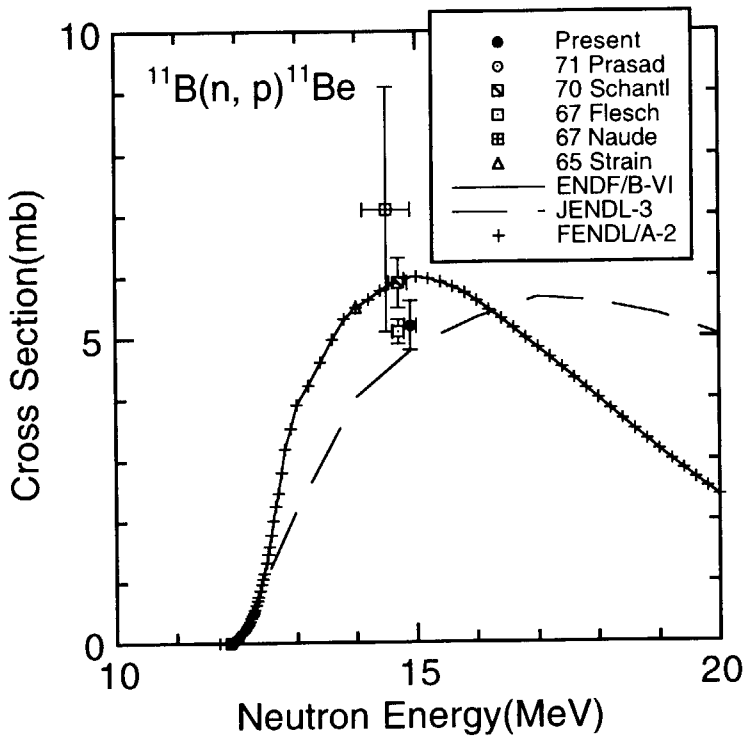

Fig. 4.1 Cross section data for ^{11}B(n, p)^{11}Be.

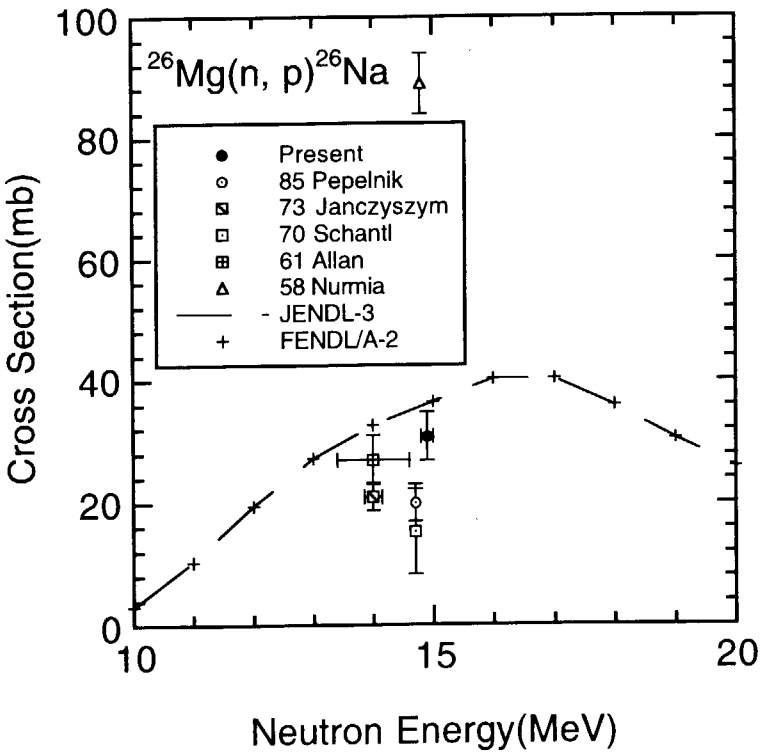

Fig. 4.2 Cross section data for ^{26}Mg(n, p)^{26}Na.

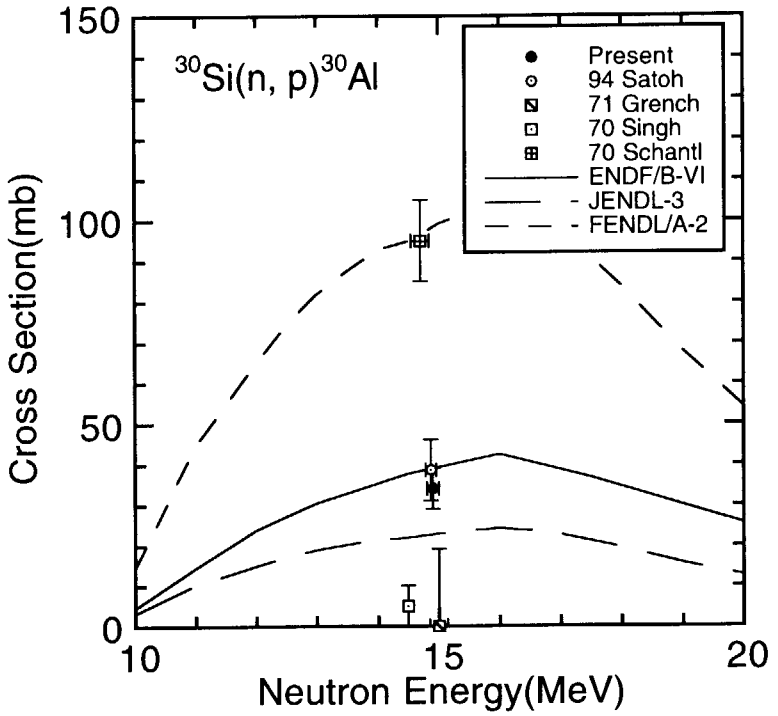

Fig. 4.3 Cross section data for ^{30}Si(n, p)^{30}Al.

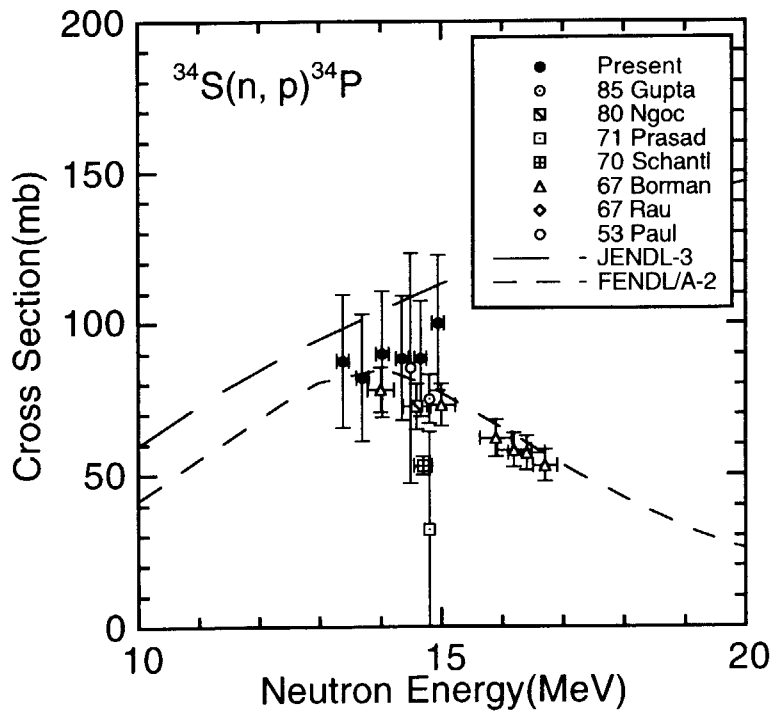

Fig. 4.4 Cross section data for ^{34}S(n, p)^{34}P.

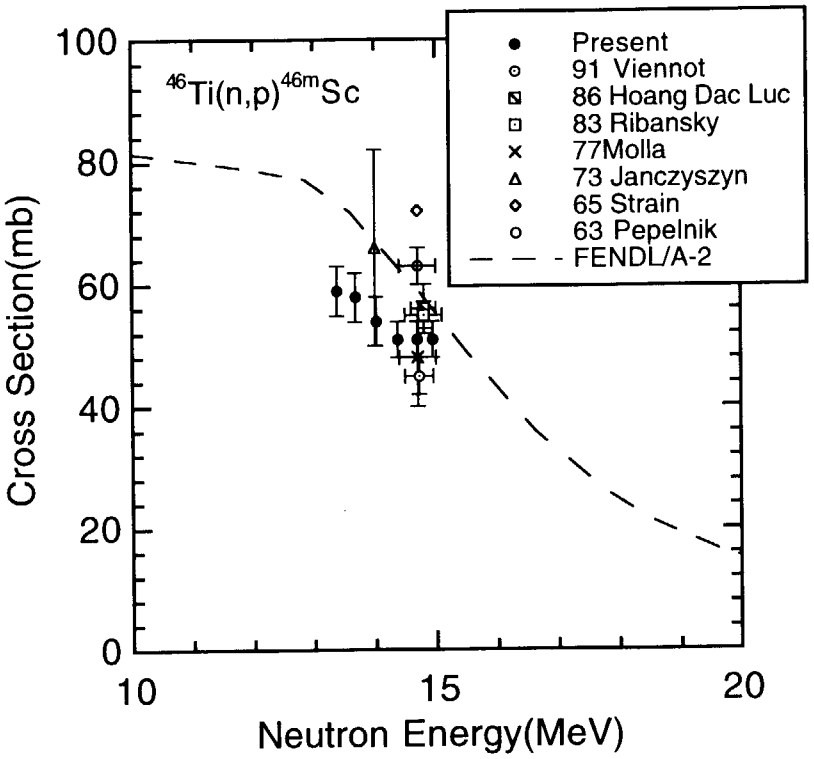

Fig. 4.5 Cross section data for ^{46}Ti(n,p)^{46m}Sc.

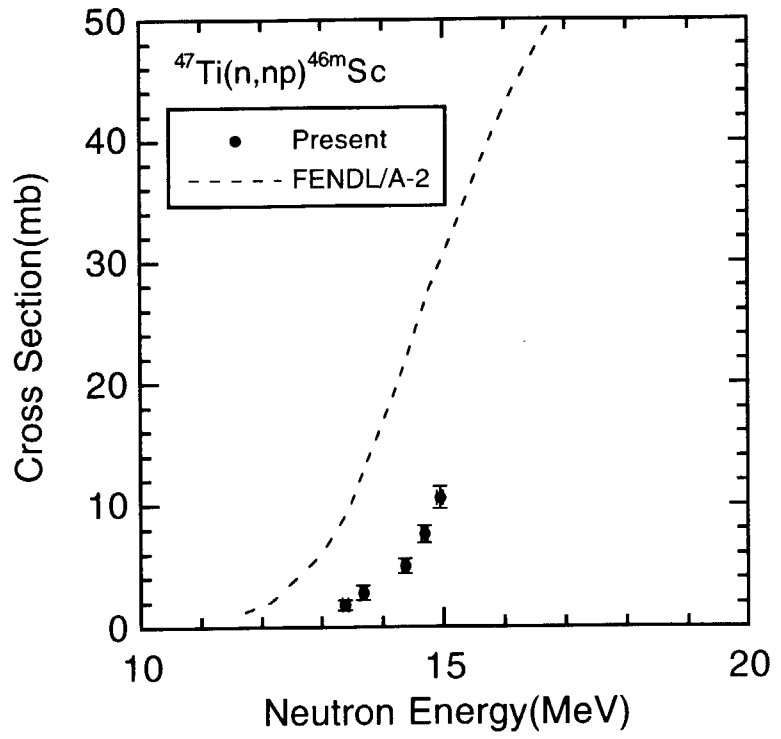

Fig. 4.6 Cross section data for ^{47}Ti(n,np)^{46m}Sc

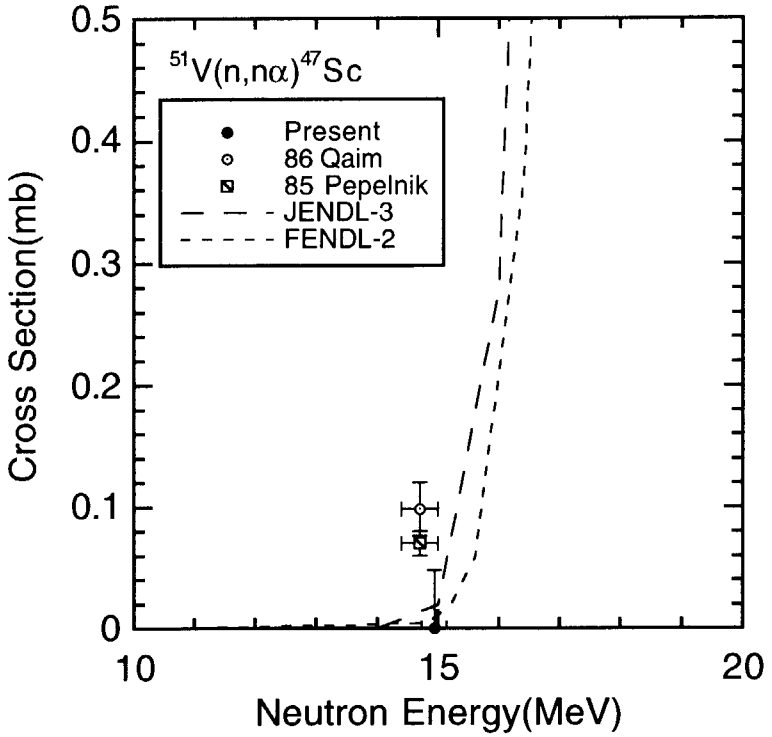

Fig. 4.7 Cross section data for ^{51}V(n, nα)^{47}Sc

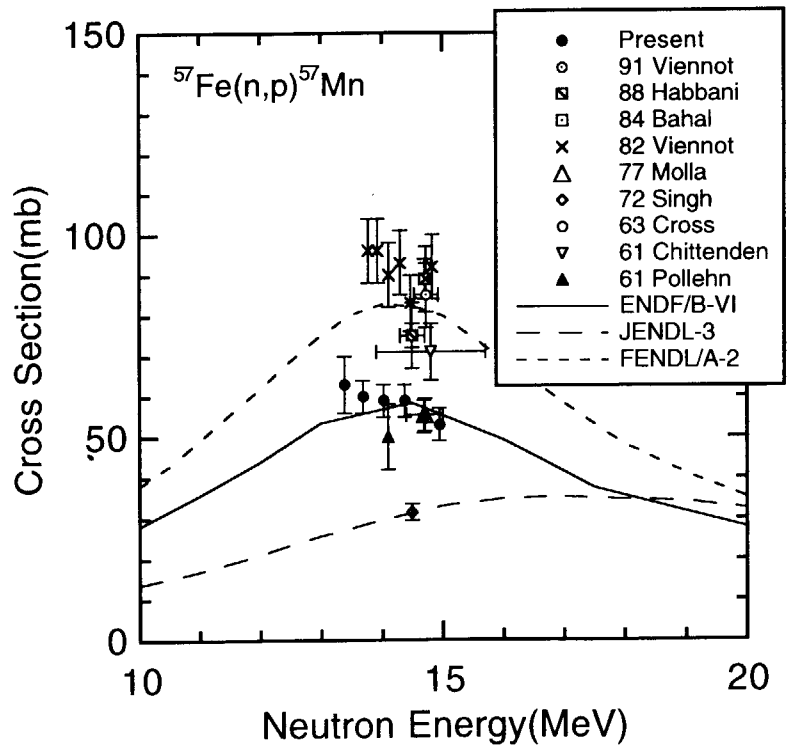

Fig. 4.8 Cross section data for ^{57}Fe(n,p)^{57}Mn

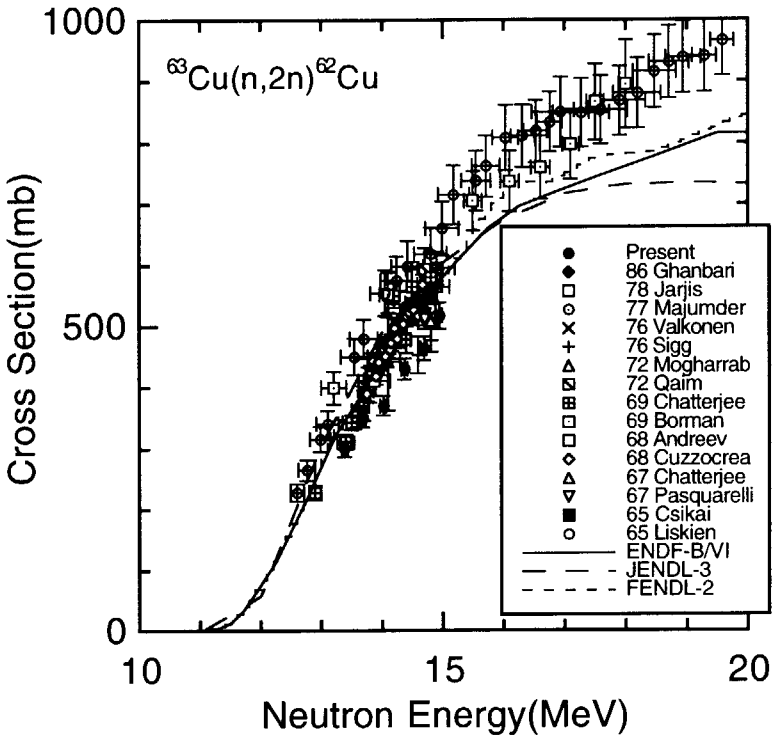

Fig. 4.9 Cross section data for ^{63}Cu(n, 2n)^{62}Cu

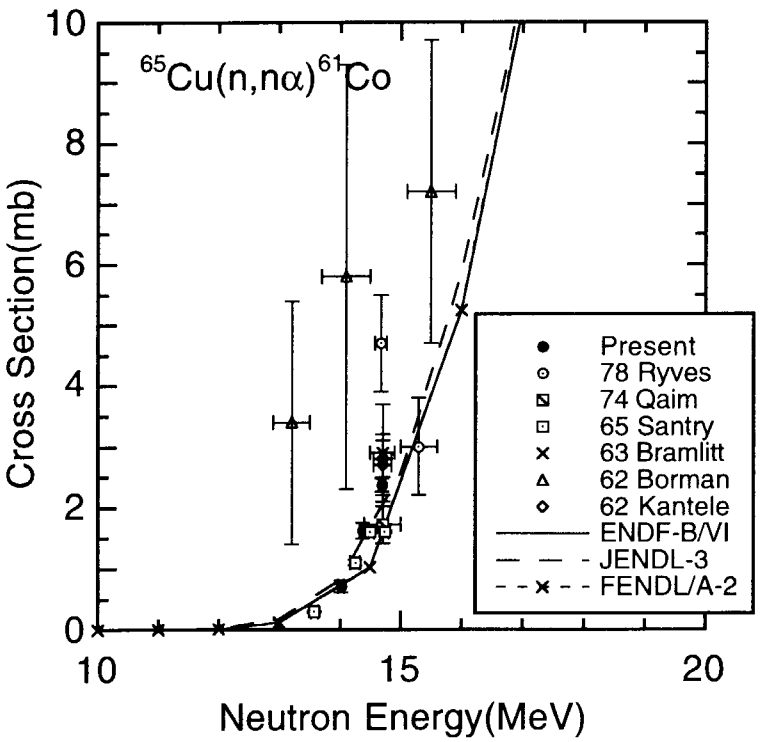

Fig. 4.10 Cross section data for ^{65}Cu(n, nα)^{61}Co

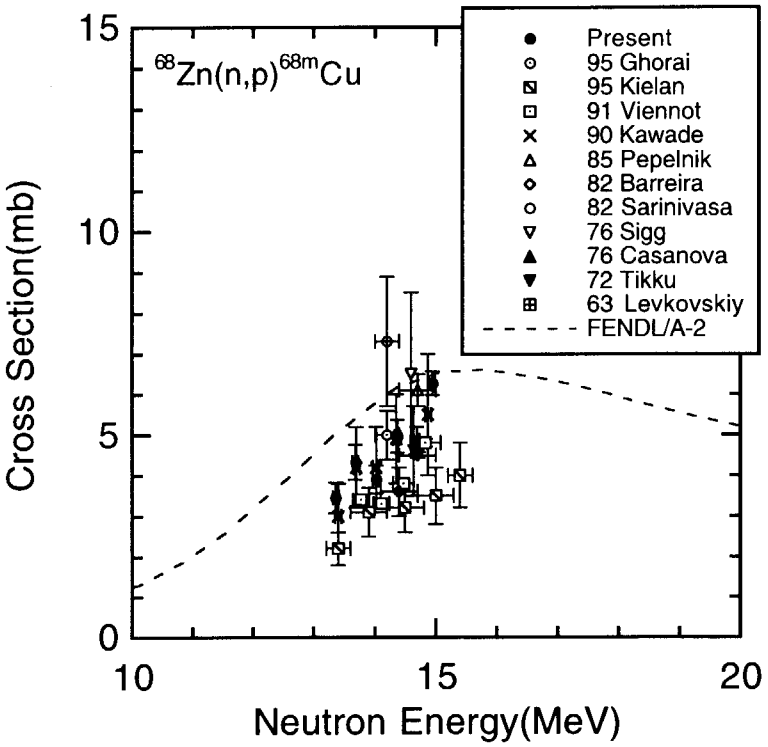

Fig. 4.11 Cross section data for ^{68}Zn(n, p)^{68m}Cu

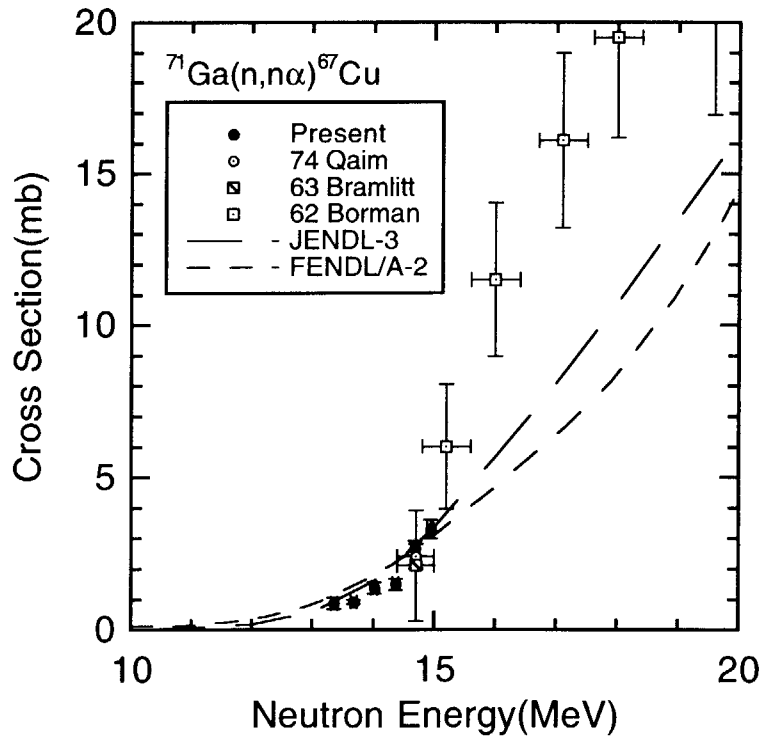

Fig. 4.12 Cross section data for ^{71}Ga(n, nα)^{67}Cu

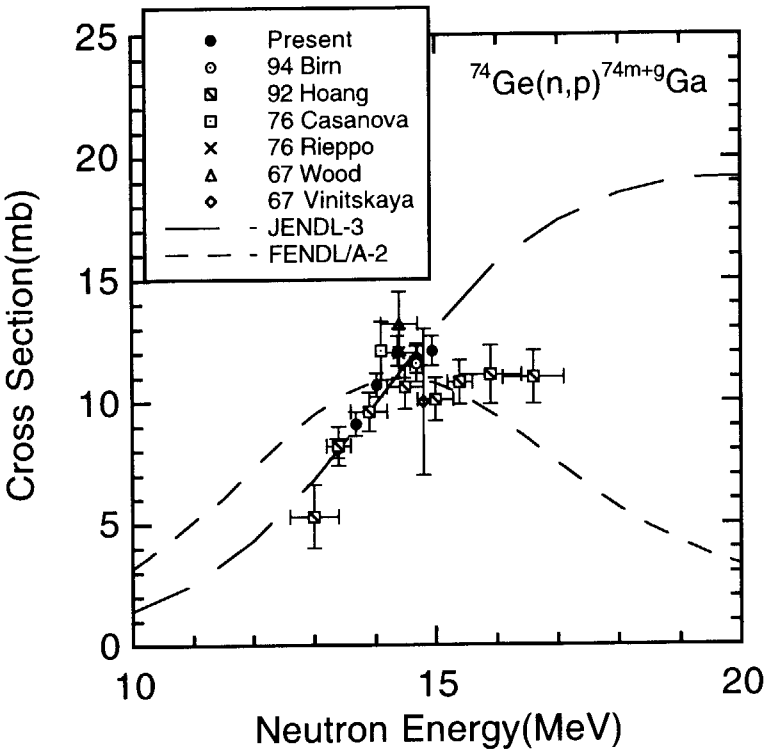

Fig. 4.13 Cross section data for ^{74}Ge(n,p)$^{74m+g}$Ga

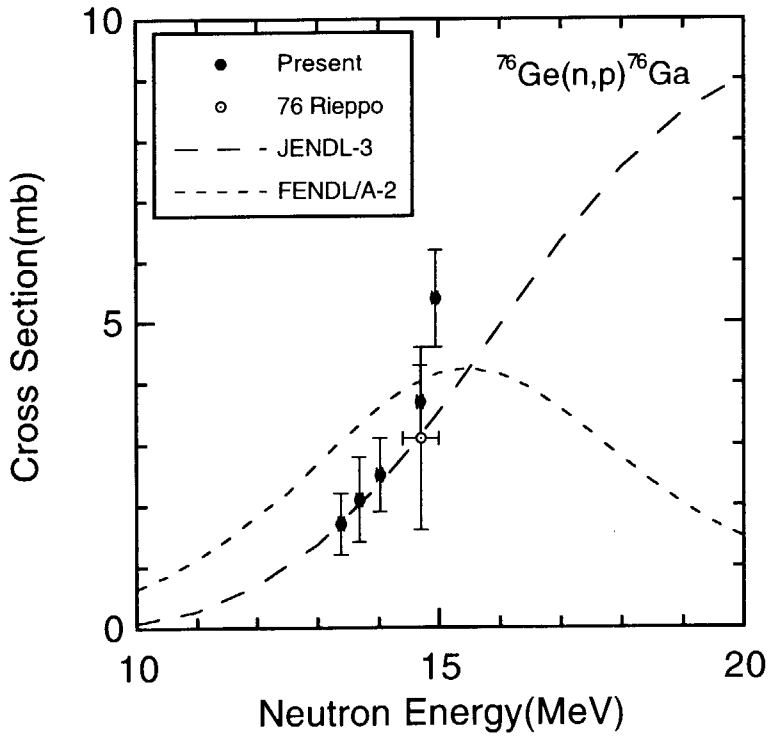

Fig. 4.14 Cross section data for ^{76}Ge(n,p)^{76}Ga

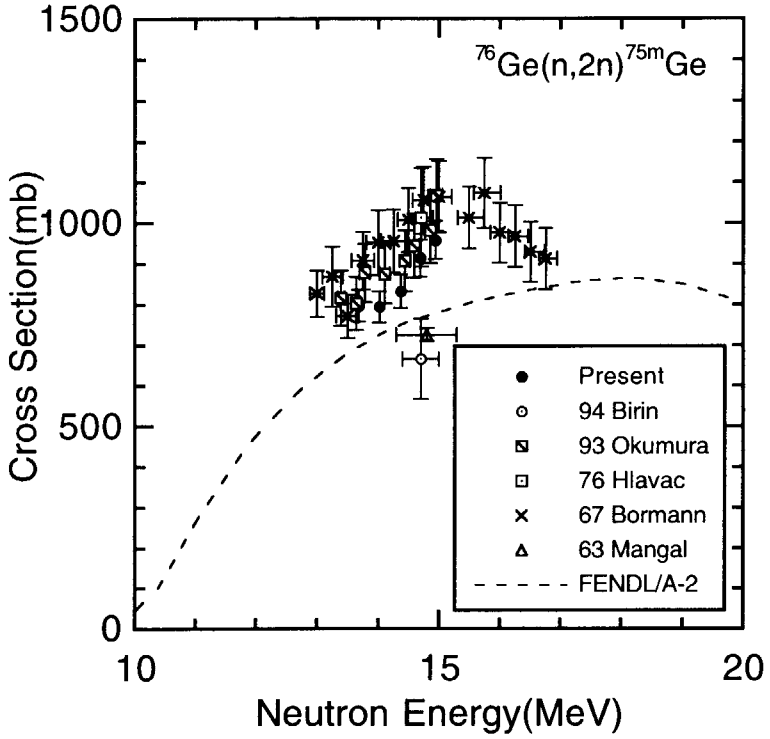

Fig. 4.15 Cross section data for ^{76}Ge(n, 2n)^{75m}Ge

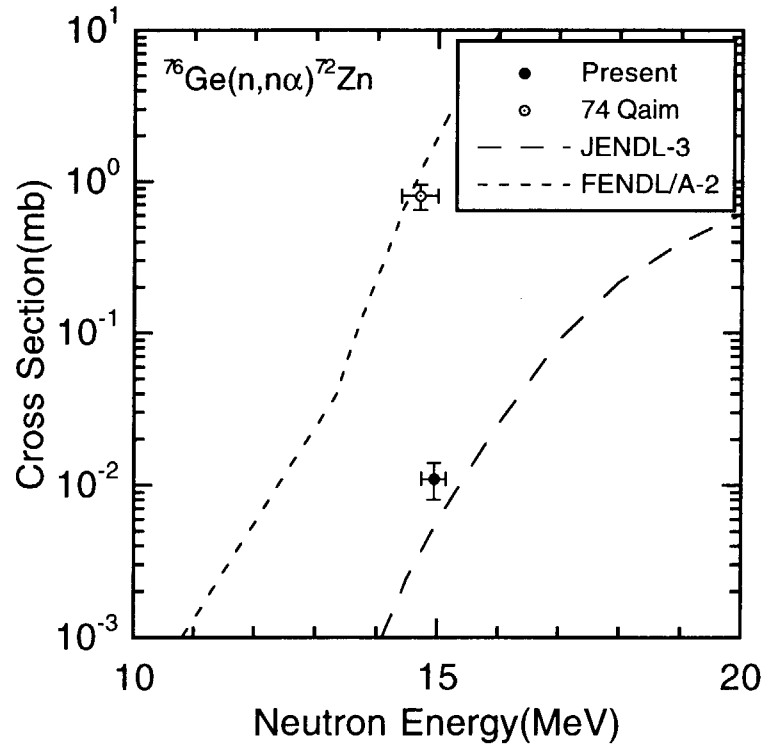

Fig. 4.16 Cross section data for ^{76}Ge(n, nα)^{72}Zn

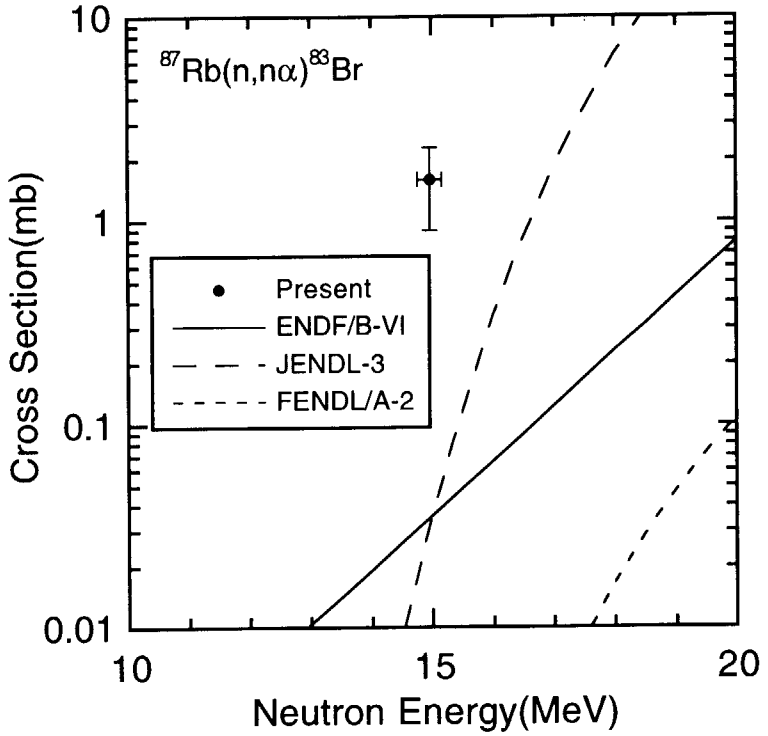

Fig. 4.17 Cross section data for ^{87}Rb(n, nα)^{83}Br

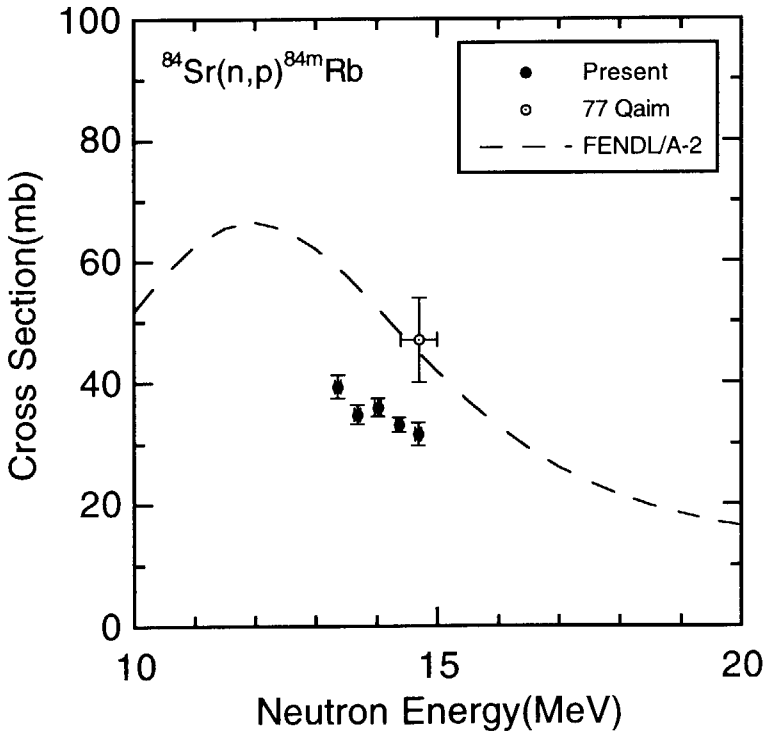

Fig. 4.18 Cross section data for ^{84}Sr(n,p)^{84m}Rb

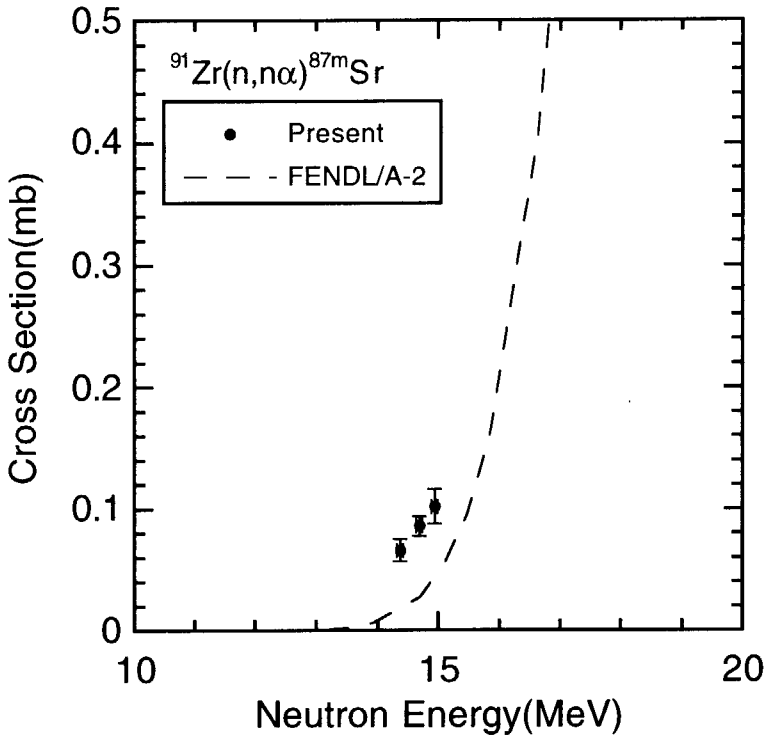

Fig. 4.19 Cross section data for ^{91}Zr(n,nα)^{87m}Sr

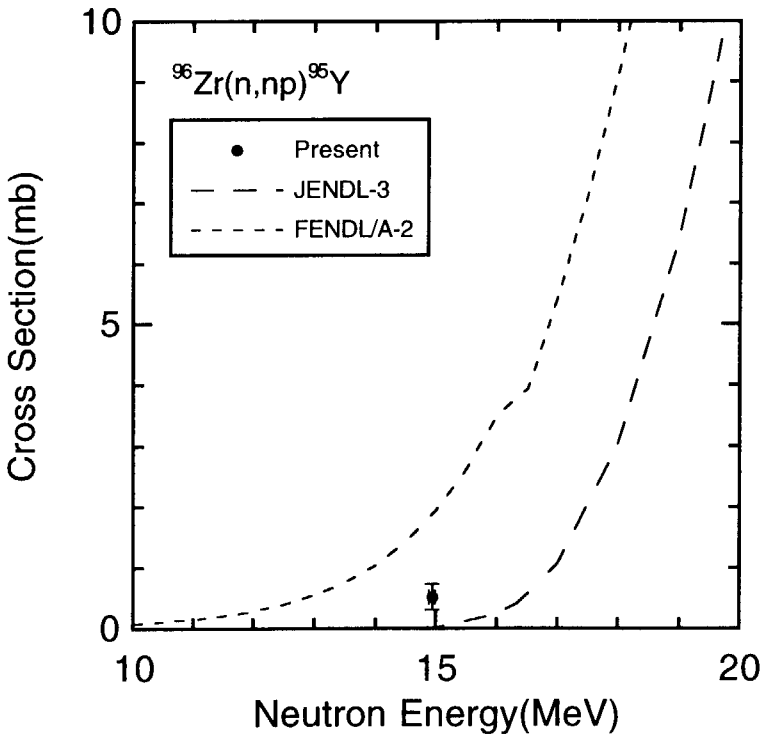

Fig. 4.20 Cross section data for ^{96}Zr(n,np)^{95}Y

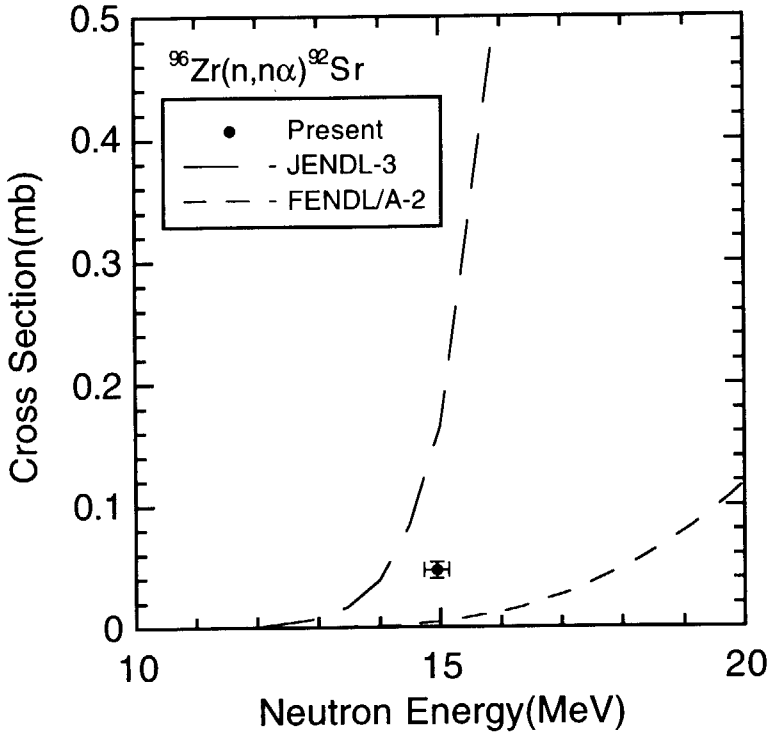

Fig. 4.21 Cross section data for ^{96}Zr(n,nα)^{92}Sr

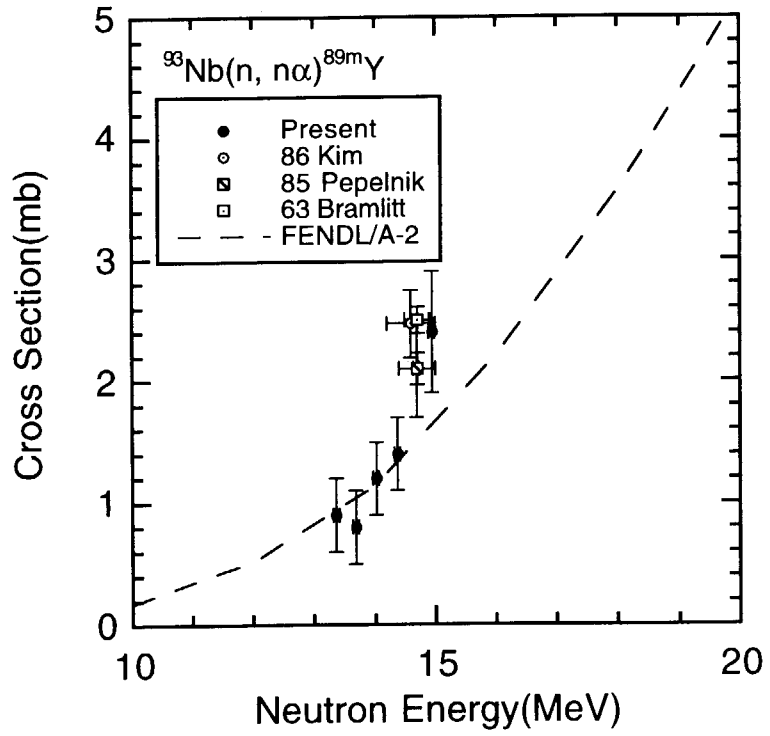

Fig. 4.22 Cross section data for ^{93}Nb(n,nα)^{89m}Y

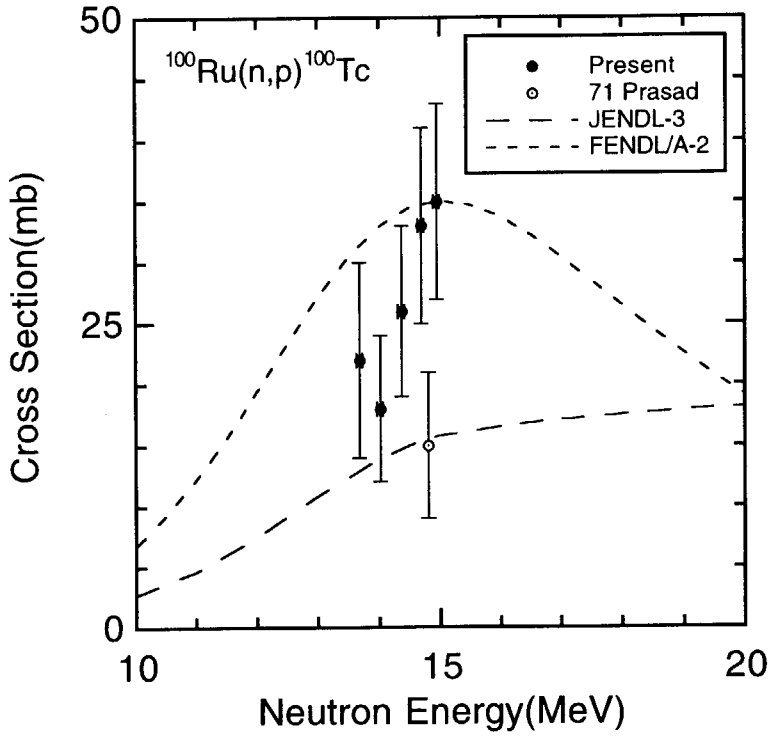

Fig. 4.23 Cross section data for ^{100}Ru(n,p)^{100}Tc

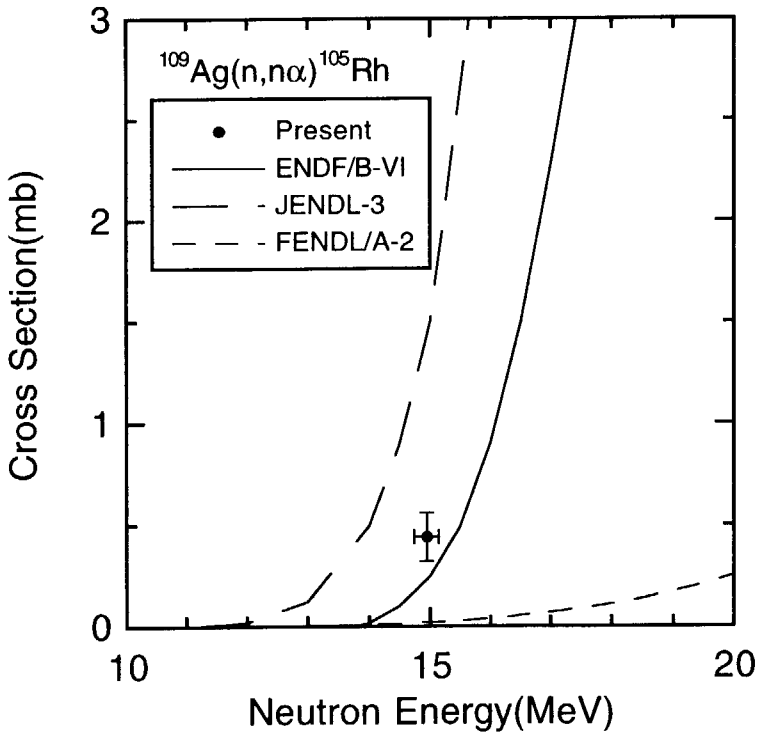

Fig. 4.24 Cross section data for ^{109}Ag(n,nα)^{105}Rh

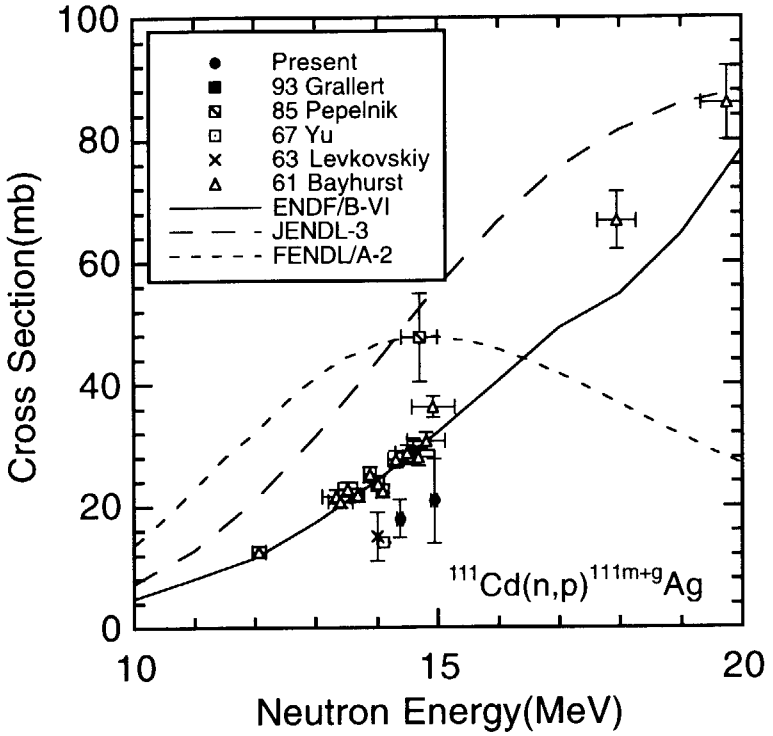

Fig. 4.25 Cross section data for ^{111}Cd(n,p)$^{111m+g}$Ag

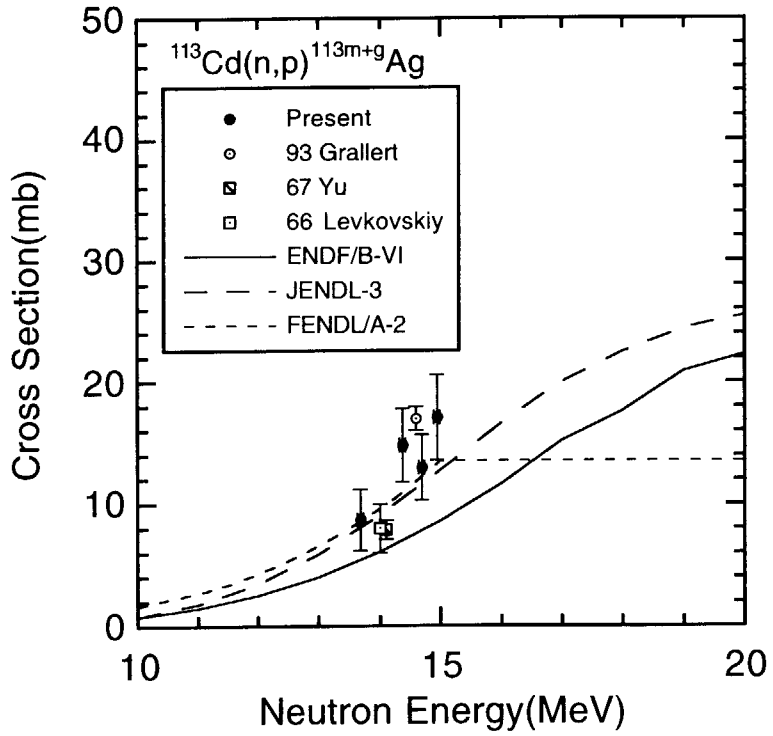

Fig. 4.26 Cross section data for ^{113}Cd(n,p)$^{113m+g}$Ag

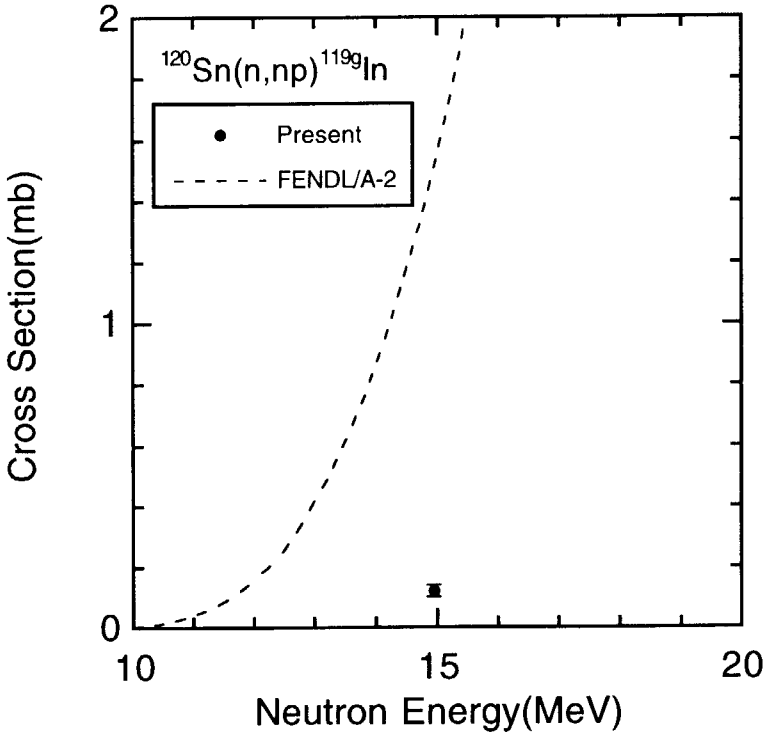

Fig. 4.27 Cross section data for ^{120}Sn(n,p)^{119g}In

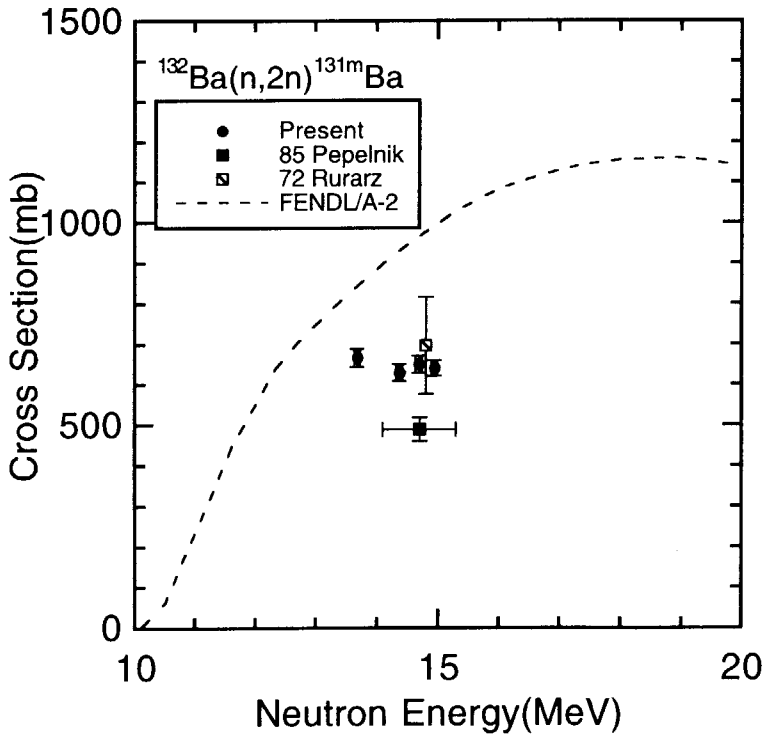

Fig. 4.28 Cross section data for ^{132}Ba(n,2n)^{131m}Ba

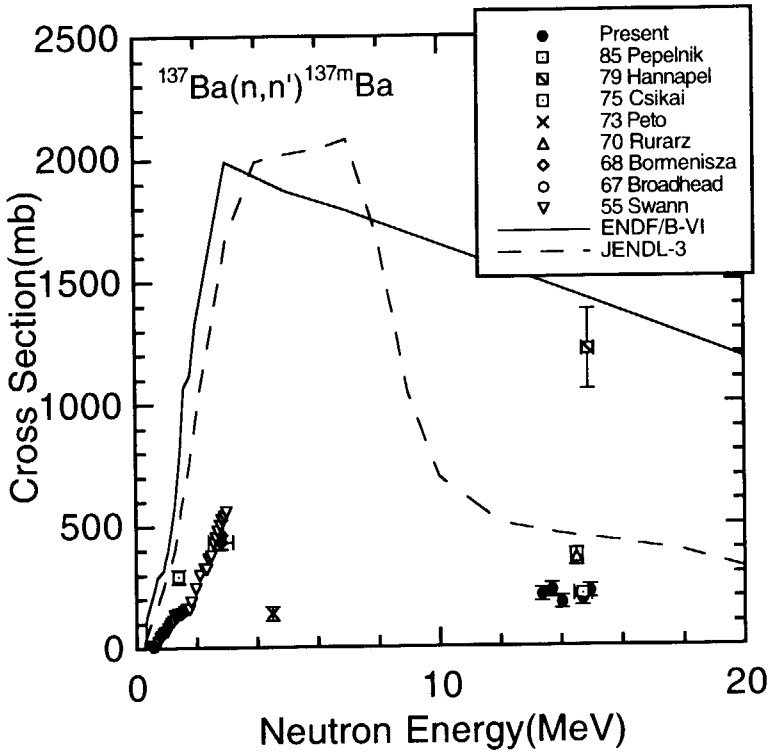

Fig. 4.29 Cross section data for ^{137}Ba(n,n')^{137m}Ba

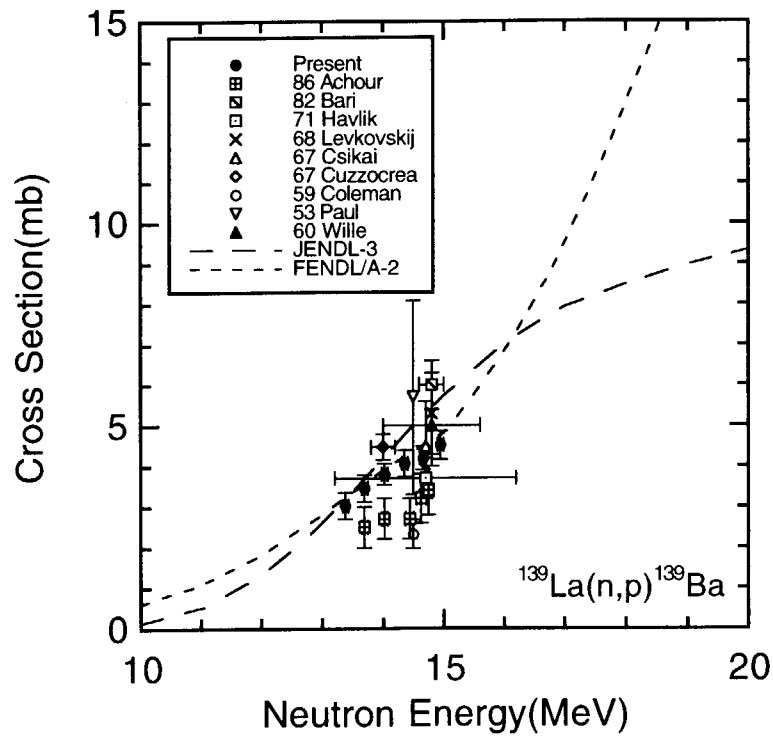

Fig. 4.30 Cross section data for ^{139}La(n,p)^{139}Ba

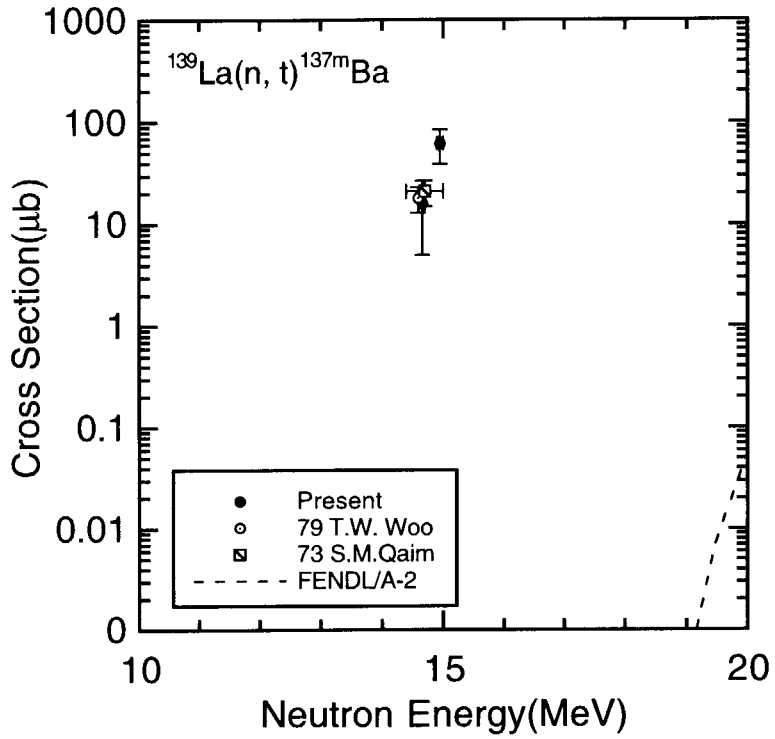

Fig. 4.31 Cross section data for ^{139}La(n,t)^{137m}Ba

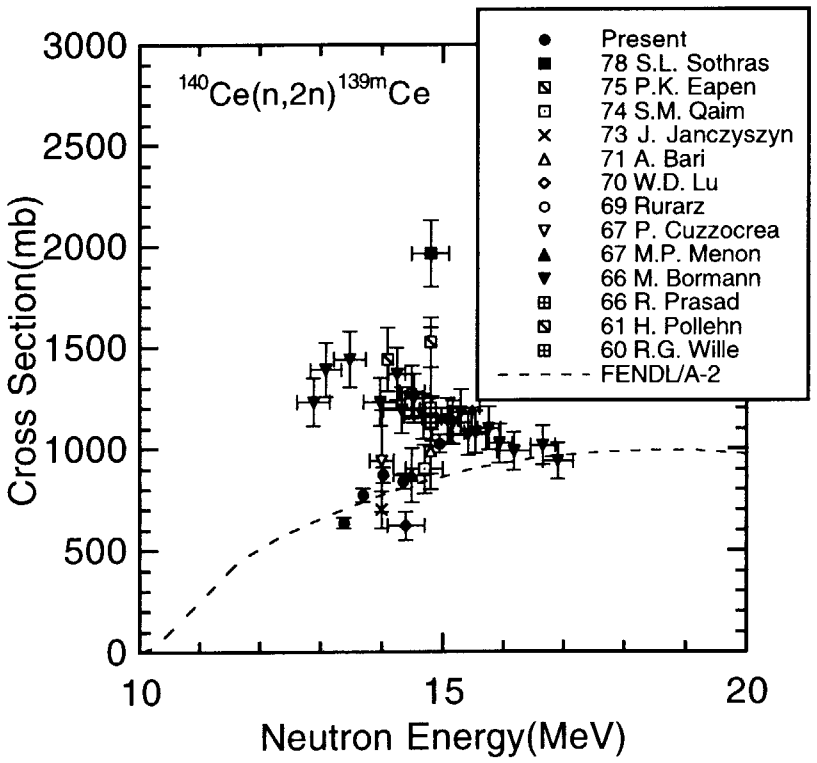

Fig. 4.32 Cross section data for ^{140}Ce(n,2n)^{139m}Ce

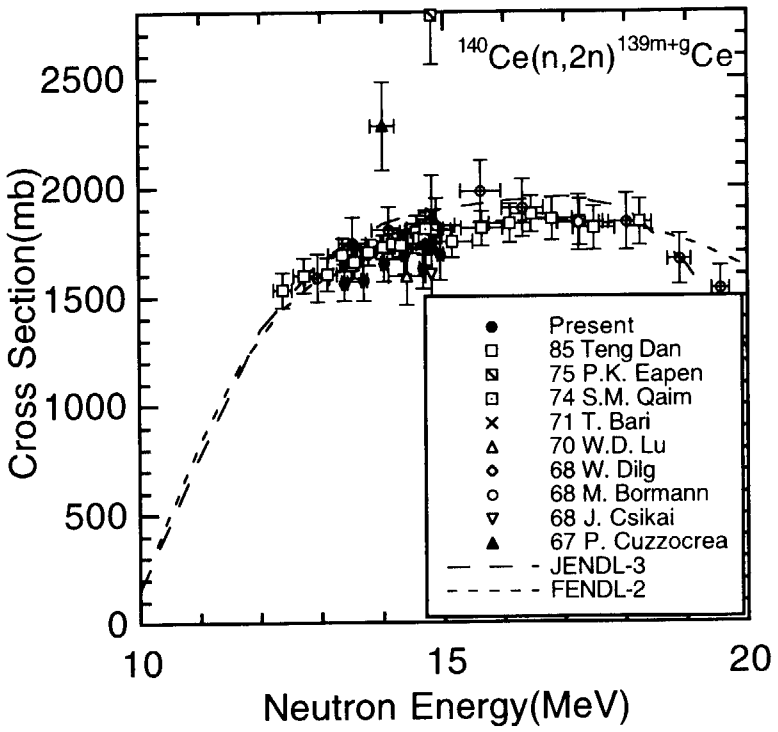

Fig. 4.33 Cross section data for ^{140}Ce(n,2n)$^{139m+g}$Ce

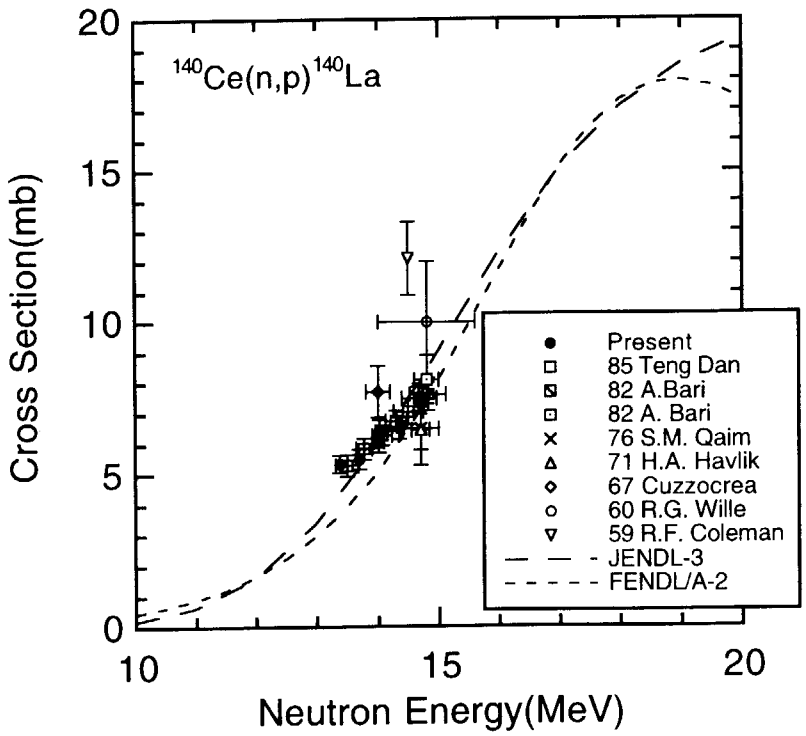

Fig. 4.34 Cross section data for ^{140}Ce(n,p)^{140}La

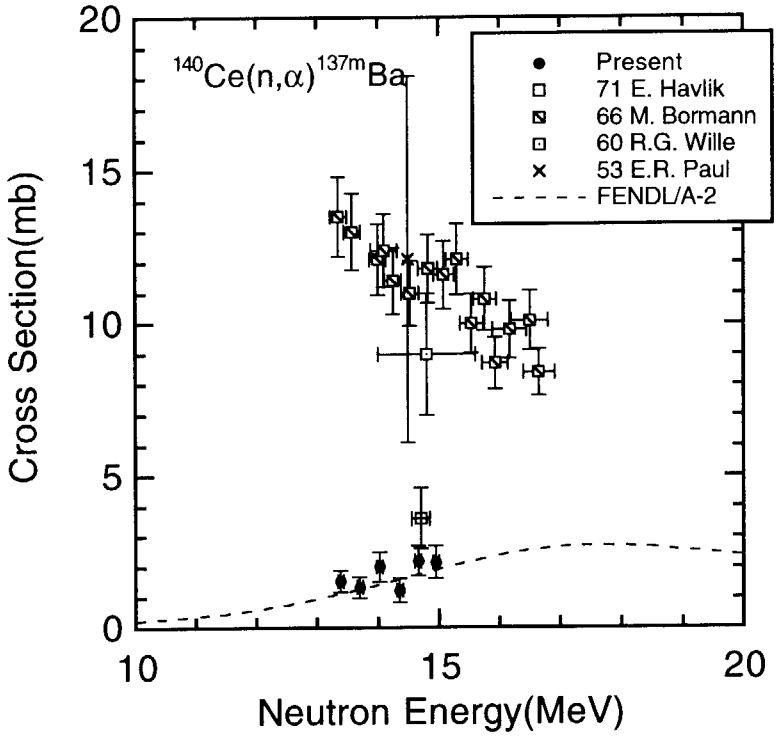

Fig. 4.35 Cross section data for ^{140}Ce(n,α)^{137m}Ba

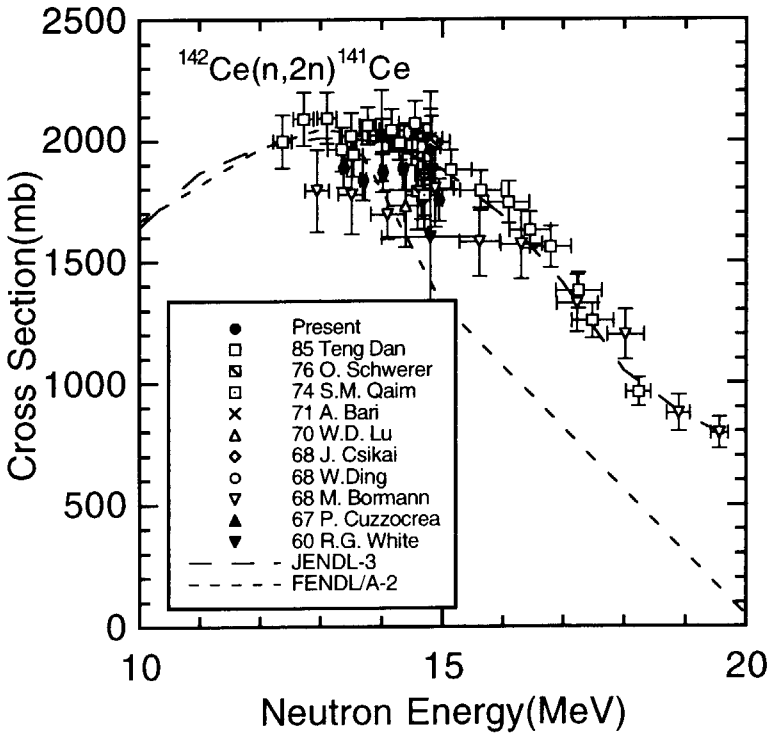

Fig. 4.36 Cross section data for ^{142}Ce(n,2n)^{141}Ce

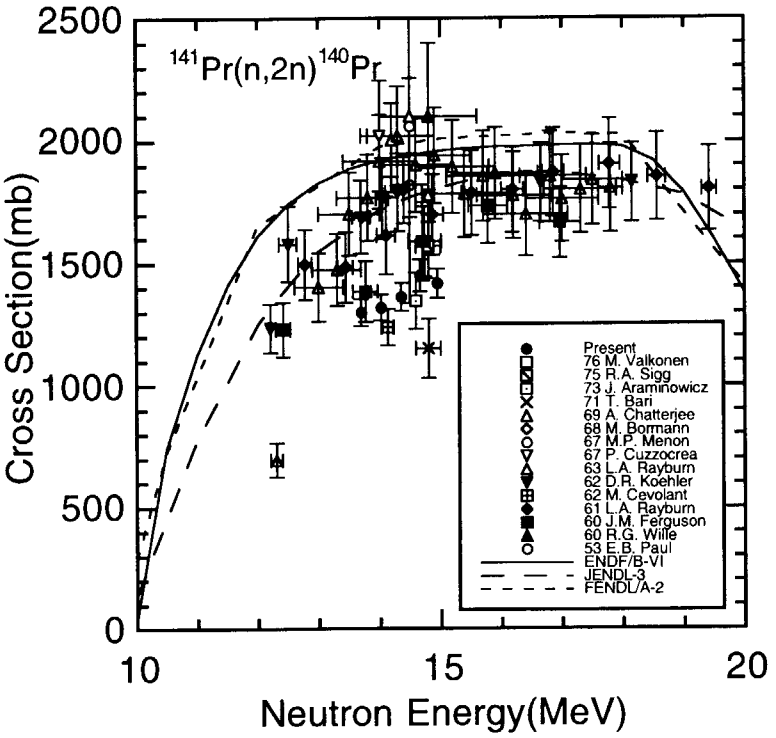

Fig. 4.37 Cross section data for ^{141}Pr(n,2n)^{140}Pr

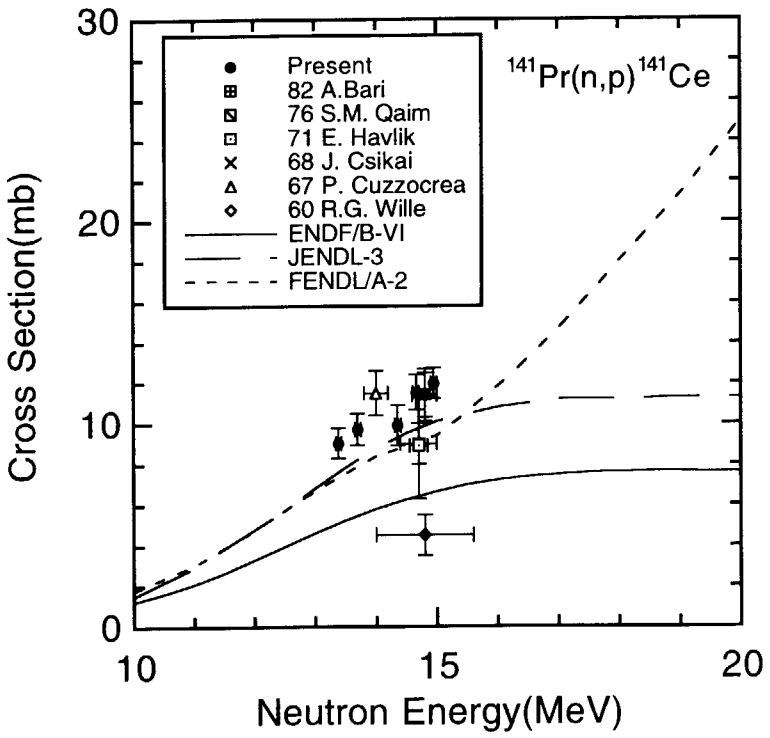

Fig. 4.38 Cross section data for ^{141}Pr(n,p)^{141}Ce

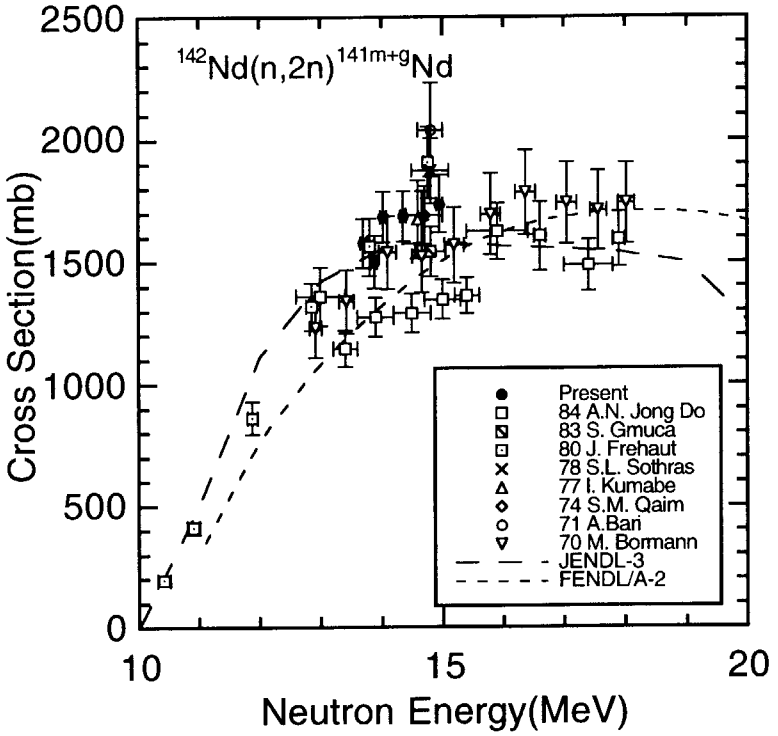

Fig. 4.39 Cross section data for $^{142}Nd(n,2n)^{141m+g}Nd$

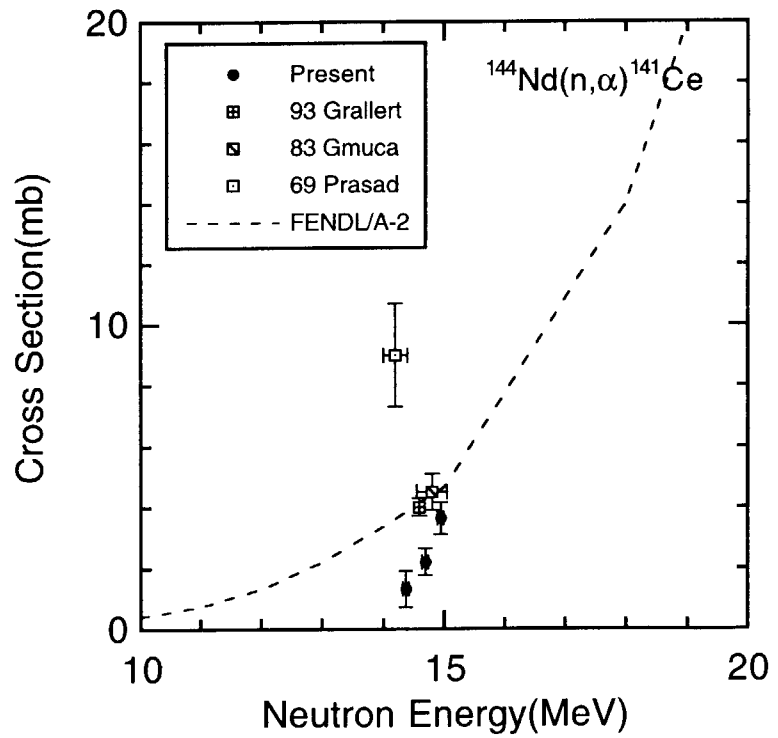

Fig. 4.40 Cross section data for $^{144}Nd(n,\alpha)^{141}Ce$

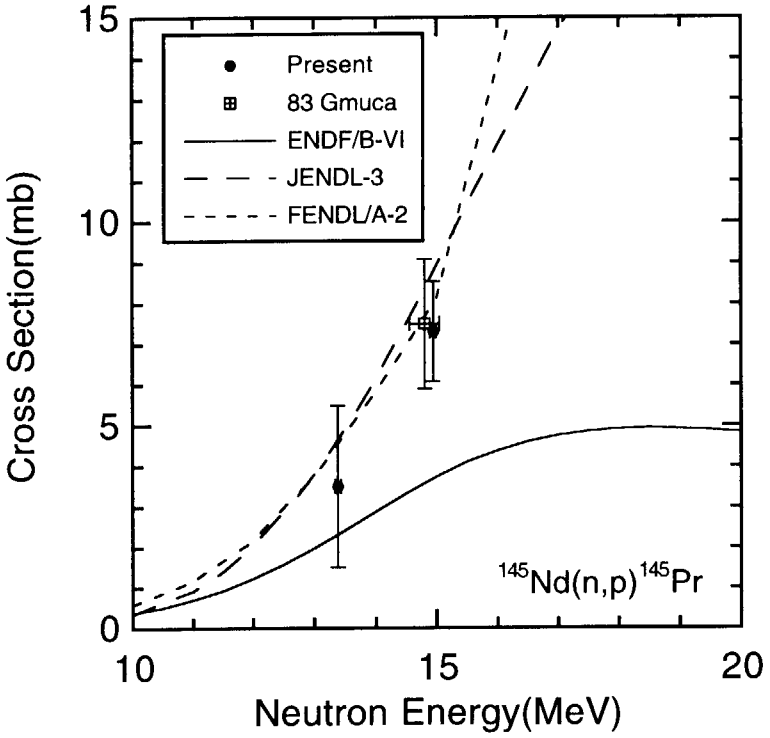

Fig. 4.41 Cross section data for ^{145}Nd(n,p)^{145}Pr

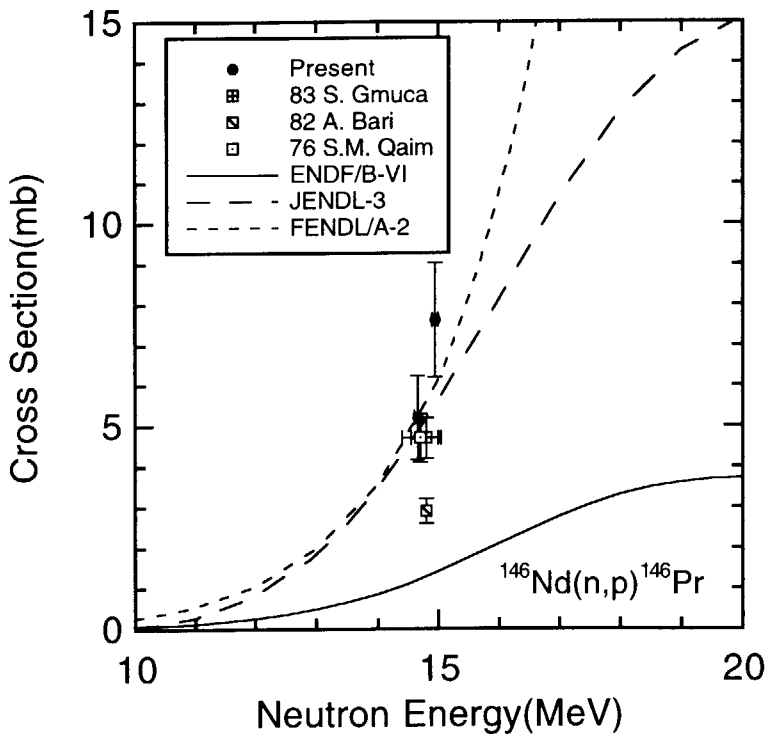

Fig. 4.42 Cross section data for ^{146}Nd(n,p)^{146}Pr

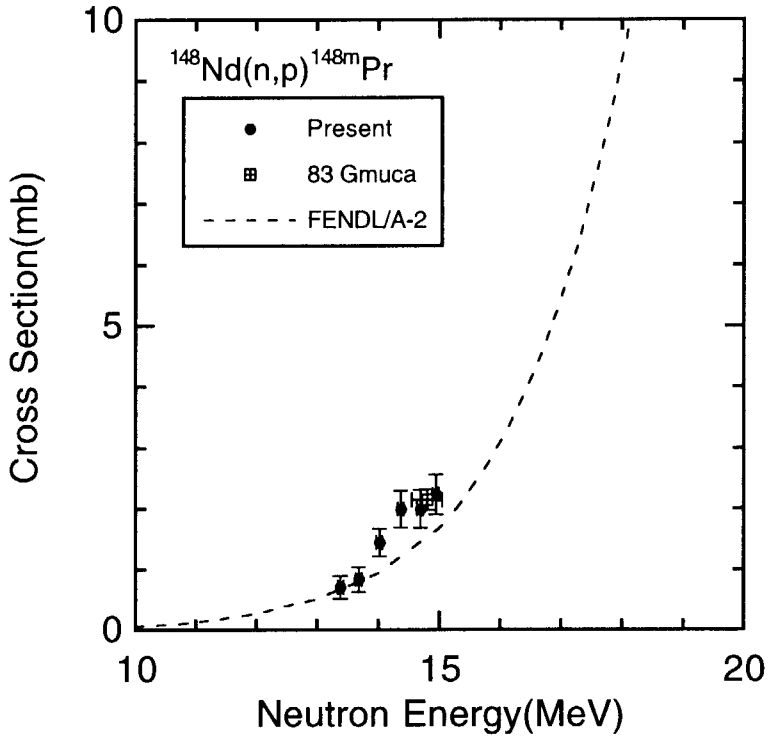

Fig. 4.43 Cross section data for ^{148}Nd(n,p)^{148m}Pr

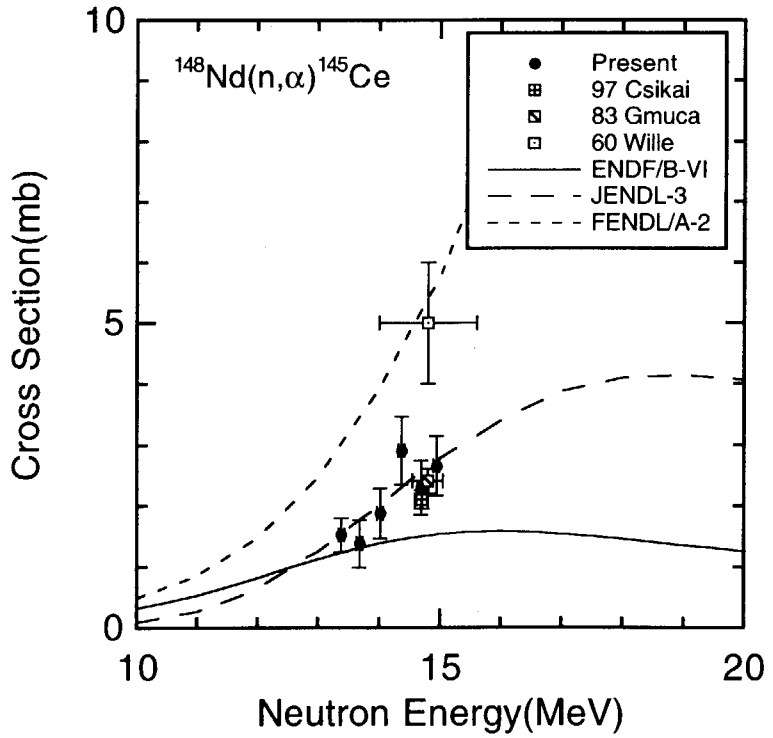

Fig. 4.44 Cross section data for ^{148}Nd(n,α)$^{145m+g}$Ce

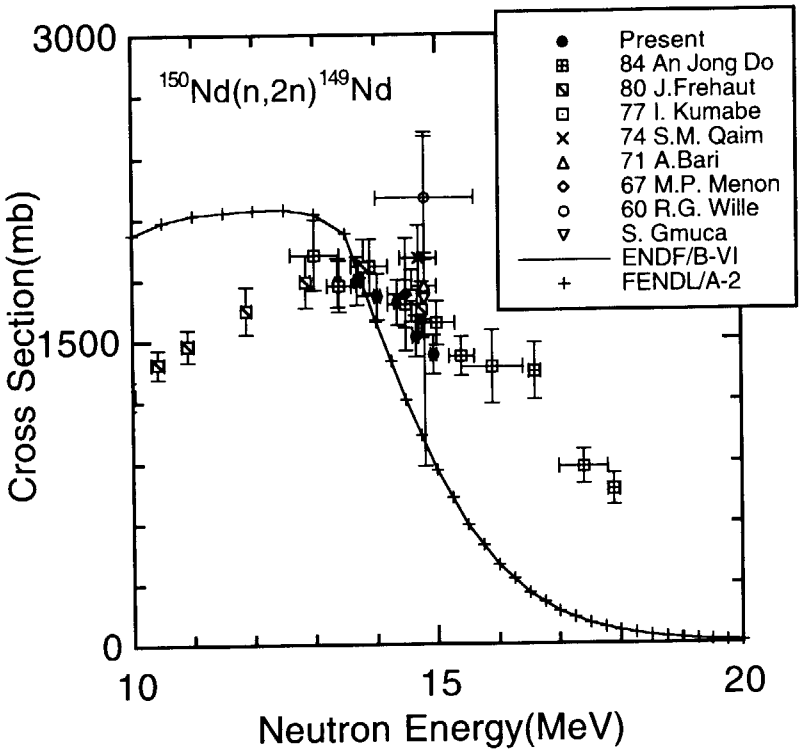

Fig. 4.45 Cross section data for ^{150}Nd(n,2n)^{149}Nd

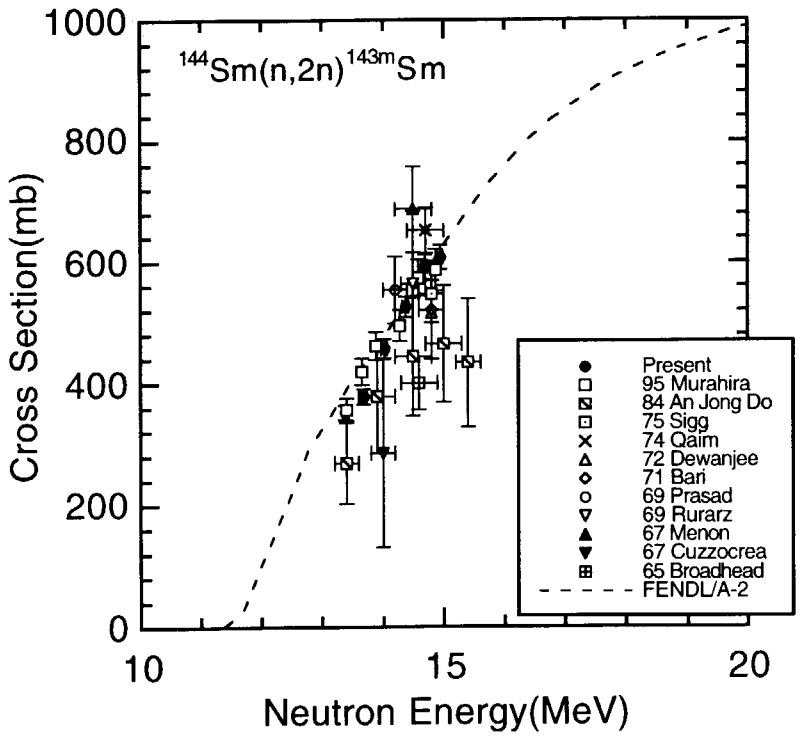

Fig. 4.46 Cross section data for ^{144}Sm(n, 2n)^{143m}Sm

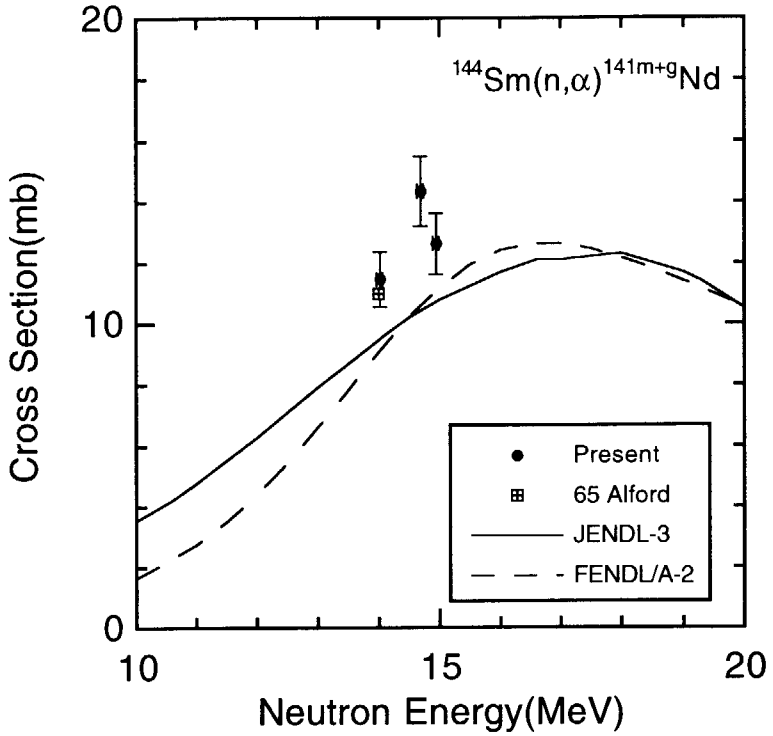

Fig. 4.47 Cross section data for ^{144}Sm(n, α)$^{141m+g}$Nd

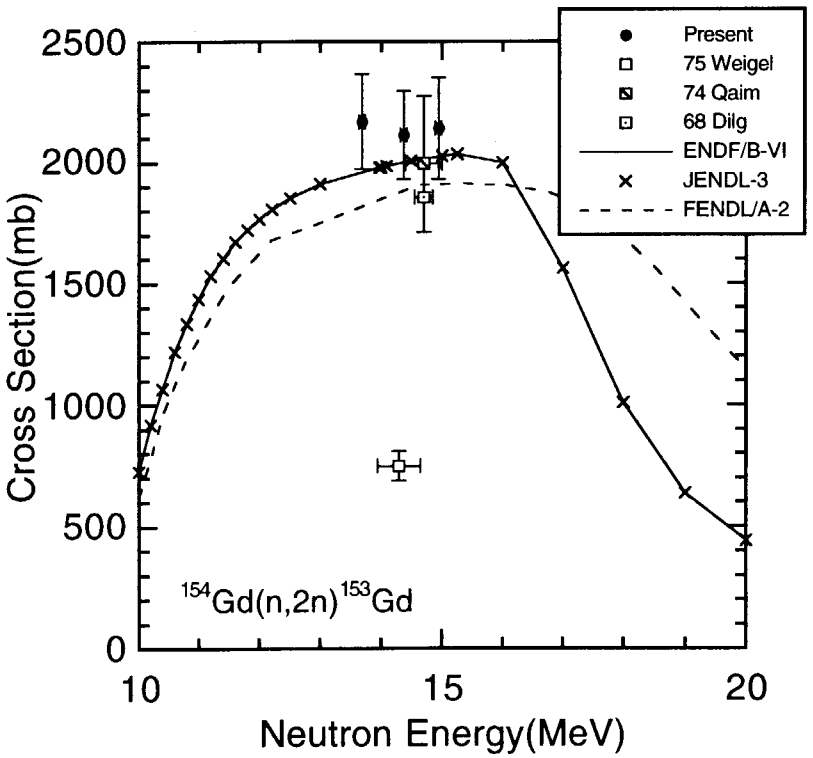

Fig. 4.48 Cross section data for ^{154}Gd(n,2n)^{153}Gd

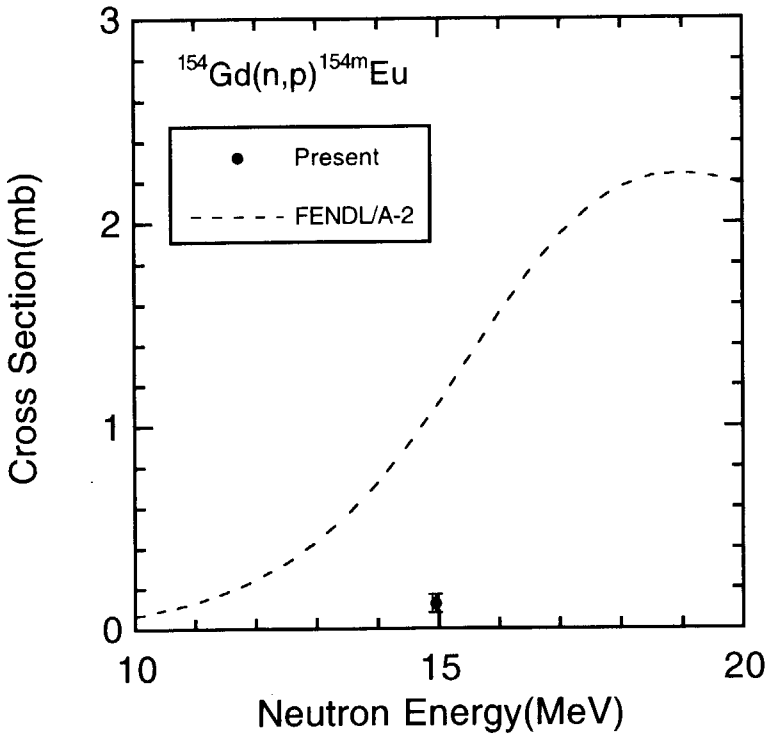

Fig. 4.49 Cross section data for ^{154}Gd(n,p)^{154m}Eu

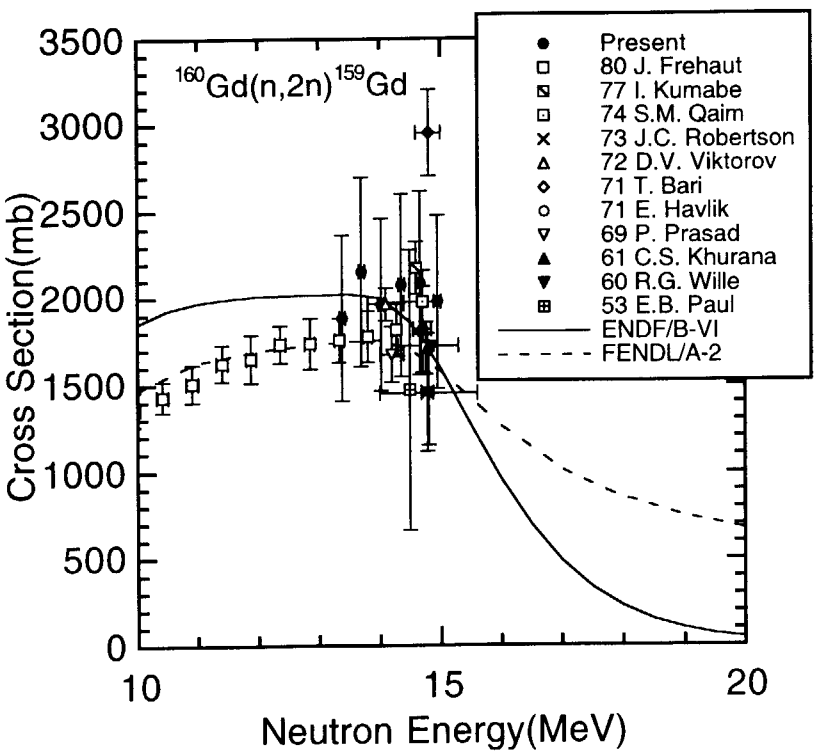

Fig. 4.50 Cross section data for ^{160}Gd(n,2n)^{159}Gd

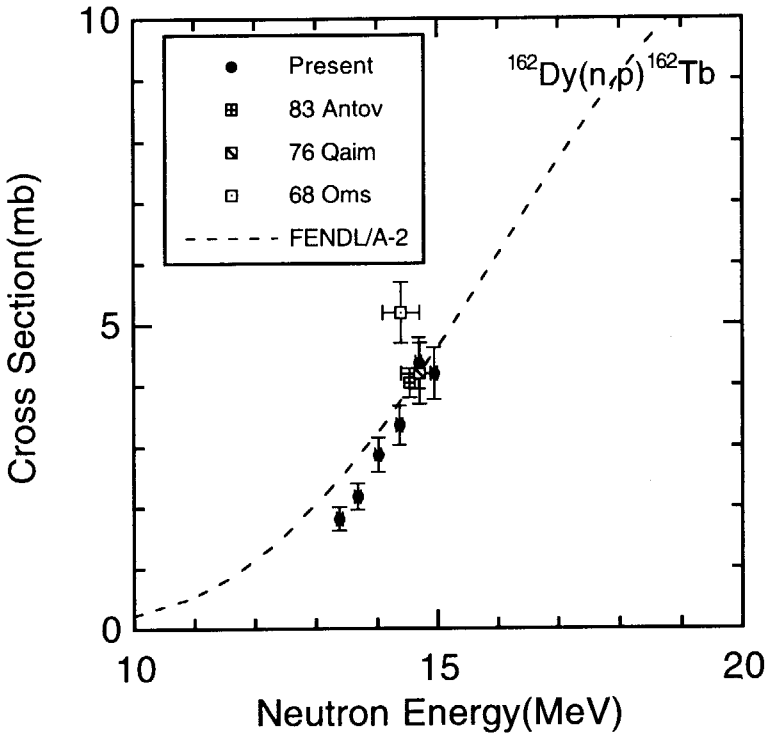

Fig. 4.51 Cross section data for ^{162}Dy(n,p)^{162}Tb

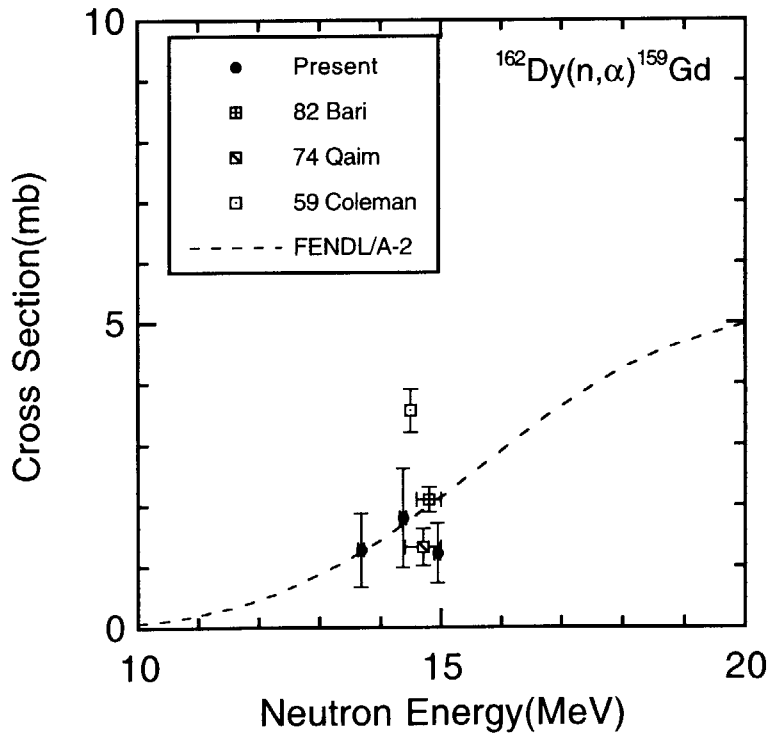

Fig. 4.52 Cross section data for ^{162}Dy(n,α)^{159}Gd

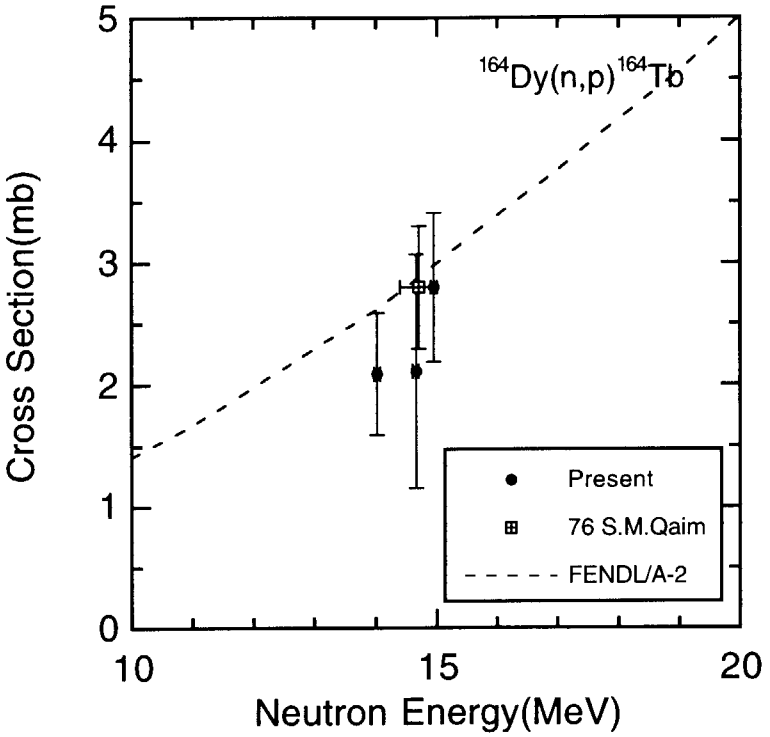

Fig. 4.53 Cross section data for ^{164}Dy(n,p)^{164}Tb

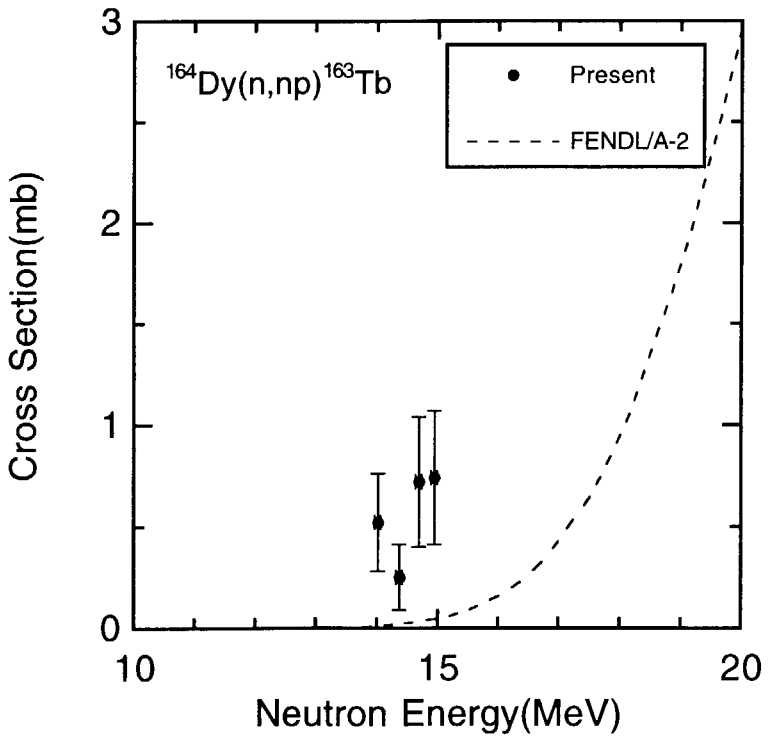

Fig. 4.54 Cross section data for ^{164}Dy(n,np)^{163}Tb

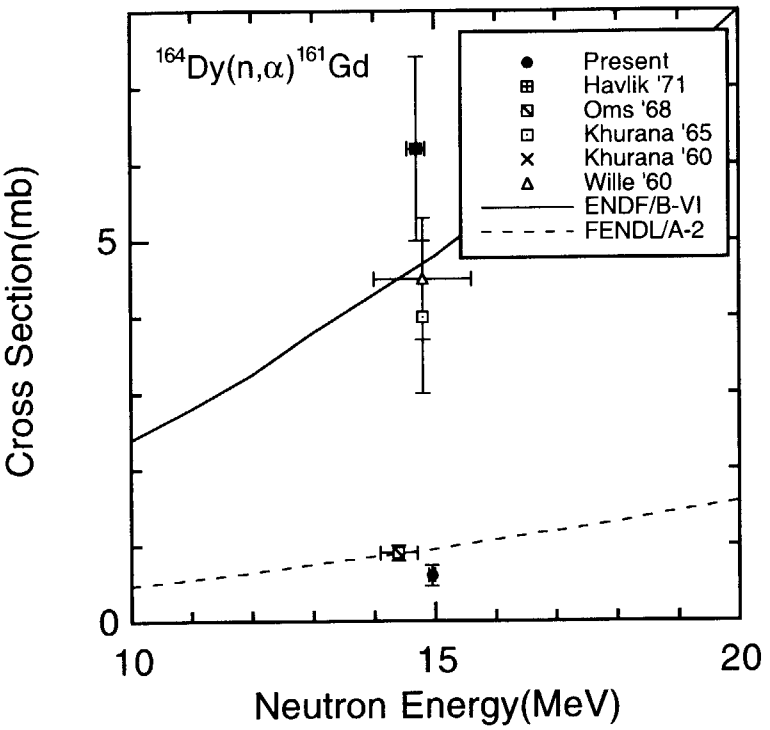

Fig. 4.55 Cross section data for ^{164}Dy(n, α)^{161}Gd

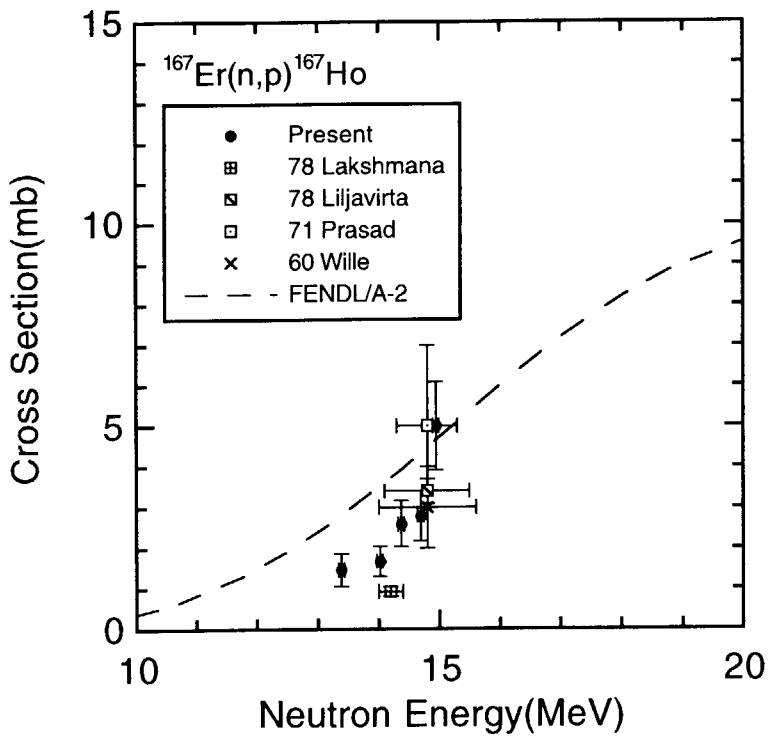

Fig. 4.56 Cross section data for ^{167}Er(n,p)^{167}Ho

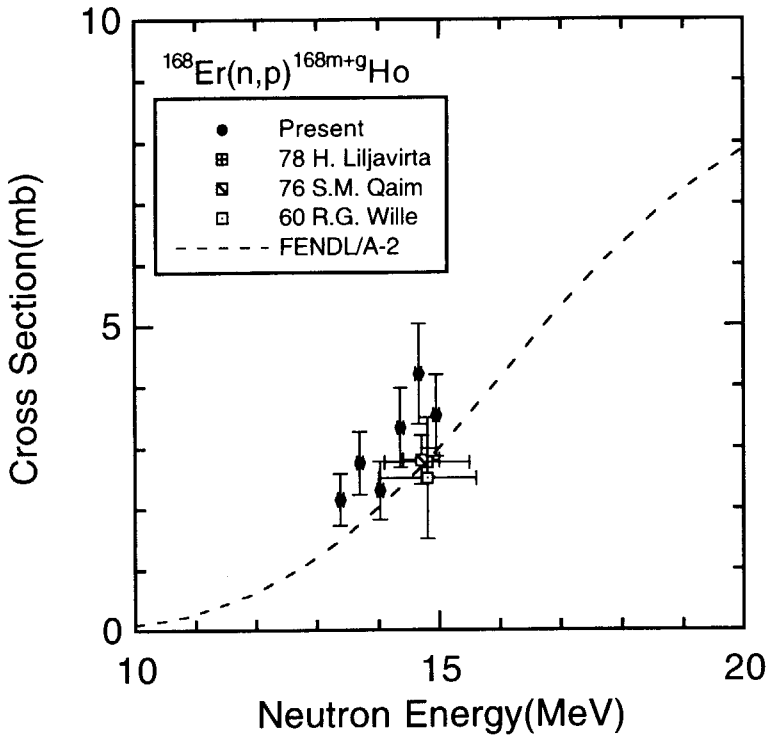

Fig. 4.57 Cross section data for ^{168}Er(n,p)$^{168m+g}$Ho

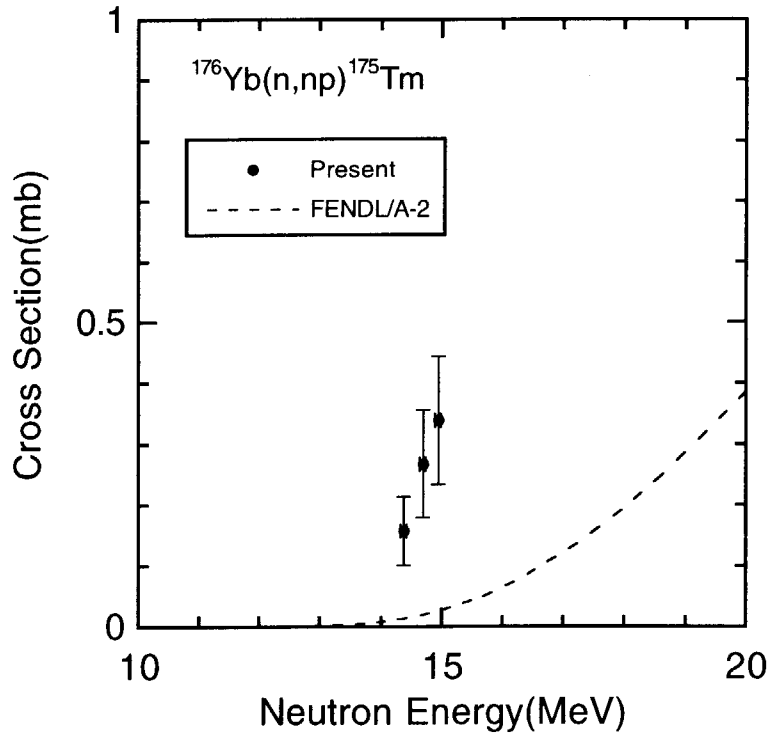

Fig. 4.58 Cross section data for ^{176}Yb(n,np)^{175}Tm

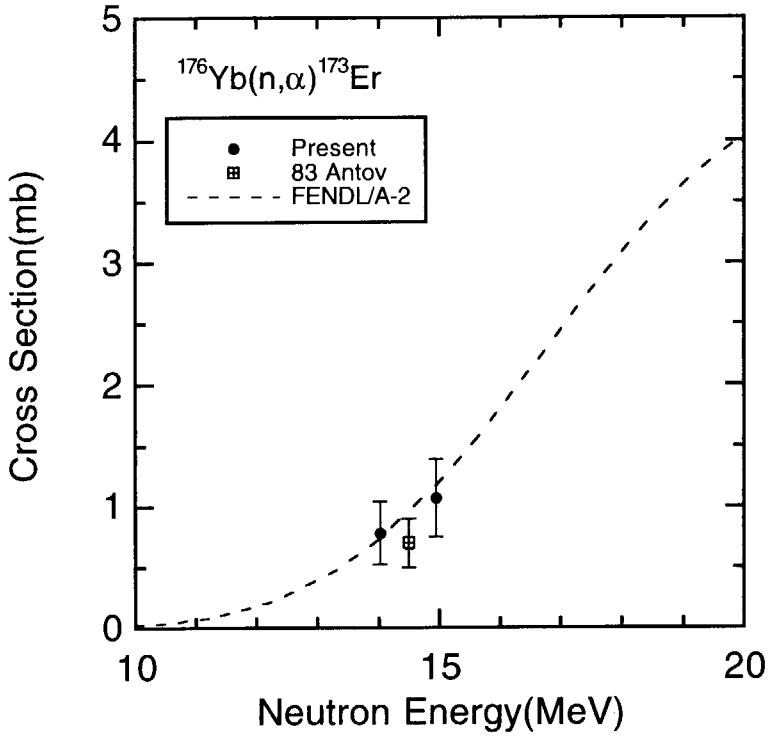

Fig. 4.59 Cross section data for $^{176}Yb(n,\alpha)^{173}Er$

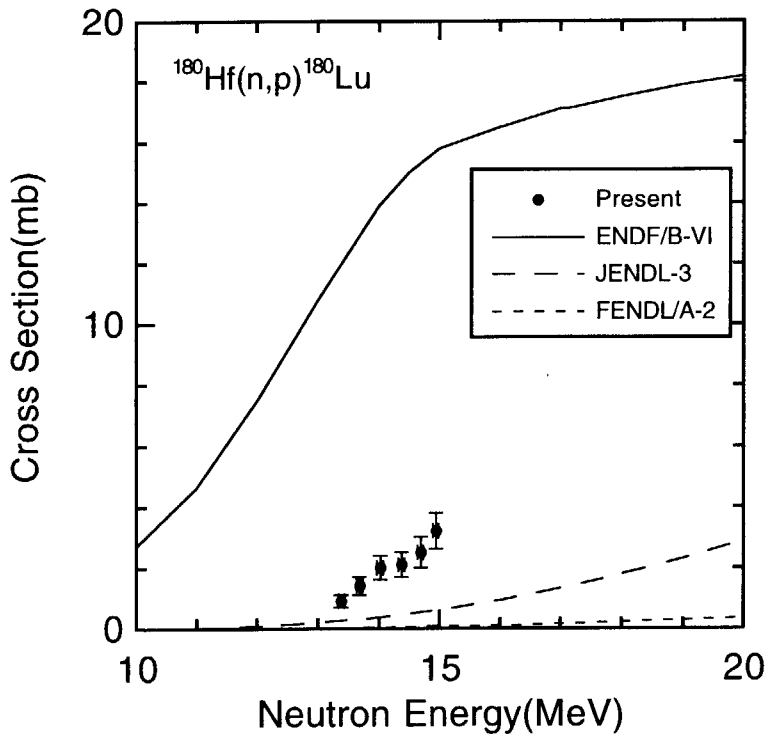

Fig. 4.60 Cross section data for $^{180}Hf(n,p)^{180}Lu$

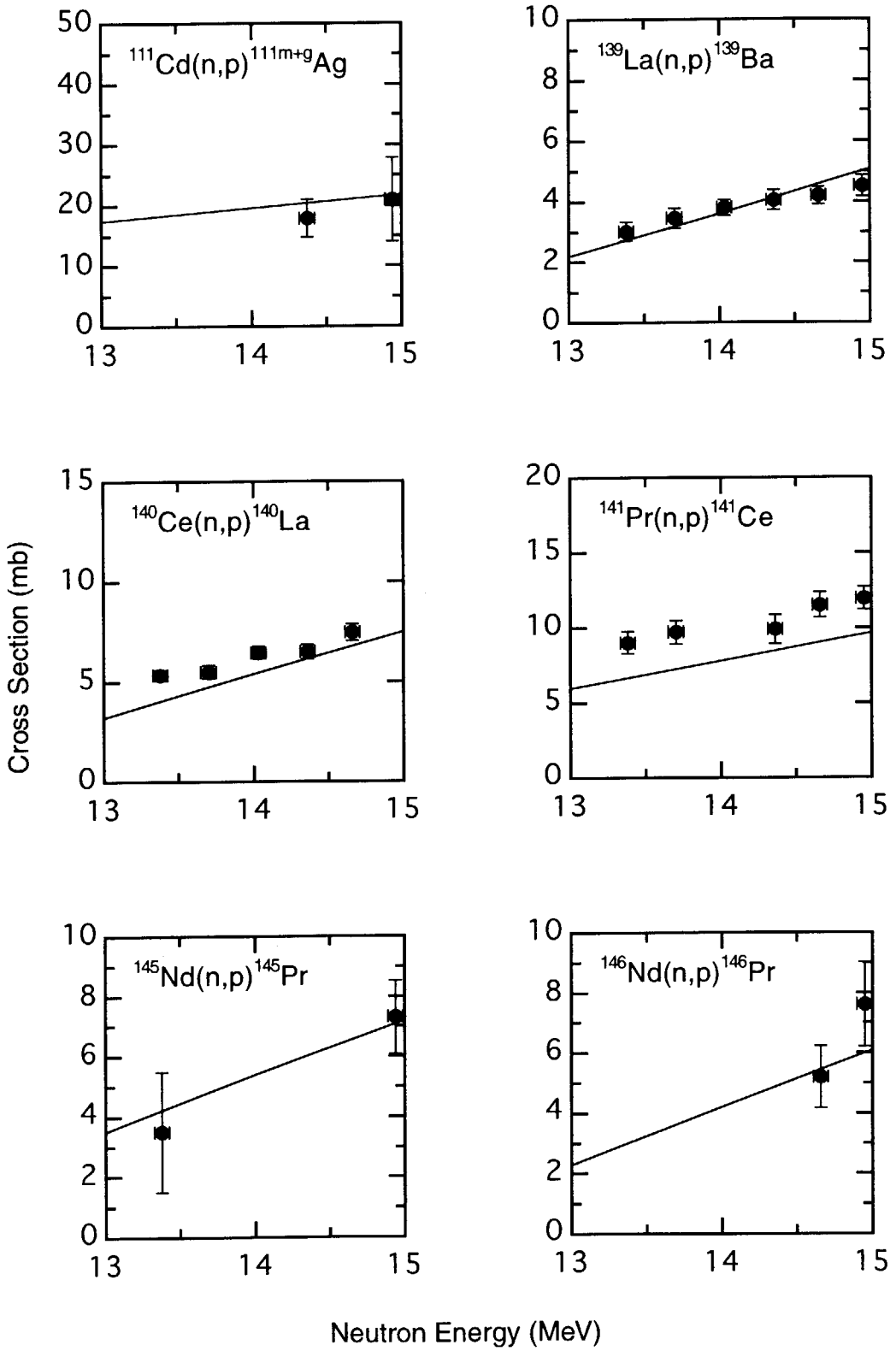

Fig. 5.1 Comparison between the present experimental data of the (n,p) reactions and the excitation function estimated by using the empirical formula. The closed circles show the experimental data, and the lines show the excitation function estimated by using the empirical formulae.

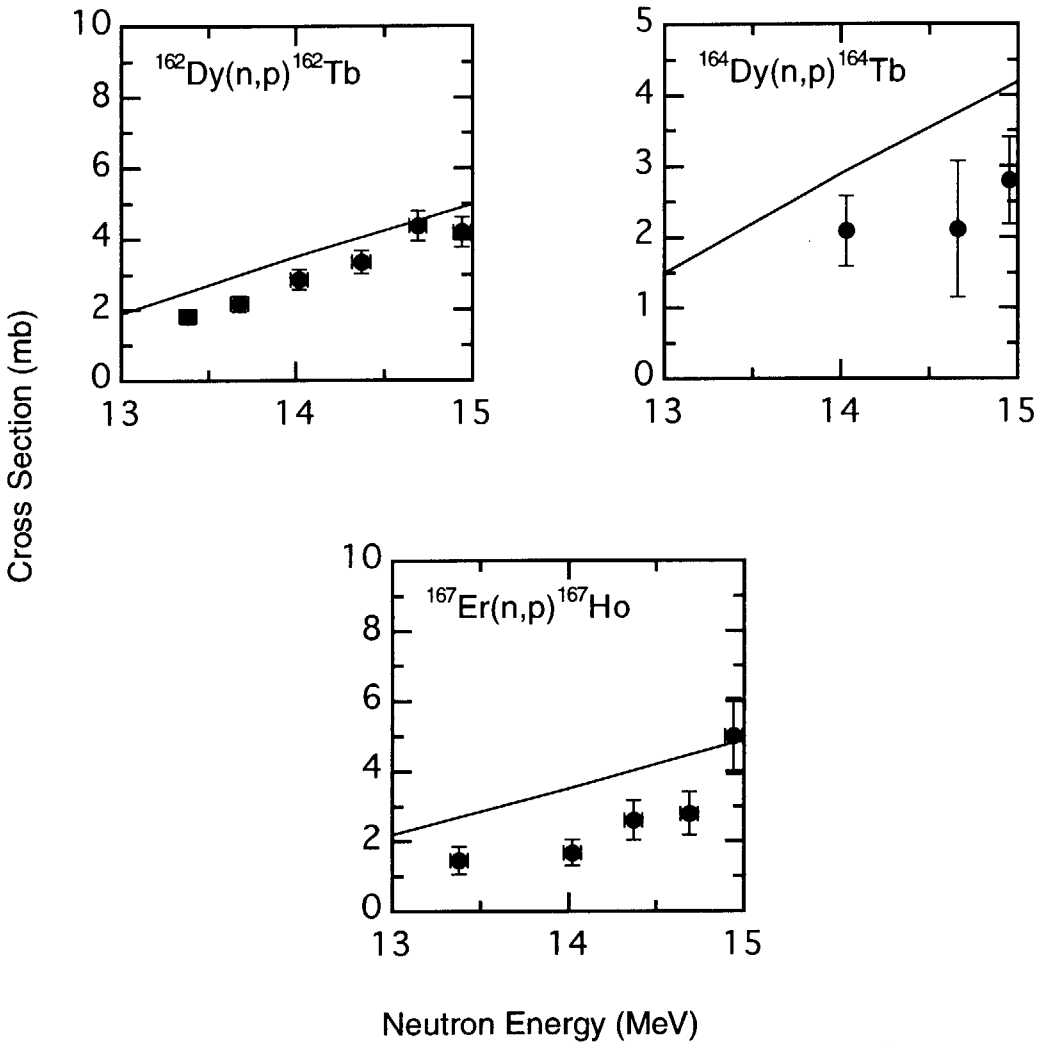

Fig. 5.1 Comparison between the present experimental data of the (n,p) reactions and the excitation function estimated by using the empirical formula. The closed circles show the experimental data, and the lines show the excitation function estimated by using the empirical formulae. (continued)

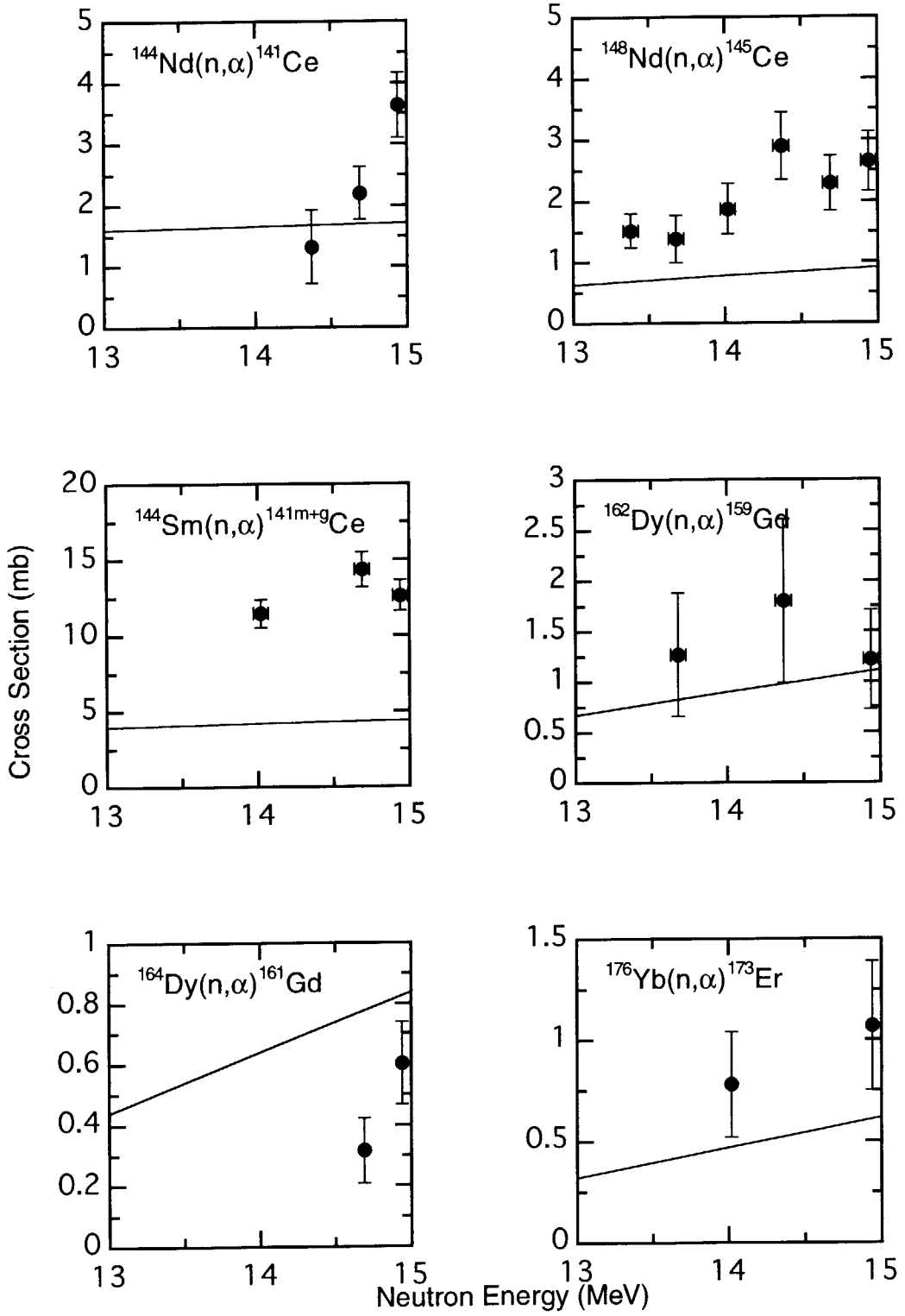

Fig. 5.2 Comparison between the present experimental data of the (n,α) reactions and the excitation function estimated by using the empirical formula. The closed circles show the experimental data, and the lines show the excitation function estimated by using the empirical formulae.

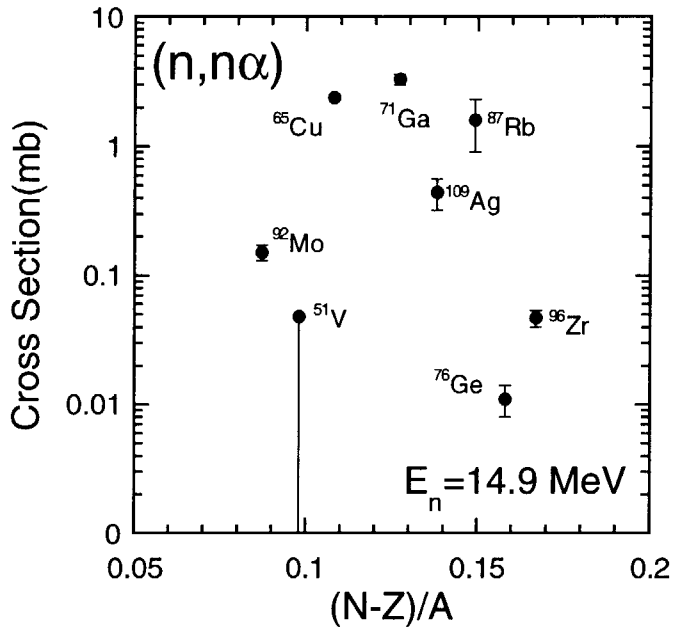

Fig. 5.3 Systematics of the (n, nα) cross sections at 14.9 MeV as a function of (N-Z)/A.

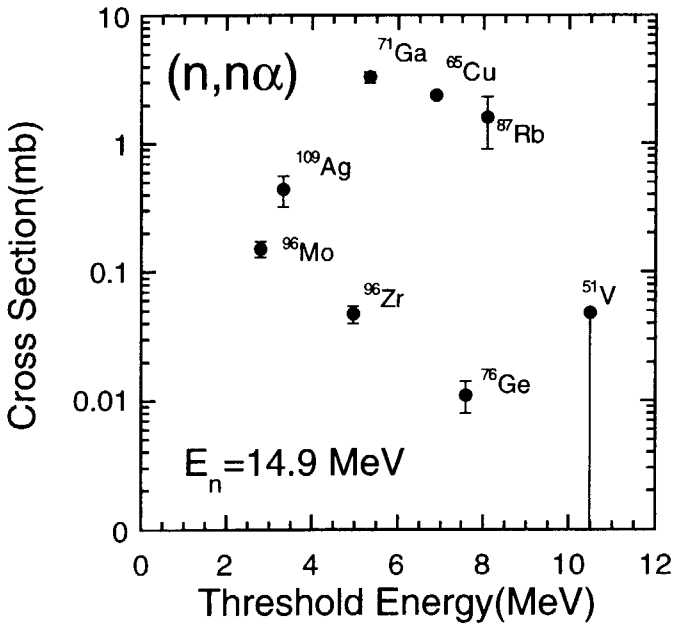

Fig. 5.4 Systematics of the (n, nα) cross sections at 14.9 MeV as a function of the threshold energy.

Appendix Summary of the systematics for (n,p) and (n,α) partial excitation functions in the neutron energy between 13.4 and 15.0 MeV

The systematics for (n,p) and (n,α) partial excitation functions in the neutron energy between 13.3 and 15.0 MeV are summarized. The details were described in Refs. 8 and 9.

The cross section curves in the energy range from 13.3 and 15.0 MeV are approximately represented by the linear function as

$$\sigma = a(E_n - 14.0) + \sigma_{14}$$

where,

σ : cross sections [mb]
E_n : neutron energy [MeV]
a : slope of excitation curve [mb/MeV]
σ_{14} : cross section at 14.0 MeV [mb].

A relative slope, S, is defined as

$$S = a/\sigma_{14}.$$

For the (n,p) reaction, the empirical formulas of σ and σ_{14} are described as

$$\sigma_{14} = 1830(N - Z + 1)\exp\left(-50.7\frac{N - Z + 1}{A}\right),$$

$$S = -0.271 + 0.811\frac{N - Z}{A} + 14.57\left(\frac{N - Z}{A}\right)^2 + 0.037E_{th}$$

where

N : neutron number of the target
Z : proton number
A : mass number
E_{th} : threshold energy of the reaction [MeV].

For the (n,α) reactions, the empirical formulas of σ and σ_{14} are described as

$$\sigma_{14} = 434.8\exp\left(-33.4\frac{N - Z}{A}\right),$$

$$S = -1.076 + 0.0788(E_{th} + V_\alpha)$$

where V_a is a coulomb barrier for an α-particle emission from a compound nucleus. N, Z, A and E_{th} are the same as for the (n,p) reaction. The value of V_a is calculated by using the following equation:

$$V_a = \frac{2Z_r e^2}{r_0 A_r^{1/3}}$$

where

A_r : mass number of a residual nucleus ($= A - 3$)
Z_r : proton number of a residual nucleus ($= Z - 2$)
e : elementary charge (e^2=1.4 MeV•fm)
r_0 : a constant value (=1.4 fm).

The value of $r_0 A^{1/3}$ corresponds to a radius of a residual nucleus, and "2" in the equation corresponds to charge of α-particle.

国際単位系 (SI) と換算表

表 1　SI基本単位および補助単位

量	名称	記号
長さ	メートル	m
質量	キログラム	kg
時間	秒	s
電流	アンペア	A
熱力学温度	ケルビン	K
物質量	モル	mol
光度	カンデラ	cd
平面角	ラジアン	rad
立体角	ステラジアン	sr

表 2　SIと併用される単位

名称	記号
分，時，日	min，h，d
度，分，秒	°，′，″
リットル	l，L
トン	t
電子ボルト	eV
原子質量単位	u

1 eV = 1.60218 × 10^{-19} J

1 u = 1.66054 × 10^{-27} kg

表 5　SI接頭語

倍数	接頭語	記号
10^{18}	エクサ	E
10^{15}	ペタ	P
10^{12}	テラ	T
10^{9}	ギガ	G
10^{6}	メガ	M
10^{3}	キロ	k
10^{2}	ヘクト	h
10^{1}	デカ	da
10^{-1}	デシ	d
10^{-2}	センチ	c
10^{-3}	ミリ	m
10^{-6}	マイクロ	μ
10^{-9}	ナノ	n
10^{-12}	ピコ	p
10^{-15}	フェムト	f
10^{-18}	アト	a

表 3　固有の名称をもつSI組立単位

量	名称	記号	他のSI単位による表現
周波数	ヘルツ	Hz	s^{-1}
力	ニュートン	N	m·kg/s^2
圧力，応力	パスカル	Pa	N/m^2
エネルギー，仕事，熱量	ジュール	J	N·m
工率，放射束	ワット	W	J/s
電気量，電荷	クーロン	C	A·s
電位，電圧，起電力	ボルト	V	W/A
静電容量	ファラド	F	C/V
電気抵抗	オーム	Ω	V/A
コンダクタンス	ジーメンス	S	A/V
磁束	ウェーバ	Wb	V·s
磁束密度	テスラ	T	Wb/m^2
インダクタンス	ヘンリー	H	Wb/A
セルシウス温度	セルシウス度	℃	
光束	ルーメン	lm	cd·sr
照度	ルクス	lx	lm/m^2
放射能	ベクレル	Bq	s^{-1}
吸収線量	グレイ	Gy	J/kg
線量当量	シーベルト	Sv	J/kg

表 4　SIと共に暫定的に維持される単位

名称	記号
オングストローム	Å
バーン	b
バール	bar
ガル	Gal
キュリー	Ci
レントゲン	R
ラド	rad
レム	rem

1 Å = 0.1 nm = 10^{-10} m

1 b = 100 fm^2 = 10^{-28} m^2

1 bar = 0.1 MPa = 10^5 Pa

1 Gal = 1 cm/s^2 = 10^{-2} m/s^2

1 Ci = 3.7 × 10^{10} Bq

1 R = 2.58 × 10^{-4} C/kg

1 rad = 1 cGy = 10^{-2} Gy

1 rem = 1 cSv = 10^{-2} Sv

（注）

1. 表1－5は「国際単位系」第5版，国際度量衡局 1985年刊行による。ただし，1 eVおよび1 uの値はCODATAの1986年推奨値によった。
2. 表4には海里，ノット，アール，ヘクタールも含まれているが日常の単位なのでここでは省略した。
3. barは，JISでは流体の圧力を表わす場合に限り表2のカテゴリーに分類されている。
4. EC閣僚理事会指令ではbar，barnおよび「血圧の単位」mmHgを表2のカテゴリーに入れている。

換　算　表

力	N(=10^5 dyn)	kgf	lbf
	1	0.101972	0.224809
	9.80665	1	2.20462
	4.44822	0.453592	1

粘　度　1 Pa·s(N·s/m^2) = 10 P(ポアズ)(g/(cm·s))

動粘度　1 m^2/s = 10^4 St(ストークス)(cm^2/s)

圧力	MPa(=10 bar)	kgf/cm^2	atm	mmHg(Torr)	lbf/in^2(psi)
	1	10.1972	9.86923	7.50062 × 10^3	145.038
	0.0980665	1	0.967841	735.559	14.2233
	0.101325	1.03323	1	760	14.6959
	1.33322 × 10^{-4}	1.35951 × 10^{-3}	1.31579 × 10^{-3}	1	1.93368 × 10^{-2}
	6.89476 × 10^{-3}	7.03070 × 10^{-2}	6.80460 × 10^{-2}	51.7149	1

エネルギー・仕事・熱量	J(=10^7 erg)	kgf·m	kW·h	cal(計量法)	Btu	ft·lbf	eV
	1	0.101972	2.77778 × 10^{-7}	0.238889	9.47813 × 10^{-4}	0.737562	6.24150 × 10^{18}
	9.80665	1	2.72407 × 10^{-6}	2.34270	9.29487 × 10^{-3}	7.23301	6.12082 × 10^{19}
	3.6 × 10^6	3.67098 × 10^5	1	8.59999 × 10^5	3412.13	2.65522 × 10^6	2.24694 × 10^{25}
	4.18605	0.426858	1.16279 × 10^{-6}	1	3.96759 × 10^{-3}	3.08747	2.61272 × 10^{19}
	1055.06	107.586	2.93072 × 10^{-4}	252.042	1	778.172	6.58515 × 10^{21}
	1.35582	0.138255	3.76616 × 10^{-7}	0.323890	1.28506 × 10^{-3}	1	8.46233 × 10^{18}
	1.60218 × 10^{-19}	1.63377 × 10^{-20}	4.45050 × 10^{-26}	3.82743 × 10^{-20}	1.51857 × 10^{-22}	1.18171 × 10^{-19}	1

1 cal = 4.18605 J(計量法)
= 4.184 J　(熱化学)
= 4.1855 J　(15 °C)
= 4.1868 J(国際蒸気表)

仕事率　1 PS(仏馬力)
= 75 kgf·m/s
= 735.499 W

放射能	Bq	Ci
	1	2.70270 × 10^{-11}
	3.7 × 10^{10}	1

吸収線量	Gy	rad
	1	100
	0.01	1

照射線量	C/kg	R
	1	3876
	2.58 × 10^{-4}	1

線量当量	Sv	rem
	1	100
	0.01	1

(86年12月26日現在)

Activation Cross Section Measurement at Neutron Energy From 13.3 to 14.9 MeV Using FNS Facility